



Contributions to Rock Fracture Induced by High Ground Stress in Deep Mining: A Review

Huaming An¹ · Xinghai Mu¹

Received: 13 February 2024 / Accepted: 2 August 2024

© The Author(s), under exclusive licence to Springer-Verlag GmbH Austria, part of Springer Nature 2024

Abstract

With the shallow resources dwindling, many countries have entered into deep mining one after another. Rock fracture caused by high stress mining disturbances is a significant concern. Destabilization caused by rock fracture not only diminishes productivity, but can also poses the risk of injuries and property damage. Therefore, it is of great significance to investigate the rock fracture mechanism of deep mining to ensure mining safety and improve production efficiency. This paper begins by summarizing key challenges associated with deep mining. Subsequently, it categorizes the outcomes of previous research on this issue into various themes, encompassing laboratory tests, theoretical analyses, numerical simulations and field measurement. This paper provides an overview of a number of representative studies that the growing scenarios and an increase in our understanding of this issue. A summary of the limitations of each contribution is presented, as well as the expected aspects that need to be optimized in the future research. It is found that our knowledge is far from complete, and there are still gaps to be narrowed, particularly concerning the theory of deep rock mechanics, identification of deformation and fracture in deep rock, establishment of three-dimension strength criterion, accuracy of numerical modelling and accuracy of field measurement. The review aims at providing researchers and engineers with a comprehensive understanding of the pertinent issue and guiding them for more in-depth exploration and research.

Highlights

- Deep mining poses significant challenges and risks due to rock rupture caused by high stress mining disturbances, which directly impact productivity, safety, and property.
- The review provides a comprehensive understanding of the key challenges associated with deep mining induced by high ground stress and categorizes previous research outcomes into various themes, including laboratory tests, theoretical analyses, numerical simulations, and field measurement.
- The study highlights the urgent need for a consensus on the concept of "deep" in deep rock mechanics, as it significantly affects the ground stress and requires specialized approaches beyond traditional rock mechanics theories and methods.
- The advancements in dynamic and static true triaxial apparatus offer crucial technology for accurately measuring various physical and mechanical properties of rocks under deep burial conditions, promoting the development of deep rock mechanics.
- The comparison and analysis of different strength criteria underscore the significance of establishing a three-dimensional strength criterion that considers geological structure, intermediate principal stress, lode angle, and excavation disturbance, enabling more accurate detection and understanding of the rock fracture mechanism in deep mining.
- This study focuses on the high ground stress in deep mining has some limitations. Therefore, other influencing factors in deep mining are prospected.

✉ Huaming An
huaming.an@kust.edu.cn

¹ Faulty of Public Security and Emergency Management,
Kunming University of Science and Technology,
Kunming 650093, China

Keywords Deep mining · Rock fracture · Laboratory tests · Theoretical analysis · Numerical simulation · Field measurement

1 Introduction

With the growth of the world's economy and the escalating in human needs, there has been a compelling impetus to utilize underground space and extract underground resources. This trend has given rise to a multitude of deeply buried underground projects across diverse sectors including transportation, energy extraction, water conservancy, and hydropower (Jiang and Zou 2023). The development and utilization of underground spaces, such as transportation tunnels, underground chambers, nuclear waste storage sites, and geothermal energy facilities, have significantly enhanced transportation and storage efficiency (Jiang et al. 2023; Qian and Li 2008). Moreover, the extraction of underground resources, including coal, metal ores, oil, and natural gas, is fundamental to global economic development. (Meng et al. 2021). However, with the gradual depletion of shallow mineral resources, it has become inevitable for different countries and regions to go deeper and deeper into the earth, and explores deeper resources by 1,000-m-deep wells has gradually become the new normal for resource development (Chen et al. 2022; Feng et al. 2019; Heping 2019; Xie et al. 2022). At present, there are more than 110 mines with a depth of more than 1,000 m. These deeply buried mines are mainly metal mines, mainly located in South Africa, Canada, the United States, India, Russia, and other countries and regions, and most of them are mined at a depth of more than 2,000 m (Vogel and Rast 2000; Yong et al. 2023). The deepest gold mine in the western part of South Africa has reached 3,700 m (Malan et al. 1998); in terms of waste disposal, the deep cavern disposal method is used, with a depth of 500–1,000 m (Wang et al. 2006); in terms of transportation, the diversion tunnel of China's Jinping II Hydropower Station has an excavation diameter of 13 m, a length of 16.7 km, and a maximum burial depth of 2,525 m (Li et al. 2023d). Overall, underground engineering presents the characteristics of considerable buried depth, significant mining height and large sections (Maolin et al. 2022; Tang et al. 2010).

Once underground engineering enters deep mining, the complex high-stress environment, the nonlinear mechanical behavior of the rock, and the significant difference of the principal stresses become the common characteristics that distinguish it from shallow engineering (Chen et al. 2021; Hoek and Brown 1997; Meng et al. 2021; Yong et al. 2023). Deep mining inevitably leads to high three-dimensional stress readjustment, resulting in deformation and fracture of the rock, which in turn presents features such as zonal disintegration and slabbing and may eventually lead to

the production of unpredictable hazards such as spalling, large deformations, collapsing, and rock burst (Jiang et al. 2021; Li et al. 2019; Sun et al. 2018b). In addition, the deep rock body shows prominent anisotropic characteristics ($\sigma_1 > \sigma_2 > \sigma_3$) under the influence of geological structure and engineering perturbation, which makes the theories and methods for studying rock fracture in shallow mining no longer applicable to deeply buried projects (Cai et al. 2022b; He and Wang 2022; Lu et al. 2021a; Wang et al. 2022; Zhao et al. 2021). For example, shallow mining of the surrounding rock produces fractured, plastic, and elastic zones. While deep mining shows zonal fracturing with alternating fractured and intact zones. The lack of theoretical methods has brought unprecedented challenges to deep underground engineering. The key to preventing and controlling deep engineering disasters is to clarify the characteristics and mechanism of rock failure under true three-dimensional stress adjustment. This can not only help to identify the possibility of deep rock fracture as early as possible to facilitate the adoption of effective reinforcement measures to ensure the safety of construction and long-term stability of operation but also promote the innovation of deep mining methods and theories to promote rock mechanics to a new level (Feng et al. 2017a, 2022; Han et al. 2020a). The key to understanding the mechanisms of rock fracture in deep mining is to choose the suitable method. A large number of papers have been written on the study of rock fracture mechanisms in deep resource extraction, which can be categorized into four groups based on the research methods of the papers: laboratory tests, theoretical analysis, numerical simulation, and field measurement. The core of any research method is how to clarify the microscopic damage and macroscopic fracture of rock under the constant adjustment of true three-dimensional stress. Each of the four research methods summarized in the literature has its characteristics. Laboratory tests can avoid difficulties in the field of mathematics and mechanics, which becomes the mainstream research method using the corresponding equipment to reflect the physical and mechanical phenomena and deformation and fracture laws of rocks (Li et al. 2015a; Zhao et al. 2022b; Zhao and Zhang 2015). Many scholars also favor theoretical analysis and numerical simulation because of their low cost, high efficiency, and high repeatability (Sun et al. 2021b; Wu et al. 2019; Zheng et al. 2021).

In general, the current research work has been fruitful and has provided a wealth of information for developing deep engineering theory and underground engineering construction. However, so far, there has not been a single

piece of literature that has systematically reviewed rock fracture research methods for deep resource extraction. In this study, the contributions of previous scholars to this problem are divided into four parts: laboratory tests, theoretical analysis, numerical simulation, and field measurement. This paper will analyze and summarize some of the key issues involved in deep underground space mining and the characteristics and prospects of four methods.

2 Problems Related to Deep Mining Induced by High Ground Stress

After entering the deep mining environment, high-ground stress is the first problem. A large number of experiments and studies have proved that the mechanical properties and mechanical responses of deep rock and shallow rock are very different. If the technology adapted to the high-stress environment is not adopted, it will inevitably cause severe engineering disasters and inhibit the efficiency of deep mining. Therefore, the definition of "deep" is necessary before the review.

Different countries have different definitions of "deep" in deep resource mining engineering. China and Japan believe that when the mining depth exceeds 600 m, it enters deep mining; Canada, Russia, and Australia set 1,000 m as the boundary to enter deep mining; the initial limits of deep mining in South Africa and the United States are 1,500 m and 1,542 m respectively (Diering 1997; Li et al. 2017b). In addition, after the concept of "Ultra deep" was first proposed by the South African industry in 1996, other countries have also divided the Ultra deep boundaries accordingly. The specific division is shown in Fig. 1. Different countries have not reached a unified boundary for the deep, but entering deep mining means that high-ground stress has become an indisputable

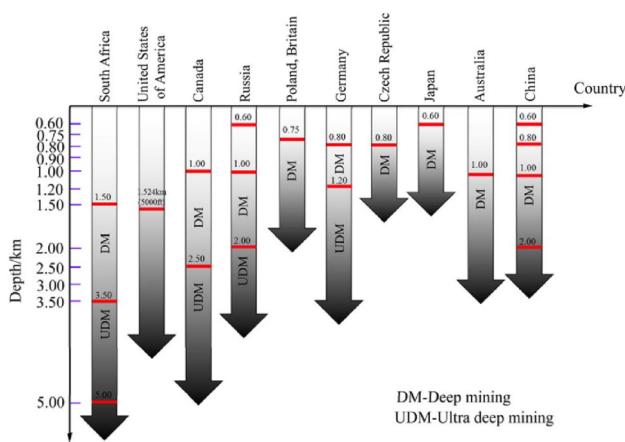


Fig. 1 Definition of deep in different countries, after Li et al. (2017b)

fact. It is generally believed that when the mining enters the deep part, the self-weight stress plus the structure stress is usually greater than 20 Mpa, and the stress concentration caused by the engineering disturbance often makes the rock stress exceed 40 Mpa, far exceeding its strength (He et al. 2005; Li et al. 2007). Therefore, "deep" is not only related to depth but should also be a concept related to the mechanical properties of rock. Therefore, in the academic field of deep mining, some scholars try to use rock mechanics phenomena, empirical formulas, lifting capacity, and ground temperature to determine the boundaries of the deep. These methods have been described in detail in the article "Probabilistic analysis of tunnel displacements based on correlative recognition of rock mass parameters" and will not be repeated in this paper. It is worth noting that ergonomics theory is used when considering the factors of ground temperature to define deep burial. The method considers that when the limit of deep burial when the mining depth exceeds a certain limit, it is also difficult to meet the workers' needs for underground work comfort with the existing cooling and ventilation technology. The method breaks the limitation of the traditional method of considering only the research object and fully considers the staff's working environment. Therefore, "Deep" is a mechanical state that should be comprehensively defined regarding stress level, stress state, and mechanical behavior of the surrounding rock.

Although scholars have proposed some methods to define the critical value of "deep", this field has no unified international standard. This has considerably hindered the development and exchange of this field, so it is urgent to unify the concept of "deep" and its scientific evaluation index to study the basis of deep rock mechanics.

Rock fracture under high-ground stress conditions is directly related to the stability of the project, so the problem has received extensive attention from the academic and engineering communities. In the mining of deep resources, the stress of rock mass will be constantly adjusted. To simplify the study of this problem, some scholars have transformed it into a plane strain problem (Cui et al. 2017; Song et al. 2016; Zhang et al. 2017a). That is, the tangential stress σ_t (σ_θ) and radial stress σ_r are the maximum principal stress σ_1 and minimum principal stress σ_3 , respectively, and the axial stress σ_a is the intermediate principal stress σ_2 , ignoring the effect of the σ_2 . However, many scholars have concluded that the intermediate principal stress significantly influences the strength, mechanical properties, damage patterns, crack development, and dynamic hazards of deeply buried rocks (Du et al. 2015; Feng et al. 2020, 2022; Kong et al. 2018; Lu et al. 2020; Zhang et al. 2021b; Zhao et al. 2018). For example, as shown in Fig. 2, the evolution of the damage mode of deep granite is affected by σ_2 , with the



Fig. 2 Failure mode evolution process of granite specimens under different σ_2 (MPa): **a** $\sigma_2=0$, **b** $\sigma_2=10$, **c** $\sigma_2=20$, **d** $\sigma_2=30$, **e** $\sigma_2=40$, after (Du et al. 2015)

increase of σ_2 , the damage mode of granite changes from shear damage to plate damage (Du et al. 2015). As shown in Fig. 3, the strength of the deep hard rock is characterized by asymmetric variation with increasing σ_2 , and the peak strength of the rock increases with increasing σ_2 (Feng et al. 2020). Crack extension in sandstone is closely related to the σ_2 , which affects the crack initiation stress σ_{ci} , as shown in Fig. 4 (Kong et al. 2018). As shown in Fig. 5, the composite dynamic hazard (coal and gas protrusion) generated by deep coal mining increases and then decreases with the rise of σ_2 (Lu et al. 2020). As shown in Fig. 6, with the increase of the σ_2 , the Jinping marble gradually changes from ductile to brittle (Zhao et al. 2018). In addition, the effect of the σ_2 on the rock increases with the depth of burial, and the σ_2 cause axial plastic flow, leading to increased deformation of the surrounding rock (Cai et al. 2022b; Guan et al. 2018). When using the plane strain model to solve the deformation of surrounding rock, it is often assumed that all the deformations are in the plane perpendicular to the axis of the roadway. The plane strain model mainly focuses

on the variation of radial stress-displacement and tangential stress-displacement of surrounding rocks (Cai et al. 2022a; Sun et al. 2021a). The plane strain model does not consider the underground cavern's axial stress, overemphasizes the surrounding rock's radial convergence deformation, and ignores the extrusion and pre-convergence deformation of the core surrounding rock (Cai et al. 2022a; Sun et al. 2021a). However, the ground stress in the axial direction will not be released entirely at excavation, which will be gradually released as the working face advances. Therefore, using the plane strain model to study rock fracture due to deep mining leads to results that are too conservative and does not effectively consider the strength and self-supporting effects of the rock mass.

It is well known that the ground stress will be redistributed during the excavation process. As shown in Fig. 7, the surrounding rock rapidly changes from a three-dimensional stress state to a one-way stress, two-way stress, or five-sided stress state (Su et al. 2017b; Sun et al. 2021a). The results of redistribution of ground stress by different

Fig. 3 Effect of σ_2 on rock strength: **a** Turkey andesite, **b** CJPL-II marble, **c** Hornblende granite, **d** Porphyritic basalt, after Feng et al. (2020)

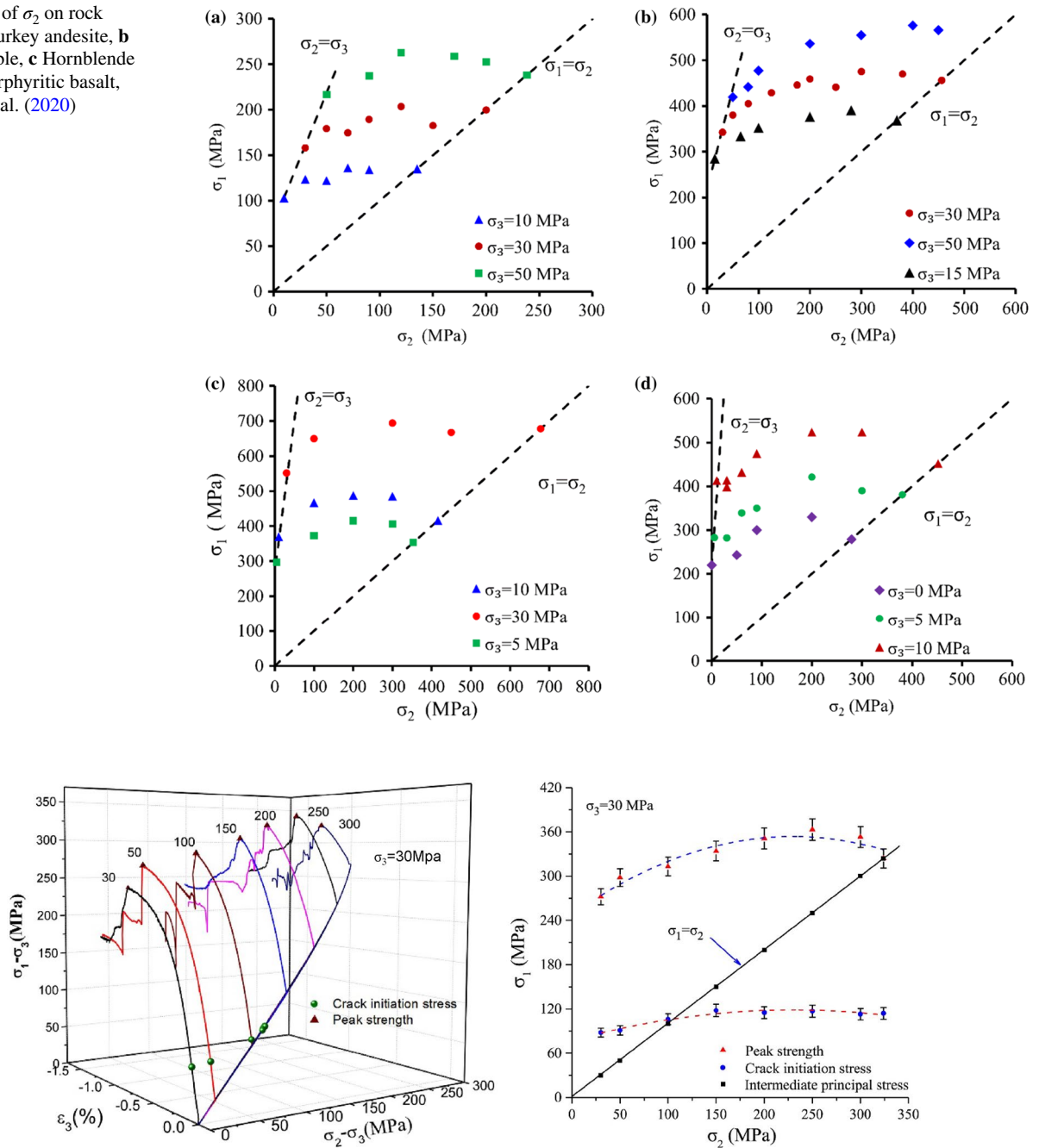


Fig. 4 Effect of different σ_2 on initiation cracking stresses in sandstones, after Kong et al. (2018)

excavation methods or excavation along different principal stress directions are different. Specifically, the rock is affected by the "excavation unloading" effect and the "stress concentration" effect. As shown in Fig. 8, a free surface is formed in the surrounding rock after excavation. On the one hand, the radial stress σ_r decreases gradually with the approaching of the free surface and decreases to zero at the roadway wall; on the other hand, the tangential stress σ_t (σ_θ) increases with the approaching the free surface and even

doubles the original rock stress at the chamber wall (Chen et al. 2021; Yang et al. 2019b; Zhao et al. 2022a). He and Wang (2022) called it digging effect I and digging effect II, respectively. In addition, with the advancement of the tunnel face, the stress concentration zone will be generated in front of the tunnel face. The stress adjustment in the whole excavation process can be divided into four stages: (1) initial stage, (2) stress concentration stage, (3) stress unloading stage, (4) stable stage. The stress adjustment

Fig. 5 Effect of σ_2 (MPa) on coal-rock dynamic hazards: **a** $\sigma_2=15$, **b** $\sigma_2=25$, **c** $\sigma_2=35$, after Lu et al. (2020)

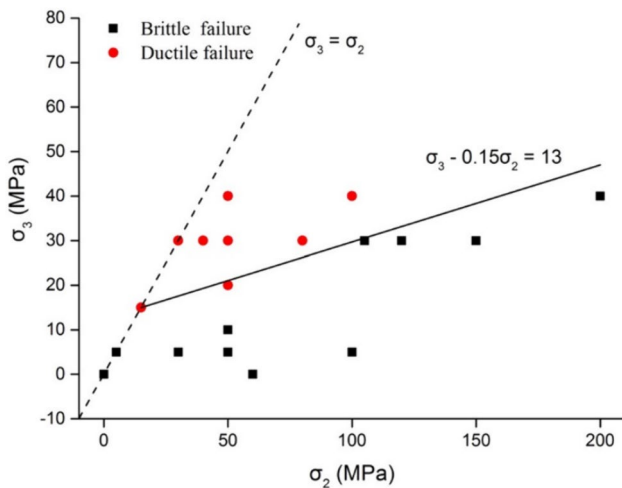
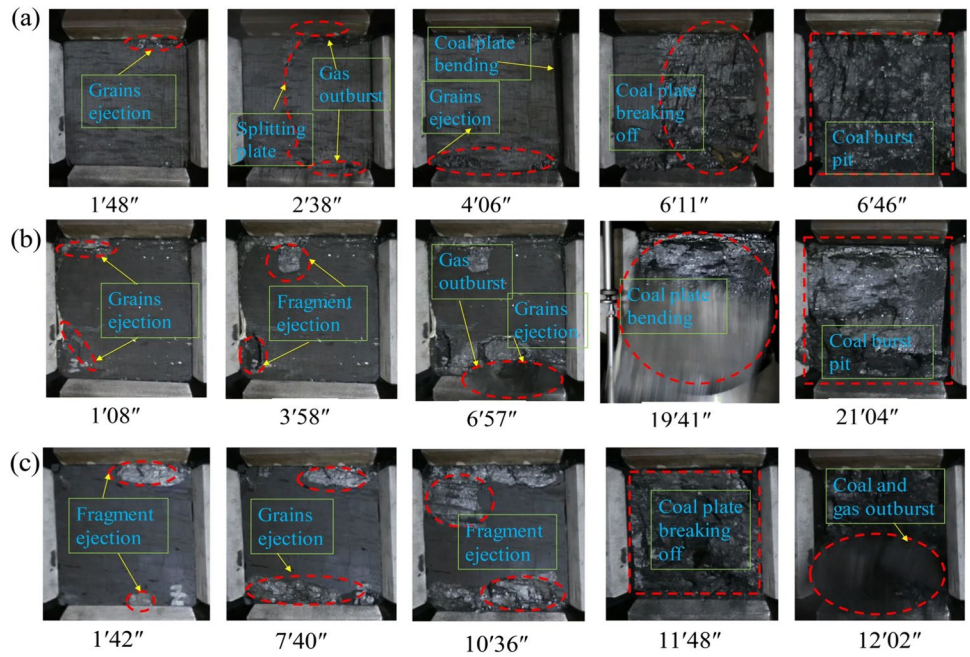


Fig. 6 The effect of σ_2 on the mechanical properties of granite, after Zhao et al. (2018)

process is sharp, so the deviatoric stress increases rapidly to form a stress concentration zone. On the one hand, as a unique natural material, rock is affected by stratum and geological structure, and there are many randomly distributed natural defects. On the other hand, under the action of load, the randomly distributed defects of rock are constantly changing. New microcracks are generated and expanded when the stress on the rock is exceeded by the minimum stress for crack initiation (CI) (Meng et al. 2021). Microcracks first appear at the tip, which gradual development leads to the continuous damage of the rock, making it a dominant meso-fracture and macro-crack. In

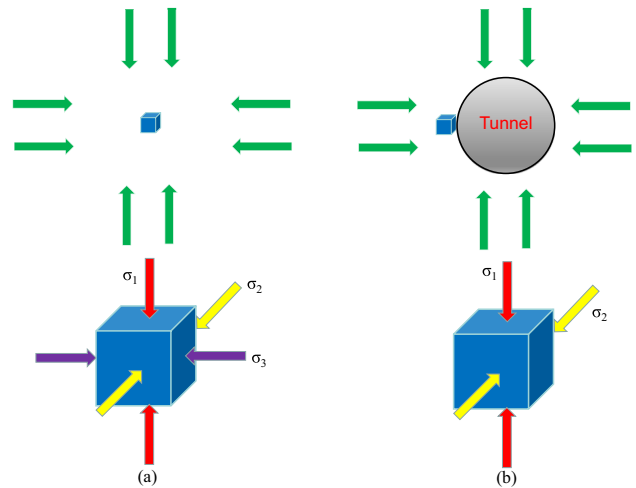


Fig. 7 Change in stress state before and after excavation: **a** before excavation, **b** after excavation

other words, when the stress reaches the extreme strength of the rock, the rock begins to break and then generates a macroscopic fracture surface. It is worth noting that in the coal mining process, the vertical stress increases and the horizontal stress decreases, which is slightly different from the above description (Huang et al. 2001). However, the core of the rock fracture is still due to the rapid increase of bias stress caused by excavation to form a stress concentration area. The excavation of deep underground caverns changes the original stress state. The peak stress of the surrounding rock shifts to the deep part. The magnitude of stress controls the degree of stress concentration. The stress direction

Fig. 8 Variation of σ_r and σ_θ for different distances from the excavated surface, after Zhao et al. (2022a)

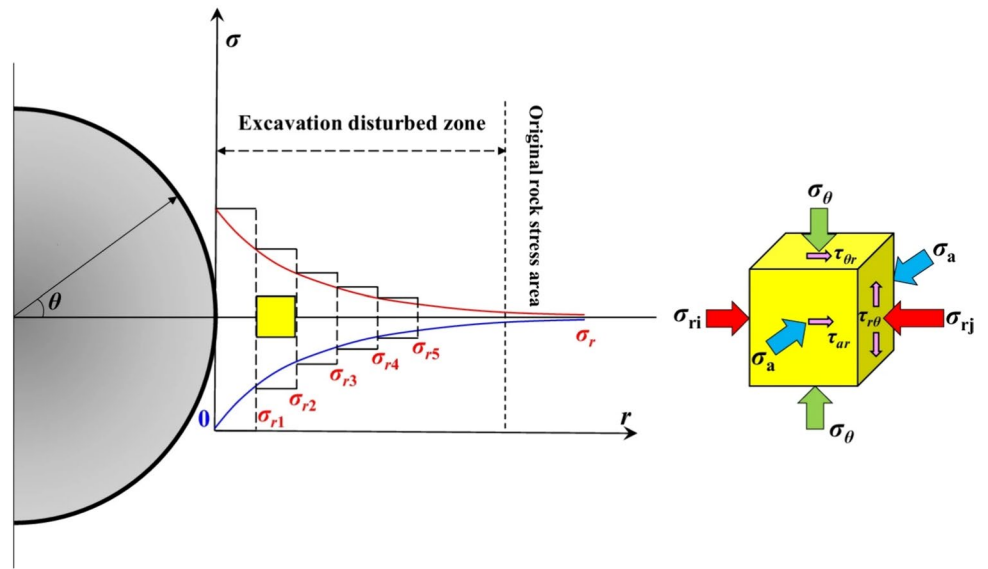
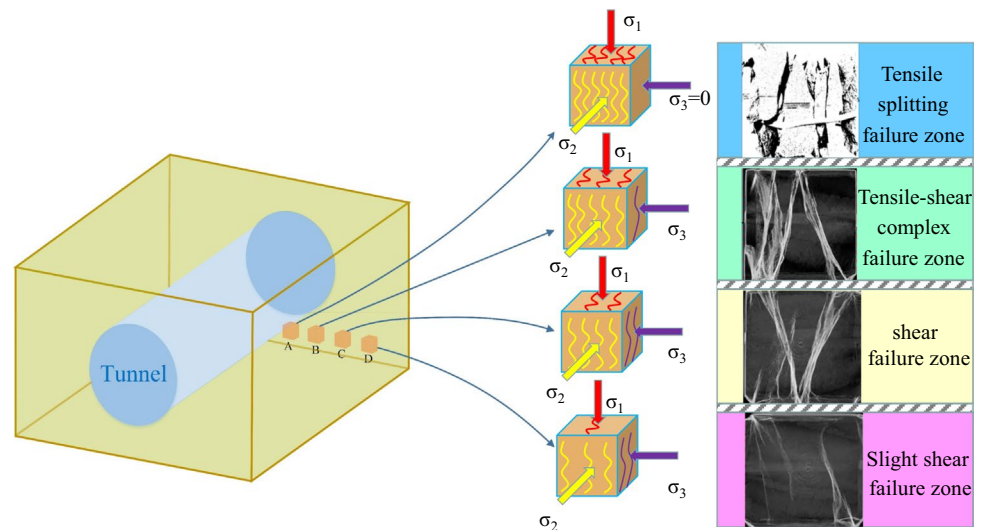


Fig. 9 Typical damage schematic of surrounding rock at different depths of the cave chamber, after Sun et al. (2022a) and Zhao et al. (2022a)



determines the position of stress concentration after excavation (Gu et al. 2023). Therefore, as shown in Fig. 9, the typical forms of microscopic damage in the surrounding rock at different depths are not the same.

Deep rocks have long been stored to high geothermal temperatures, high ground stress, and high karst water pressures, and their past history will influence the rocks' present and future mechanical behavior (Brown and Hoek 1978; Cai et al. 2022b; Qian and Zhou 2018). Deep rocks exhibit nonlinear mechanical properties, which are quite different from shallow buried rocks. In shallow buried areas, rocks generally satisfy an elastic state with a limited plastic zone, which can be explained using elasticity theory. In addition, Yan et al. (2015) measured the ground stress in the Jinping II diversion tunnel using hydraulic fracturing, and the principal stresses varied linearly in the shallow

burial zone, while increased nonlinearly in the deep burial zone (see Fig. 10). The nonlinear variation of ground stress in deeply buried rocks is the primary factor that causes their physicochemical properties to differ from those of shallow rocks. Second, as shown in Fig. 11, the basic physicochemical parameters of deep rocks, such as modulus of elasticity, Poisson's ratio, and strength, change continuously with depth (Zhang et al. 2019b; Zhou et al. 2010). However, traditional rock mechanics theory assumes that rocks' microstructure and physicochemical parameters are constant. This is one of the reasons why conventional rock mechanics theories and methods are inapplicable to deeply buried projects. At present, researchers have conducted extensive studies on the mechanical properties of deep rock (Kaiser and Kim 2015; Verman et al. 1997; Wang et al. 2016b; Zhang et al. 2015). The related studies

Fig. 10 Non-linear variation of principal stresses with depth, after Yan et al. (2015)

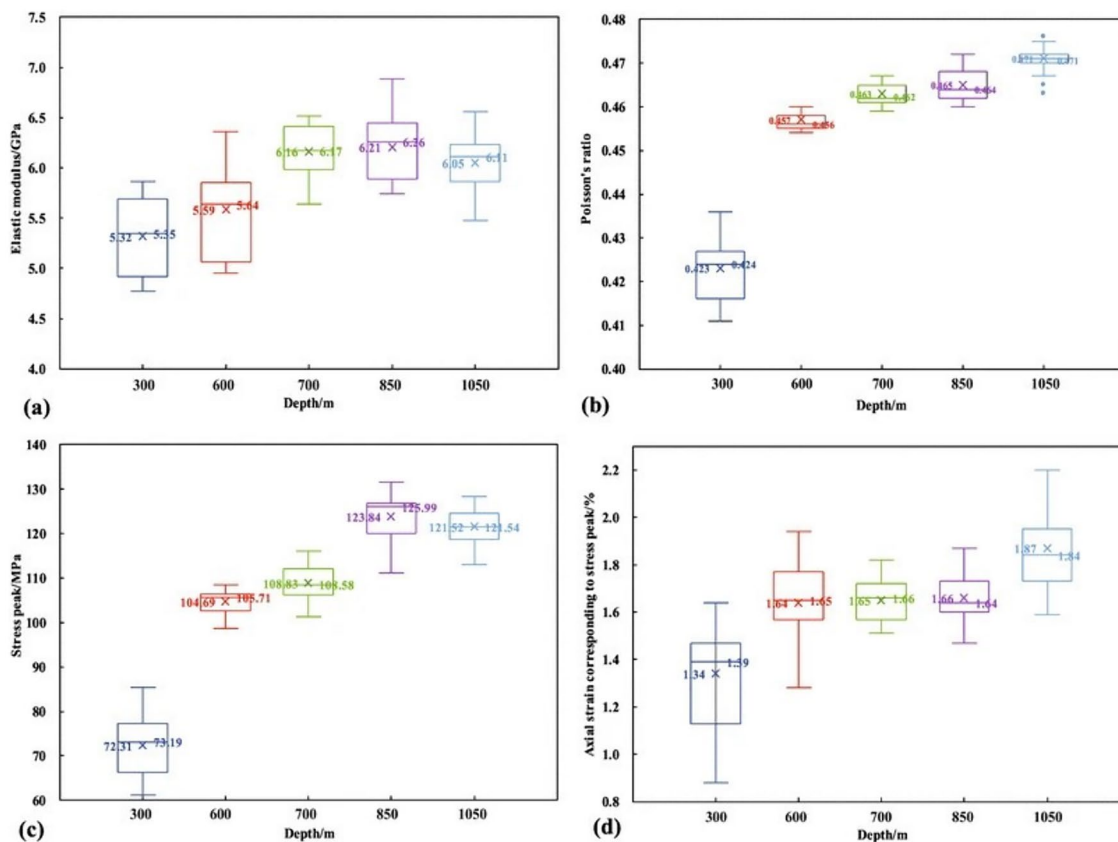
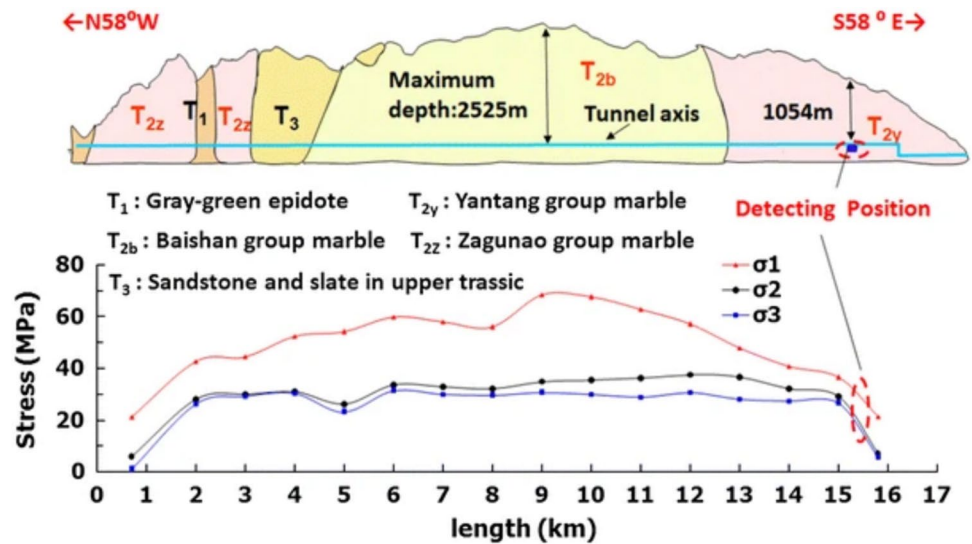


Fig. 11 Variation of rock mechanical parameters with depth: **a** Elastic modulus, **b** Poisson's ratio, **c** strength, **d** axial strain corresponding to stress peak, after Zhang et al. (2019b)

can be divided into two categories. In the first category, the deformation and damage behavior at different depths was simulated by applying different temperatures and circumferential pressures for rocks at the same position, but this method must consider the variability of rock's physical

properties due to different depths. In the second category, only the differences in the physical properties of the rocks as affected by the depths were taken into account, without considering the stress environment (Zhang et al. 2019b). Therefore, to accurately characterize the physicochemical

properties of the rock mass at the microscopic (presence and extension of defects at different scales and levels, interactions in the formation of tectonic units) and macroscopic (cohesion, internal friction, dilatation, and energy release properties) it is necessary to take into account both the depth of the rock storage and the environment in which the rock exists.

At present, the study of deep rock mass mechanics has lagged behind the practice of geotechnical engineering, and factors such as depth, engineering activities, and ground stress environment have yet to be fully understood, resulting in a lot of uncertainty and inefficiency in practice (Xie et al. 2005). Therefore, promoting the development of deep rock mechanics and the innovation of theoretical methods is the key to the deep earth.

3 Laboratory Tests

The mechanical properties of rock, such as compressive strength (including uniaxial compressive strength and compressive strength under confining pressure), tensile strength, shear strength, and fracture angle, are related to the stress state, temperature and loading rate of rock, but the stress state has the most significant influence on the mechanical properties of rock. Laboratory tests, especially true triaxial apparatus, are considered one of the most practical test methods due to their ability to simulate real underground stress conditions and a unique understanding of the three-dimensional stress state of the rock mass. The laboratory test can compensate for the lack of relevant theories of deep rock mechanics and clarify the rock's failure mechanism under a three-dimensional stress state. Xie et al. (2022) has systematically described a variety of

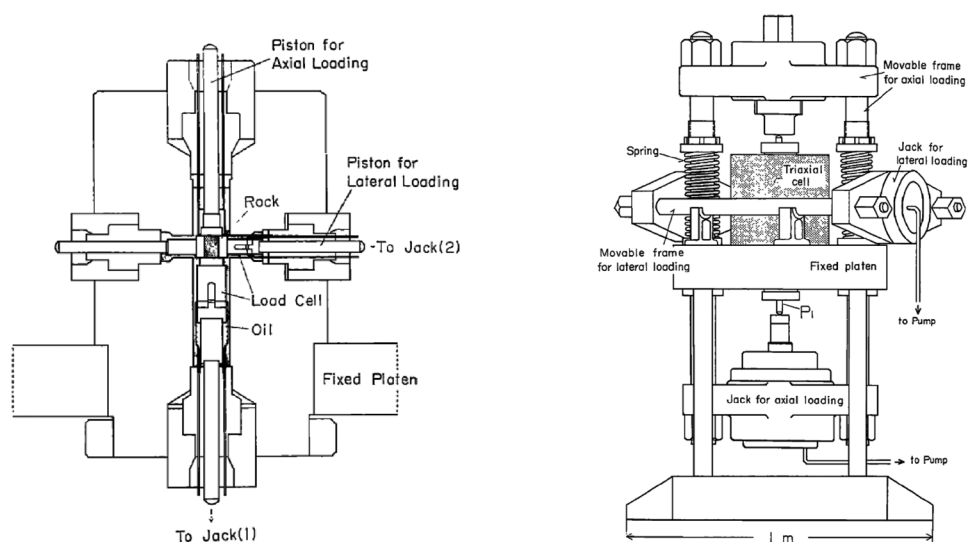
typical triaxial test apparatus in the "Experimental study on the mechanical and failure behaviors of deep rock subjected to true triaxial stress: A review". Therefore, this paper will briefly summarize the true triaxial test apparatus of rock, and focus on the discussion and summary of several key issues involved in the triaxial tests (end effect and eccentric loading, stress path, similar experiment, crack initiation stress, and characterization methods).

3.1 True Triaxial Apparatus

The true triaxial apparatus is divided into quasi-static true triaxial apparatus and dynamic triaxial apparatus according to its loading speed and loading mode. The quasi-static triaxial testing machine applies a stable and continuous static loading during the test. A hydraulic cylinder or screw drive generally realizes the loading method, and the loading rate can be adjusted to meet the experimental requirements. The dynamic triaxial apparatus applies dynamic loading during the test to simulate dynamic loads such as earthquakes and blasting, which can be achieved quickly and instantly using an electromagnetic drive and hydraulic drive. True static triaxial apparatus can study rocks' strength, deformation, stability, and other mechanical properties under different stress conditions. True dynamic triaxial apparatus can be used to study the response, strength, damage mode, and other dynamic mechanical properties of rocks under dynamic loads such as earthquakes and explosions.

As shown in Fig. 12, the first true triaxial experimental apparatus for rocks was developed in 1970 by Mogi Kiyoo, a seismologist at the University of Tokyo, and it used a hybrid loading structure (Mogi 1967, 1971). For the loading structure, the maximum principal stress (σ_1) and the intermediate principal stress (σ_2) are loaded by rigid loading plate, and the minimum principal stress (σ_3)

Fig.12 Mogi type testing apparatus, after Mogi (1971)



is loaded by hydraulic flexible loading. The true triaxial apparatus is also known as the Mogi test machine or the "two rigid and one flexible" true triaxial test machine. The test machine uses a small sample ($15\text{ mm} \times 15\text{ mm} \times 30\text{ mm}$). The maximum fluid pressure that can be applied is 0.8 Mpa , the maximum principal stress is 700 KN , and the maximum intermediate principal stress is 300 KN . Mogi concluded that the intermediate principal stress plays a vital role in the mechanical properties of deep rock through the developed triaxial testing machine. Since then, the intermediate principal stress effect has gradually become a research topic in rock mechanics. The test machine has a milestone significance, so most of the subsequent true triaxial experimental equipment is based on this idea. However, the test machine is suitable for low-confining pressure soft rock, which will produce large errors in measuring small specimens (Xie et al. 2022).

When the triaxial apparatus was first created, its function was uncomplicated, and it was mainly used to study the strength and stress-strain relationship of rocks under specific stress conditions, which had little requirement for equipment refinement. However, with the increasing mining depth, the academic community has higher expectations for understanding and studying the mechanism of deep rock fracture (Yu et al. 2020). Therefore, many scholars have

developed different types of rock true triaxial apparatus, which promotes the development of true triaxial apparatus. According to the loading method, true triaxial apparatus can be divided into three types: (1) mixed loading type (see Fig. 13), which is also the Mogi test machine. In addition to the Mogi type, there are Spetzler et al. (1981), Wawersik et al. (1997), Haimson and Chang (2000), Feng et al. (2021; 2016; 2018), Li et al. (2016a), etc. (2) Rigid loading type (see Fig. 14), this instrument's three principal stress directions are all imposed by rigid loading plates. Typical representatives include Furuzumi and Sugimoto (1986), Skoczylas and Henry (1995), Sibai et al. (1997), Cheon et al. (2006), He et al. (2012), Nasser et al. (2014), etc. (3) Flexible loading type (see Fig. 15). The three principal stresses of this type of instrument are all applied by flexible loads, such as Smart et al. (1995), Lee et al. (1999), etc. Xie et al. (2022) also classified it as: (a) true triaxial compression under three rigid platens. (b) compression and torsion of the hollow cylinder under fluid confining pressure, and (c) triaxial compression under a biaxial solid piston and fluid confining pressure corresponds to the above rigid loading type, flexible loading type, and mixed loading type, respectively.

In the actual project, the deeply buried rock is in the static high true triaxial stress state before the disturbance,

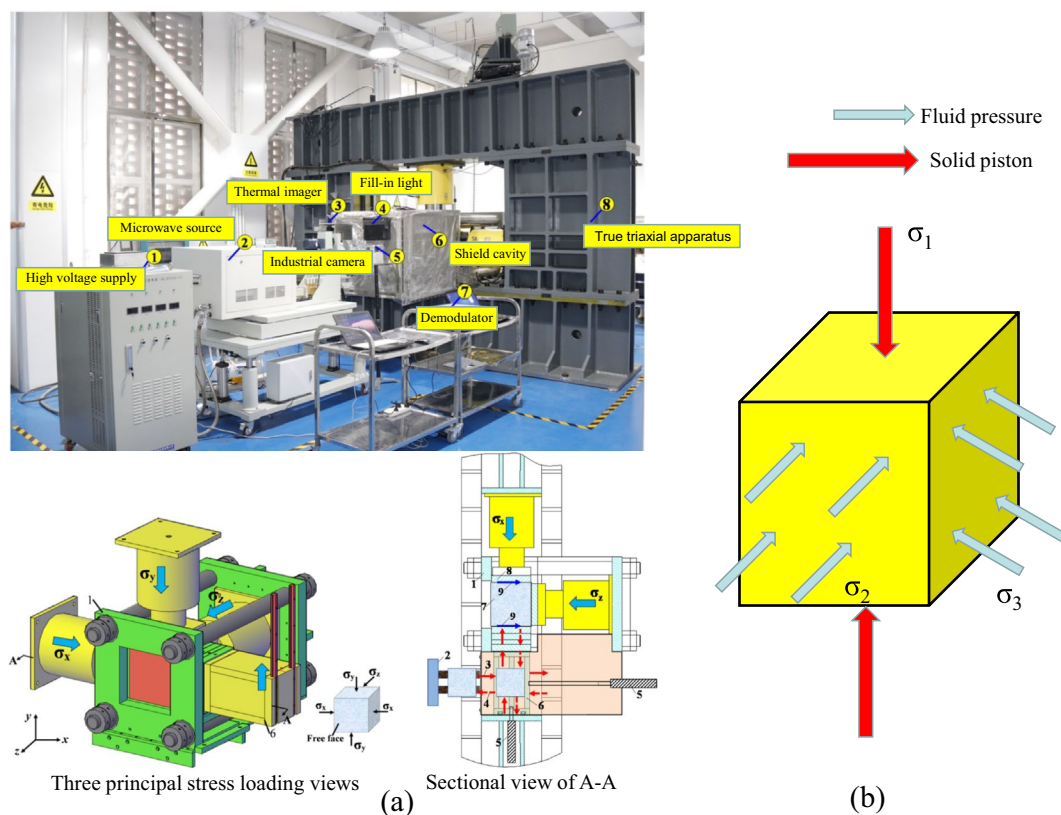


Fig. 13 Schematic diagram of a mixed loading true triaxial apparatus: **a** Actual apparatus, **b** loading method, after Feng et al. (2021)

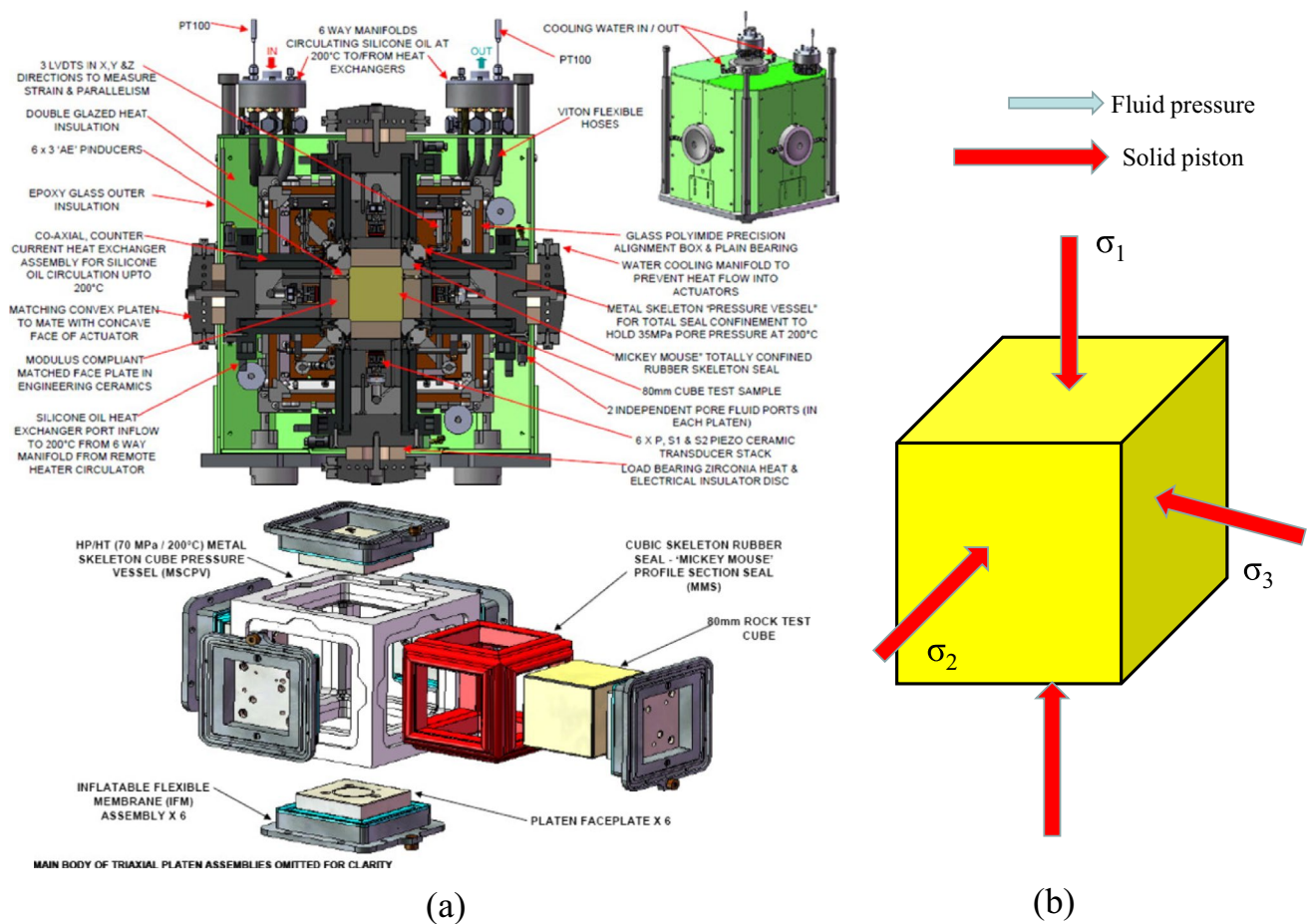


Fig. 14 Schematic diagram of a rigidly loading true triaxial testing apparatus: **a** Actual apparatus, **b** loading method, after Nasseri et al. (2014)

and the dynamic load impact will be generated after the excavation disturbance and blasting. To meet the actual engineering situation, the dynamic true triaxial perturbation instrument was developed. He et al. (2021) developed an impact rock burst test system that applies multi-directional periodic disturbance load and single-sided rapid unloading based on true triaxial loading. Li et al. (2015b) and Su et al. (2017a) have also developed high-pressure servo dynamic true triaxial experimental instruments that can realize periodic disturbance load application and single-sided rapid unloading, respectively, and studied the mechanism of rapid unloading leading to deterioration of rock mechanical properties and inducing engineering disasters such as rock burst. Feng et al. (2023) developed a true triaxial test device for low-frequency disturbance and high-speed impact of high-pressure hard rock.

The true triaxial apparatus is in the stage of rapid development, which is developing in the direction of high tonnage, high rigidity, super precision, and strong disturbance. In the future, multi-field coupling rock true triaxial apparatus can be considered to reveal rock

deformation and failure law under complex environmental conditions and promote the development of rock mechanics.

3.2 End Effect and Eccentric Loading

As shown in Fig. 16a, when the rock sample is subjected to true triaxial loading, the fixed-end constraint produces additional shear stresses, resulting in an uneven distribution of stresses in the sample (Zhang et al. 2017b). Two methods can be considered to ensure that the center position of the rock sample remains constant during compression. One method is to use four or six actuators simultaneously in a true three-axis setup to compress the specimen using a master–slave control algorithm, and the other method is to use two actuators with a moving or floating loading frame (Feng et al. 2016). The first method is costly and requires high servo precision control. The second method has a low carrying capacity. To solve the problem, Feng et al. (2016) proposed a new technique of servo-controlled free up and down floating with a combined pneumatic-hydraulic drive while retaining the second method. This method realizes

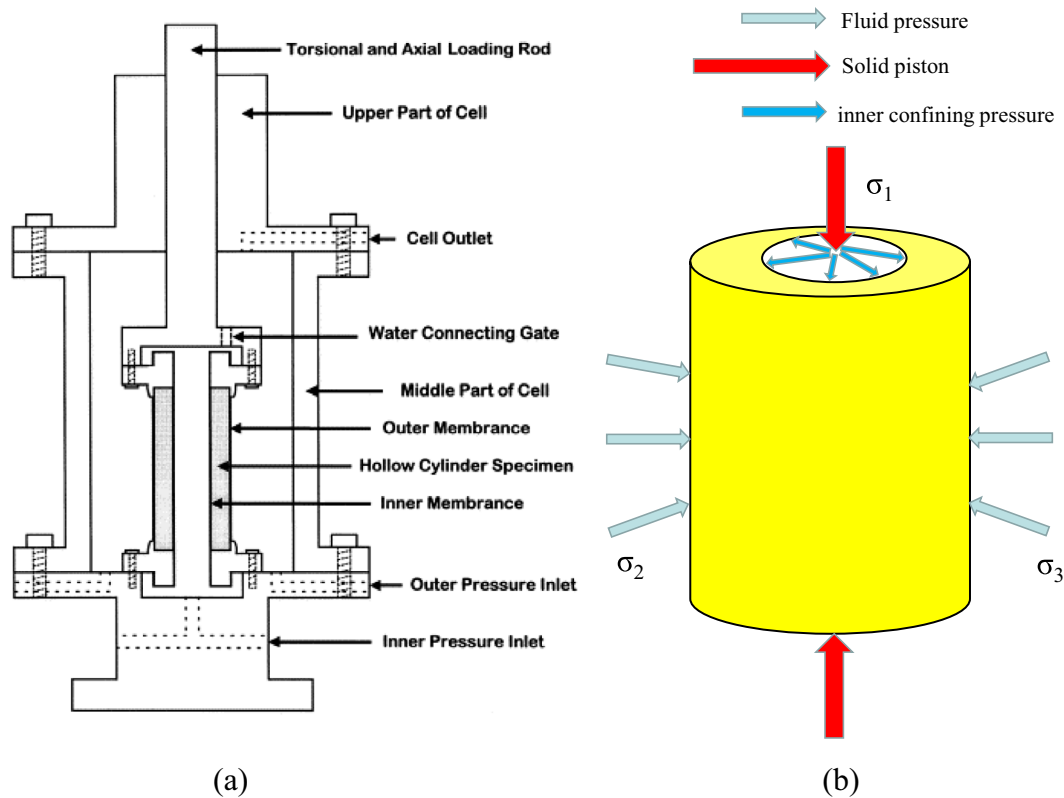


Fig. 15 Schematic diagram of a flexibly loading true triaxial apparatus: **a** Actual apparatus, **b** loading method, after Lee et al. (1999)

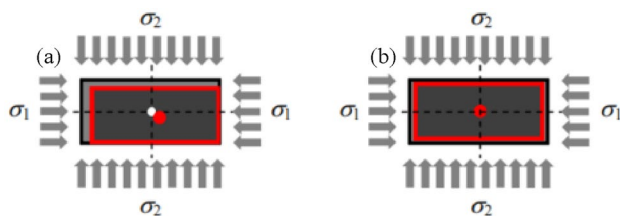


Fig. 16 Triaxial compressive stresses on specimen: **a** eccentric loading, **b** eccentric suppression technique, after Feng et al. (2016)

the free up and down movement of the vertical loading frame so that the high pressure generated by the pneumatic pressure balances the weight of the loading frame and thus realizes the concentric loading (see Fig. 16b). The end friction effect is mainly due to the friction effect between the surface of the sample and the testing machine to hinder the uniform deformation of the rock; when greater the confining pressure, the greater the axial pressure required, and the end friction effect will be more obvious (Meng et al. 2021). In rock mechanics experiments, friction reduction is usually achieved by adding cushioning material between the rock specimen surface and the testing machine. Feng et al. (2017b) conducted true triaxial tests on granite and sandstone with and without friction reducers. The

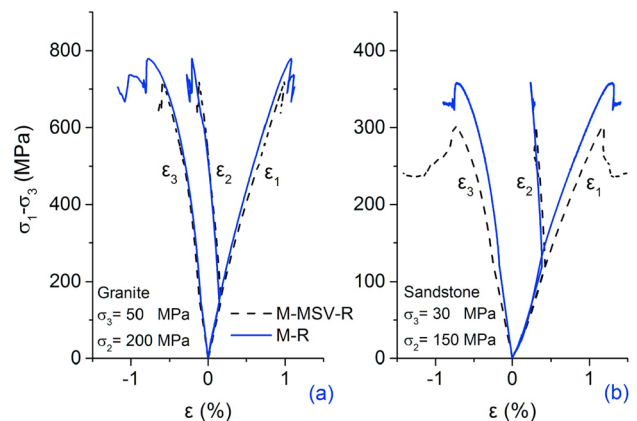


Fig. 17 Effect of friction reducer on rock strength in true triaxial test: **a** Granite, **b** Sandstone, after Feng et al. (2017b) Note: black dashed line represents use of friction reducer

experimental results showed that end friction promotes an increase in the strength of the rock, which is functionally equivalent to an improvement in the minimum principal stress (see Fig. 17). The mixture of butter, stearic acid, single-layer Teflon film, stearic acid and Vaseline has been favored by scholars because of its anti-friction effect (Haimson and Chang 2000; Lu et al. 2021b). Currently, there

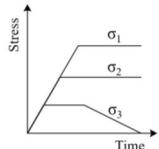
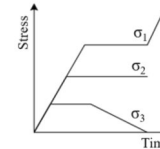
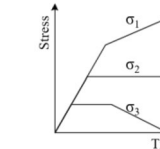
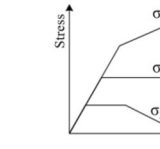
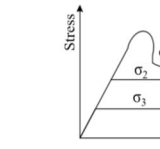
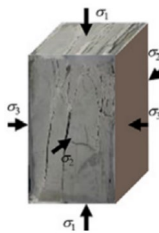
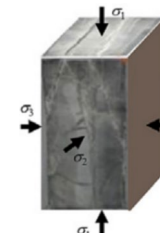
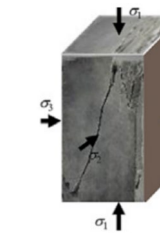
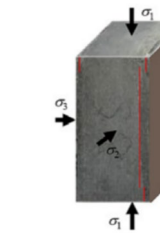

are no standards for friction reducer composition and ratios, which need to be evaluated and quantified for different materials. The end friction effect can be characterized in true triaxial experiments by minimum compressive strain rate at room temperature, high positive stress and plane friction. For this reason, Feng and Zhang et al. (2016; 2017b) proposed a multi-point strain measurement method and made a mixture (MSV) of stearic acid and Vaseline in the ratio of 1:1 as a friction reducer for true triaxial experiments with good results. In addition, Mogi believes that the friction effect can be reduced by adding metal shims between the specimen and the experimental equipment and by improving the specimen's shape. The first method is the ideal one, which can make the rock surface not produce shear stress. However, finding metal blocks identical to rock materials is difficult. The second method can be realized by increasing the height-to-diameter ratio, which will cause the rock specimen not to extend to the end when damage occurs. Therefore, this method will not affect the experiment results even if there is an end effect. Combining the characteristics of the above three methods, the measures to reduce the end effect in triaxial rock mechanics experiments can be summarized as follows: (1) select the specimen with a relatively large height and diameter, (2) try to find a gasket matching the elastic modulus of the rock material, and (3) improve the friction reducing agent.

3.3 Stress Path

The mechanical behavior of deep rock mass depends on its occurrence environment and the change of stress state. The failure mechanism of rock mass will change significantly under different stress paths. As shown in Table 1, the damage patterns of Jinping II marble under different stress

paths were demonstrated. Therefore, it is necessary to consider the loading and unloading paths to simulate the stress redistribution under three-dimensional stress states when doing true triaxial experiments on rocks (Jiang et al. 2021). Using true triaxial to simulate the stress path changes in deep mining generally consists of (1) triaxial loading, simulating the stress environment before excavation of deep rock mass mechanics; (2) unloading: stress effect caused by excavation; (3) uniaxial loading stage: used to simulate the working face to take advanced support; (4) cyclic loading–unloading: repeated loading–unloading is used to simulate the influence of unexcavated rock mass (Yuan et al. 2020). In the triaxial loading stage, it is mainly to realize the three-dimensional unequal pressure condition ($\sigma_1 > \sigma_2 > \sigma_3$). Generally speaking, the steps are: (1) hydrostatic pressure loading ($\sigma_1 = \sigma_2 = \sigma_3$); (2) biaxial loading (σ_1, σ_2 loading, σ_3 constant); (3) maximum principal stress loading (σ_1 loading, σ_2, σ_3 constant); (4) the minimum principal strain controls the maximum principal stress loading (σ_1 loading, σ_2, σ_3 constant) (Zheng et al. 2020). The accuracy of ground stress values is the first step in correctly analyzing a rock's entire deformation and fracture process. To restore the real stress environment of the rock, the most important thing at the triaxial loading stage is to determine the value of the principal stress accurately (Note: the method of determining the ground stress will describe in Sect. 6). In practical engineering, the horizontal principal stresses are different due to the different directions of the underground cavern arrangement (Gong et al. 2018). Therefore, it is necessary to design a multi-group experimental program by considering the vertical stress as a constant and adjusting the combination of the maximum and minimum horizontal principal stress (Gong et al. 2019). The unloading perturbation effect is a research hotspot in rock mechanics,

Table 1 Failure modes of CJPL-II marble under true triaxial loading and unloading paths, after Feng et al. (2022)

Item	True triaxial compression and unloading		True triaxial compression		
	I	II	III	IV	V
Stress path					
Failure mode					

and many experimental studies have been carried out on the unloading effect of excavated rock bodies in deep-buried engineering. For example, He et al. (2007) carried out an experimental study of the rock burst process in deep, highly stressed granite through unloading, which showed that rapid unloading of stress in one direction would lead to the occurrence of rock bursts. Based on the unloading rate, unloading can be divided into quasi-static unloading and intensive unloading. Quasi-static unloading refers to the process of unloading in limited equilibrium at all times; strong unloading is mainly used to study the effect of dynamic loads such as blasting (Frenelus et al. 2021; Xie et al. 2022). Different stress paths are selected to carry out the unloading tests based on the various processes of stress change induced by the engineering excavation. For underground chamber excavation, the increase of tangential stress in the surrounding rock is generally simulated by σ_1 loading path, and then the decrease of radial stress in the rock near the free surface of the chamber is simulated by σ_3 unloading at one face (Jiang et al. 2021). The unloading process corresponding to the remaining works is shown in Table 2. The biggest problem in the previous research for the unloading experiment is that it needs to remove the coupling control role of the initial damage degree and the unloading path. The controlling role of the unloading path in the experiment is masked by the initial damage degree, and the conclusion obtained may be unreliable. The triaxial test can only approximately simulate the simple change process of the stress change trend and the engineering rock mass's initial to final stress state, which usually simplifies the stress path. The simplification of the stress path often depends on the scholars' understanding of the trend of stress change and the stress state, as well as the convenience of experimental control.

3.4 Similar Experiments

Traditional true triaxial tests are often based on rock samples to study their physico-mechanical properties and microscopic damage mechanisms. To reveal the damage mechanism of deep rock works in a macroscopic way, existing underground engineering projects (prototypes) are often downsize based

on the similarity principle in the laboratory to simulate the mechanical behavior of rocks during the entire process of an underground engineering construction. Therefore, similar experiments are also called physical experiments or large-scale geomechanical experiments. The similar experiment overcomes the shortcomings of using only small samples and restores underground engineering to make it more convenient and intuitive to reveal the failure mechanism of rock during excavation, which has become one of the main research methods (Sun et al. 2018b; Wu et al. 2023; Zhu et al. 2019). Due to its features, many scholars have studied the damage mechanism of surrounding rock under different engineering geological conditions through similar experiments. For example, Lee and Schubert (2008) studied the stability of the palm face of tunnel excavation through small-scale model tests. He et al. (2009) studied the damage mechanism of the roadway in the inclined layered rock body of a deep coal mine through a physical model test combined with an infrared camera. Lin et al. (2015) studied the damage behavior of large underground caverns built in the Jinping second-level hydropower station and analyzed the causes of the damage. Li et al. (2021) conducted large-scale experiments on continuous arch tunnels with different burial depths and elucidated their damage mechanisms.

Similarity principle underlies the relationship between models and prototypes in similarity experiments (Lu et al. 2021a). Similarity principle can be described as qualitative and quantitative. The first theorem of the similarity principle states that if all the instantaneous physical quantities of the prototype and the model are proportional, the two systems (phenomena) are similar. The second theorem of the similarity principle states that if the phenomena of the two systems are similar, the relation between different parameters used to describe similar phenomena can be transformed into a functional relation between similar principle (Yang et al. 2019a). According to the connotation of the similarity principle, when conducting simulated deep mining similarity experiments, the following aspects should be considered:

Geometric conditions: The models are scaled to a certain ratio to ensure similarity in shape. For parts that cannot be strictly similar due to environmental factors, it should be

Table 2 Engineering items corresponding to different unloading paths for rocks

Number	Rock force diagram	Initial stress	Unloading process	Type of project
1		$\sigma_1 > \sigma_2 > \sigma_3$	Unload σ_3 , constant σ_1 and σ_2	slope foundation
2			Unload first σ_3 , after unload σ_2 , constant σ_1	open pit
3			Unload first σ_3 , constant σ_2 , increase σ_1	separate lanes
4			Unload first σ_3 , increase σ_1 , after unload σ_2	roadway

ensured that they have similar physical properties (Wu et al. 2023).

(2) Parameter conditions: The following parameter relationships should be satisfied Eq. (1) between the simulated material and the prototype (Zhu et al. 2019):

$$C_i = \frac{i^p}{i^m}, \tag{1}$$

where p is prototype, m is model, C is similarity constant.

As the centrifuge is not the source of gravity in similar experiments, the following relationship should also be satisfied the Eq. (2):

$$\frac{C_\sigma}{C_L C_\gamma} = 1, \frac{C_\sigma}{C_\epsilon C_E} = 1, \frac{C_\delta}{C_\epsilon C_L} = 1, \tag{2}$$

where i is physico-mechanical parameter, include stress (σ), modulus of elasticity (E), cohesion (c), angle of internal friction (φ), strain (ϵ), length (L), gravity (γ), and displacement (δ).

Finally, the similarity ratio must be 1 for dimensionless parameters and equal for parameters of the same magnitude (Yang et al. 2019a):

$$C_\sigma = C_E = C_c, \tag{3}$$

$$C_\sigma = C_E = C_u = 1. \tag{4}$$

(3) Boundary and initial conditions: Since deep engineering take place in a complex stress environment, initial ground stress simulation and boundary fixation are required.

When doing similar experiments, the production of rock models must be involved. Currently, fruitful results have been achieved in modeling rocks using different materials, and some typical modeling materials and their ratios are given as shown in Table 3. It is worth noting that it is a great challenge to simulate rocks with high brittleness, high bulk density, high strength, brittle-ductile transition, and other characteristics of deep rocks. Previous researchers have often controlled the brittleness and strength of simulated materials by gelling, but this does not fully reveal the nature of deep

rocks. Therefore, Zhu et al. (2019) proposed a new method to control the properties of simulated materials based on aggregate and developed a new simulated material similar to marble by controlling the aggregate and grain size type, which improved the similarity relation of deep hard rock. The deep hard rock should satisfy the Eq. (5) in addition to the similarity relationship:

$$C_b = C_{bd} = C_d = 1, \tag{5}$$

where b is brittleness, bd is brittle ductile transition, d is ductile.

The degree of similarity between the model and the field prototype determines the reliability of the experiment. However, the mechanical theory of deep rock isn't perfect, which leads to some lack of similarity with the theory of deep hard rock, and it's not easy to simulate some mechanical phenomena. Therefore, to reveal the destruction mechanism of deep mining rocks, firstly, we should do a lot of true triaxial experiments on deep rocks to study their physical and mechanical properties and micro destruction mechanisms to improve the mechanical theory of deep rocks. Secondly, materials consistent with rock mechanical properties and micro-fractures are made and applied to similar experiments so that micro-fractures are associated with macro-fractures. In addition, the model of similar experiments can be made with the help of 3D printing technology to construct a large-scale physical model of the roadway containing weak surfaces and defects that are consistent with the field engineering so that the indoor model specimen can be more realistically restored to the actual field engineering.

3.5 Identification of Crack Initiating Stresses

The complete stress–strain curve can analyze almost all mechanical behaviors of rocks (shear expansion, strain softening, plastic flow, etc.), which effectively reveals the strength and deformation characteristics of rocks (Cai et al. 2023; Chen et al. 2021). According to the classical complete stress–strain curve of rock, it is known that

Table 3 Some typical modeling materials and their ratios

Number	Rock type	Simulated materials and ratios	Bonding material or method	Reference
1	Granite	Iron powder, barite powder, and silica sand (1:1:0.5)	Rosin cementation	(Zhang et al. 2021a)
2	Clay rock	River sand, cement, and gypsum (8:1.4:0.6)	Cement and gypsum cementation	(Lu et al. 2021a)
3	Fine sandstone	River sand, cement, and gypsum (6:1.2:2.8)		
4	Silty sandstone	Rosin, paraffin, and river sand (3:0.8:100)	Rosin and paraffin cementation	(Yang et al. 2019a)
5	Coal rock	Gypsum and water (1.2:1)	Physical finite element plate	(He et al. 2010b)
6	Limestone	Gypsum and water (0.8:1)		
7	Mudstone	River sand, lime and gypsum (12:1:1)	Lime and gypsum cementation	(Sun et al. 2018b)

the rock undergoes crack closure, elastic deformation, crack extension, post-peak deformation, and residual deformation stages from loading to destruction (Brace et al. 1966; Eberhardt et al. 1998; Lajtai 1974). Important stress threshold points such as crack closure stress, crack initiation stress (CI), damage stress (CD), peak strength, and residual strength are included in these phases (Wen et al. 2018). It is obvious that CI is a vital node in studying the rock fracture mechanism. It is worth noting that a high-stiffness testing machine should be used to obtain the complete stress threshold point. If the stiffness of the testing machine is less than the stiffness of the rock, it will result in the strain energy of the testing machine being less than the strain energy stored in the specimen during loading. The pressure exerted by the testing machine will exceed the resistance of the specimen. Thus, the strain energy of the testing machine will be released suddenly during the loading process, resulting in the sudden destruction of the specimen and the failure of the complete stress–strain curve.

Some researchers have argued that the determination of CI is helpful in evaluating the brittleness of rocks, establishing a rock strength criterion (parameter m_i for uniaxial compressive strength in the Hoke–Brown strength criterion) (Cai 2010; Wang et al. 2014). However, it is difficult to determine the value of CI objectively. To be able to accurately determine the crack initiation stress, a large number of scholars have done extensive research and proposed a series of methods, such as the volumetric strain method (VSM), the lateral strain method (LSM), the instantaneous Poisson's ratio method (IPRM), the axial stiffness method (ASM), the crack volumetric strain method (CVSM), the lateral strain response method (LSR), the cumulative acoustic emission hitting tangent method, the relative compressive strain method (RCSR), etc. (Li et al. 2023b). Brace et al. (1966) used the volume-strain of rocks to identify the initiation stress in rocks. VSM considers the stress–volume curve to be linear until the rock reaches CI, and when the stress–volume curve deviates from the linear state, it is considered to be the onset of the initiation stress (see Fig. 18a). It is worth noting that the lateral strain of rocks is more sensitive than the axial strain. Taking this into account, Lajtai (1974) proposed the LSM, which is similar to the VSM in that the CI can be determined from the point at which the lateral stress–strain curve deviates from the linear trajectory (see Fig. 18b). Compared to VSM, LSM is simple, intuitive and accurate (Wen et al. 2018). Diederichs (2007) proposed the IPRM and the method identifies points where the curve deviates from the linear region as CI using a plot of axial stress versus Poisson's ratio (see Fig. 18d). ASM was proposed by Gao et al. (2018), who consider the onset of the deviation from the horizontal region on the axial stiffness versus the axial strain curve as the crack initiation stress point. The four methods mentioned above all determine

the CI by determining the points on the stress–strain curve that deviate from the linear trajectory. While all of these methods are highly feasible, they are heavily subjective. Second, Martin and Chandler (1994) argues that the linear trajectories referred to in the above approach do not occur when there are many joints in the rock mass. With this in mind, Martin proposed CVSM to identify CI (see Fig. 18g). This method considers that the rock fractures when the fracture volume strain deviates from 0 and continues to decrease. The calculation of the fracture volume strain is determined by Eq. (6) (Li et al. 2023c):

$$\varepsilon_{vCracks} = \varepsilon_v - \varepsilon_{vElastic}, \quad (6)$$

where $\varepsilon_{vCracks}$ is the volume of fracture, ε_v is volumetric strain, $\varepsilon_{vElastic}$ is the elastic bulk strain. The elastic bulk strain is determined by Eq. (7):

$$\varepsilon_{vElastic} = (1 - 2\mu)\sigma_1/E_s, \quad (7)$$

where μ Poisson's ratio, E_s is the modulus of elasticity. CVSM is more accurate and objective than the previous methods. However, CVSM strongly depends on elastic modulus values and Poisson's ratio. When the rock itself has defects, the elastic modulus and Poisson's ratio are uncertain, which in turn affects the judgment of CI accuracy. Later, Nicksiar and Martin (2012) proposed LSR, which follows the idea of LSM, with the most significant change being that it allows the rock to produce only one maximum lateral strain difference, eliminating subjectivity. As shown in Fig. 18f, the LSR method first establishes a reference line by connecting the stress origin point with the unstable crack growth point. Subsequently, by calculating the distance ΔLSR between the lateral stress–strain curve and the reference line, the stress corresponding to the maximum ΔLSR is identified as the CI. However, the prerequisite for applying LSR is the accurate determination of the unstable crack growth point, as different unstable crack growth point can lead to significant errors in determining the CI. And, the physical significance of LSR is unclear, and it is impossible to prove that the difference in maximum lateral strains corresponds to the cracking stress. To overcome some of the shortcomings of the above methods, Wen et al. (2018) proposed RCSR, which takes the lateral strain corresponding to the lateral displacement as the initial deformation point, reflecting the change of the rock deformation state from compression to fracture and determines the initiating stress by the maximum strain difference (see Fig. 18e). In contrast to LSR, RCSR gives a specific physical meaning of the maximum strain difference, i.e., new microcrack generation. Considering that elastic waves are generated internally during rock fracture, Zhao et al. (2013) monitored the CI by acoustic emission techniques. CI is defined as the point at which the cumulative acoustic emission hits deviate

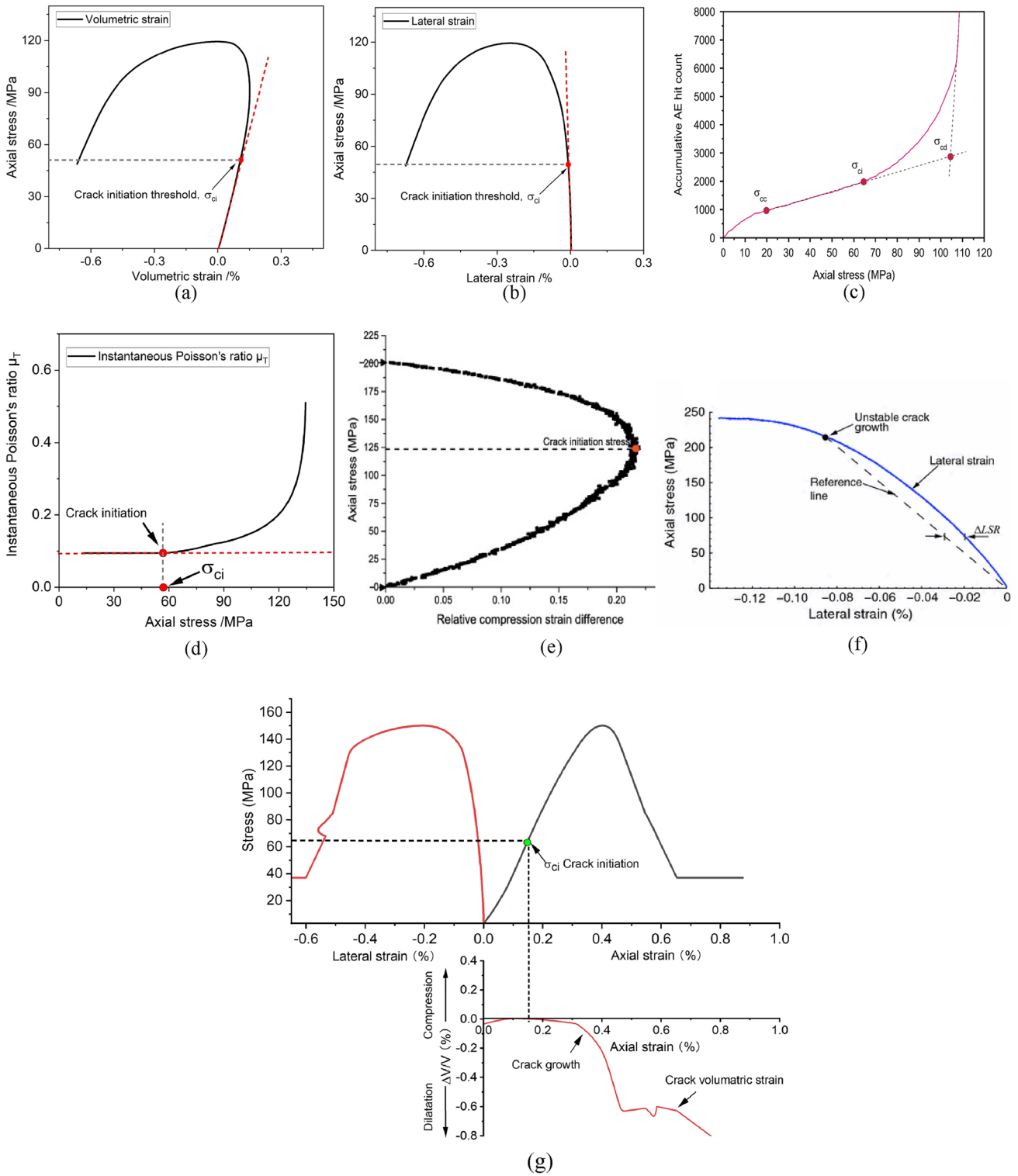


Fig. 18 Schematic diagram of the method for identifying cracking stresses: **a** VSM, **b** LSM, **c** AE, **d** IPRM, **e** RCSR, **f** LSR, **g** CVSM, after Li et al. (2023b), Nicksiar and Martin (2012), Wen et al. (2018)

from the tangent line (see Fig. 18c). The method takes into account the point at which the cumulative number of impacts deviates from linear growth as the acoustic emission impact

rate increases as CI. Moreover, the method relies on curves with a S-shaped feature when determining CI, but not all

rocks can satisfy this feature, and it is not universal (Feng et al. 2017b).

Most of the methods based on stress–strain curves to recognize rock initial cracking stresses are based on uniaxial or conventional triaxial experiments, and the validity of these methods has yet to be verified under true triaxial conditions. Although the acoustic emission-based identification method is not restricted by the experimental method, the application range of this method is limited, and its accuracy needs to be improved. Therefore, it is necessary to establish a universal method to recognize the crack initiation stress in rocks.

3.6 Characterization Methods

With the rapid development of true triaxial experimental technology, researchers are no longer limited to summarizing and describing rock damage phenomena and patterns but have begun to explore the fracture mechanisms of rock in depth. In rock mechanics experiments, strain gauges and displacement gauges are commonly used to record data on rock deformation and fracture (Liu et al. 2020). The data measured by these tools reflect the average stress and total deformation within the rock. However, rocks often exhibit anisotropy, and their stress–strain distribution is uneven, making it difficult for traditional measurement methods to characterize the deformation and fracture processes of rocks accurately. Additionally, the interior of the rock is like a "black box," making it difficult to obtain information about its internal damage state through direct measurement methods. Notably, strain energy is released through acoustic, thermal signals when external forces damage rocks. Therefore, physical signals can be utilized to infer the damage state of rocks, for instance: acoustic emission (AE), infrared radiation (IR). Additionally, image acquisition processing techniques can be used to characterize the damage of rocks in triaxial tests, such as scanning electron microscopy (SEM), and computed tomography (CT).

3.6.1 AE

AE is defined as the generation of transient elastic wave energy pulses from the rapid release of elastic properties during crack expansion or deformation within a material. At present, AE has been applied in various rock mechanics experiments such as uniaxial compression, triaxial tests, cyclic loading experiments, multi-field coupling (Kong et al. 2016; Ting et al. 2012; Yang et al. 2014; Zhou et al. 2019). In early AE experiments on rocks, the main focus was on studying the similarities between AE activities and microseismic (MS) activities (Mogi 1962). MS activities are induced by rock fracturing at engineering scales, and MS monitoring can be used to address various rock engineering problems (MS monitoring techniques will be systematically introduced in Sect. 6). Compared to MS, AE is an effective method for detecting the initiation and propagation of microcracks before macroscopic fracture occurs. As shown in Fig. 19, AE sensors are placed on rock samples in laboratory tests. When deformation, crack expansion, or other stress-releasing phenomena occur within the rock, a high-frequency elastic wave signal is generated, known as an AE phenomenon. This process is also called the occurrence of AE event. Therefore, analyzing AE events can reveal the deformation and fracture process of rocks. Jia et al. (2020) used AE to reveal the damage mechanism of deeply buried coal rocks. The study concluded that the AE events are mainly caused by the generation of new cracks and the expansion of primary cracks. A large number of primary cracks lead to fragmented deep coal structures, inducing a large number of plastic slip events along the preexisting microcracks and the destruction of rock structures.

The main principle of AE is based on the Kaiser effect, which utilizes spatial localization to analyze the internal damage state of rocks. Therefore, the localization of AE events is the key for studying the rock fracturing process (Zhao et al. 2006). Currently, the methods for AE

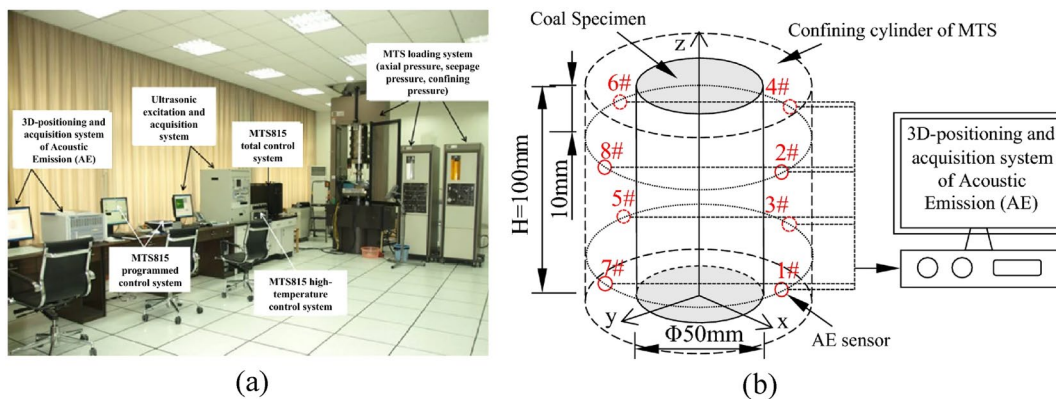


Fig. 19 AE System in a Laboratory: **a** Console, **b** AE Sensor Arrangement, after Jia et al. (2020)

localization mainly include the Geiger localization method, the simplex method, the relative localization techniques, and the generalized least squares method (Shi et al. 2022b). Although there are many methods for acoustic emission localization, a consensus on the optimal localization method has not yet been reached, and the accuracy of localization still needs to be improved. The number of AE sensors also directly affects the accuracy of the research. In true triaxial experiments, due to spatial constraints, it is not easy to install sensors on the surface of rocks, making it challenging to meet the requirements for the accuracy of AE event localization. In addition, the loading path and loading rate also affect the localization results of AE events. For example, the faster of the loading rate, the fewer AE events are received. Displacement-controlled loading is better to get accurate localization of AE events compared to force-controlled loading methods (Xu et al. 2008). The above mentioned are external factors that affect the localization of AE events. In fact, microcracks inside the rock also affect the localization effect of AE. This is because the defects inside the rock cause the elastic waves generated by acoustic emission to be refracted and reflected inside the rock. This is because defects within the rock cause the elastic waves generated by acoustic emission to be refracted and reflected within the rock.

Considering the multiple factors that affect the localization of acoustic emission events, the ratio of signal rise time (RA) to average frequency (AF) method (RA-AF method) was emerged (Dong et al. 2020; Ohno and Ohtsu 2010). RA-AF does not require localization of AE signals and has no requirement for the number of sensors. Therefore, many researchers have used RA-AF to study the fracture mechanism of rocks. Kong et al. (2021) used the RA-AF method to accurately identify the type of fracture in andesite rock, where rock fracture is dominated by tensile fractures in the previous loading period, and the number of shear fractures rises rapidly when the load exceeds the yield strength. Bi et al. (2024) determined the boundaries of tensile fracture and shear crack generation in the tested rocks based on RA-AF data from rock uniaxial compression experiments (UCS) and Brazilian splitting experiments (BTS) combined with the KDE algorithm. Du et al. (2024) performed compression and tension experiments on four types of rocks and analyzed the transition trends of rock crack types based on RA-AF data. Although RA-AF is simple and easy to use, the discriminatory criteria for shearing and tensile are not uniform and subjective. Although RA-AF is simple and easy to use, the criteria for distinguishing shear fracture and tensile fracture are not consistent, leading to subjectivity (Li et al. 2022).

It is worth noting that AE is not only applicable at the laboratory scale but also for field monitoring. The suitability of AE for field monitoring will be discussed in Sect. 6.

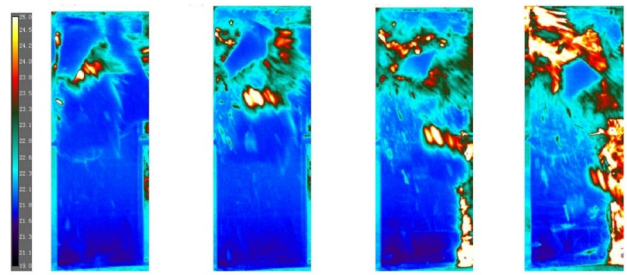


Fig. 20 Infrared thermal image of rock crack extension, after Sun et al. (2018a)

3.6.2 IR

During the fracturing process of rocks, phenomena such as friction and crack formation occur. The elastic energy accumulated during these processes can convert into thermal energy, leading to localized temperature increases. The changes in rock temperature will excite infrared electromagnetic waves (Liu et al. 2023c). Infrared thermal imaging devices can capture the infrared radiation emitted from the surface of the object and convert it into visual temperature images. As shown in Fig. 20, the localized temperature increase during rock fracture can be detected by an infrared imager and a temperature distribution map can be generated. Therefore, the fracture of rocks can be characterized using IR (Sun et al. 2017b; Wang et al. 2016a). In rock mechanics experiments, the infrared radiation temperature increment ΔT , can be explained qualitatively by the following Eq. (8) (Wu and Wang 1998):

$$\Delta T = \Delta T_1 + \Delta T_2 + \Delta T_3, \quad (8)$$

where ΔT_1 is infrared radiation temperature increment caused by the thermal-elastic effect (The value can be positive or negative), ΔT_2 is caused by the initial fissures, joints and newly produced fractures of rocks (The value is negative), ΔT_3 is caused by the friction (The value is positive). And, ΔT_1 can be determined by Eq. (9) (Wu et al. 2006):

$$\Delta T_1 = \gamma \beta^{-1} T \Delta(\sigma_1 + \sigma_2 + \sigma_3), \quad (9)$$

where γ is a transfer factor, β is a constant correction factor, T is the physical temperature of rock, $\Delta(\sigma_1 + \sigma_2)$ is the change of the rock's principal stress (If $\Delta(\sigma_1 + \sigma_2) > 0$. ΔT_1 is positive and vice versa (Sun et al. 2018a). IR can quantitatively monitor the entire rock fracture process without touching the rock specimen, which helps researchers to observe the initiation and propagation of cracks in real time (Lou and He 2018).

It is worth noting that during the process of rock fracture, the variation in infrared temperature is very small, and the

original temperature information of IR is easily obscured by noise signals (Gao et al. 2023). Meanwhile, there is significant discrete in the quantitative indicators (average infrared radiation temperature, AIRT) used to characterize the IR features of rocks under load in different studies (Sun et al. 2017a). This is largely attributed to the influence of noise on the IR information during the experimental process (He et al. 2010a). The impact of noise often makes experimental conclusions unreliable, making it difficult to accurately assess the rock fracture process (Shi et al. 2022a). Therefore, reducing infrared radiation noise during experiments is particularly crucial. During the experimental process, noise mainly originates from experimental operations and the experimental environment. To mitigate experimental operational noise, it is imperative to maintain closed doors and windows throughout the experimental process, prohibiting personnel movement, and employing high-precision infrared observation equipment (Sun et al. 2018a). Currently, two main methods are used to reduce

background noise in experimental environments: median filtering noise reduction method (Gong et al. 2013) and reference sample noise reduction method (Sun et al. 2022b). The median filtering noise reduction method can enhance the clarity of infrared images; however, it remains ineffective in eliminating noise values from the AIRT curve. The principle of the reference sample noise reduction method is to place a reference rock sample next to the experimental rock sample, and subtract the AIRT value of the reference rock sample from the AIRT value of the experimental rock sample to eliminate the influence of environmental noise. This method effectively improves the signal-to-noise ratio. The method requires that the change trend of the AIRT curve between the experimental rock sample and the reference rock sample remain consistent.

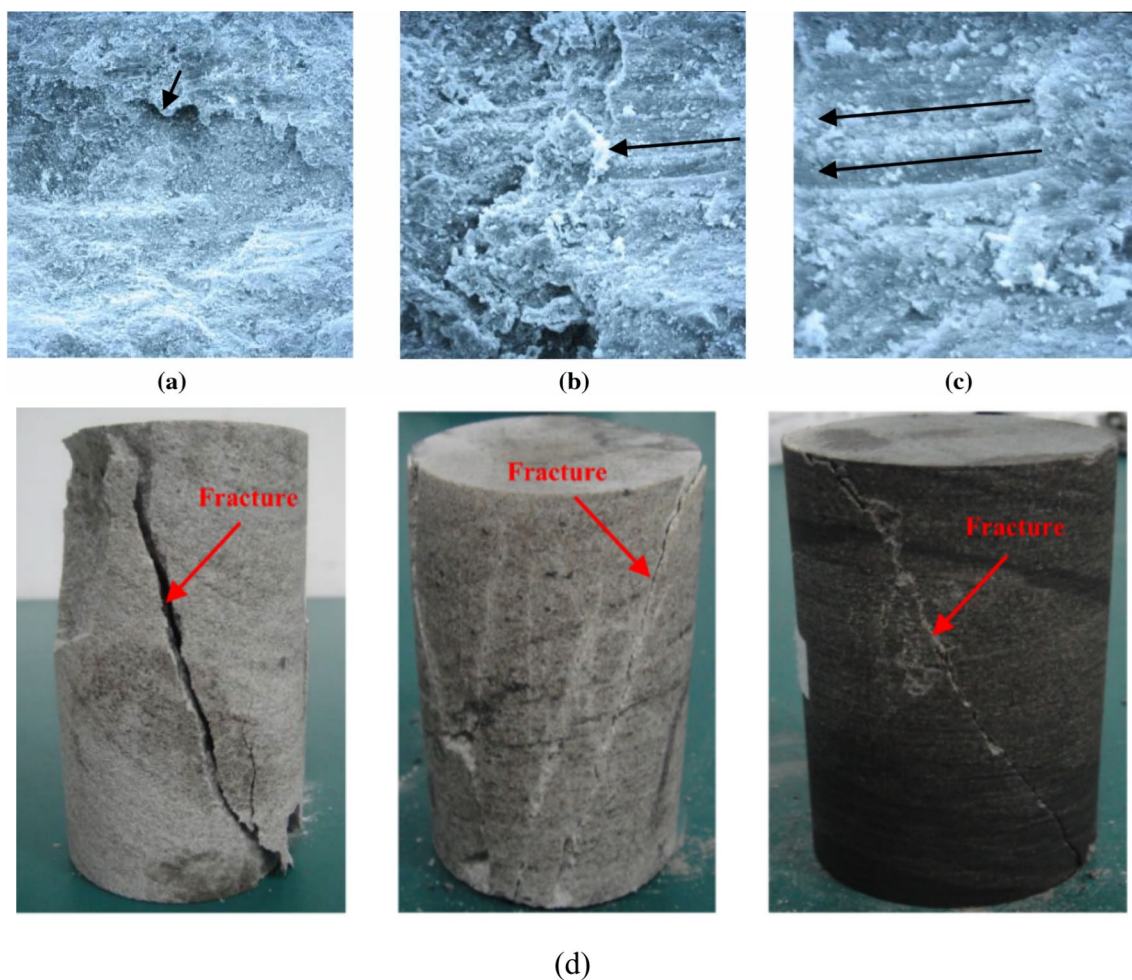


Fig. 21 Micro-damage and macro-damage of sandstone under true triaxial compression: **a** SEM100x, **b** SEM500x, **c** SEM1000x, **d** Macro-damage, after Zhang et al. (2019a)

3.6.3 SEM

The microscopic fracture characteristics of rocks are the most direct reflection of the fracture mechanism. SEM can observe changes in the microstructure of rocks, thereby qualitatively revealing the rock fracture mechanism from a microscopic perspective (Tao et al. 2020). SEM analyzes rock fracture based on scanned rock surface images. Since the introduction of SEM in rock mechanics, which has played a significant role in studying rock fracture mechanism. Zhang et al. (2019a) investigated the fracture mechanism of sandstone under triaxial conditions. The study indicates that the primary reason for the reduction in rock strength is the formation of microcracks on the fracture surfaces of highly hydrophilic clastic sandstone during shear. The fracture mechanism is mainly due to shear slip in the direction of the maximum shear stress in the rock (see Fig. 21). SEM focuses on the destruction and changes in rock crystals when analyzing microscopic fractures in rocks. From a microscopic point of view, rock fracture can be categorized into along-crystal fracture and through-crystal fracture. In triaxial experiments, rocks typically exhibit through-crystal fracture due to severe friction between crystals. The microscopic fracture characteristics can only qualitatively reflect local fracture mechanisms, and cannot quantitatively depict the mechanisms of fracture surfaces on a macroscopic scale (Li et al. 2022). To make SEM more powerful in rock mechanics, it is necessary to establish a connection between microscopic fracture and macroscopic fracture in rocks. Liu et al. (2022) suggested that measuring a sufficient amount of data and conducting statistical analysis can establish a connection between microscopic damage characteristics and macroscopic fracture characteristics.

3.6.4 CT

CT is a non-destructive testing technique, which is a significant achievement stemming from the collaboration between physics and computer science. The development of CT technology can be traced back to the early 1970s and was first used for biomedical imaging. In 1972, British

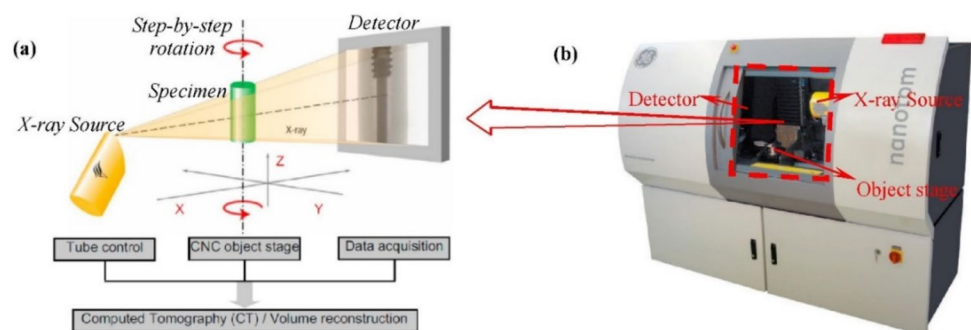
engineer Hounsfield (Hounsfield 1973) invented the first CT scanner, revolutionizing the field of medical imaging. CT technique maintains the integrity of the sample and can be used for subsequent evaluation (Košek et al. 2024). As rock damage processes make it difficult to accurately observe internal structures and describe fracture processes, CT technology has gradually found applications in the field of rock mechanics (Duan et al. 2020). CT technology can achieve high-resolution acquisition of information about various materials through computer image reconstruction. When X-rays penetrate substances, their intensity decays exponentially. The density of a material affects the degree of X-ray attenuation, manifested specifically as the attenuation coefficient of the object under measurement. The light intensity of the X-rays as they penetrate the detected object follows Beer's theorem as shown in Eq. (10) (McCullough 1975):

$$I' = I_0 \exp \mu(x), \quad (10)$$

where I_0 is the incident intensity of the X-ray, and I is the transmitted intensity after it traverses a thickness (x) of material characterized by a linear attenuation coefficient $\mu(x)$ (Wang and Miller 2020).

Over the past 20 years, many researchers have utilized CT image reconstruction technology to study the mesoscopic fracture characteristics of rock specimens, greatly advancing the application of CT technology in rock fracture analysis. Duan et al. (2022) and Feng et al. (2004) used in situ CT to study the mechanical properties and microstructural evolution of rock samples under uniaxial and triaxial compression conditions. These studies can capture information on the internal damage during loading processes. However, due to the limited resolution of CT apparatus, the images cannot provide detailed damage or microcracks. Micro-CT technology can generate smaller focal spots and has higher resolution, providing a new method for detailed exploration of the internal damage processes of rocks. Commonly used tomography systems can be roughly classified as conventional milli-CT (focal spot sizes larger than 0.1 mm), micro-CT (spot sizes down to one

Fig. 22 Illustration of high-resolution micro-CT: **a** micro-CT scanning principle, **b** micro-CT scanning machine, after Yang et al. (2019c)



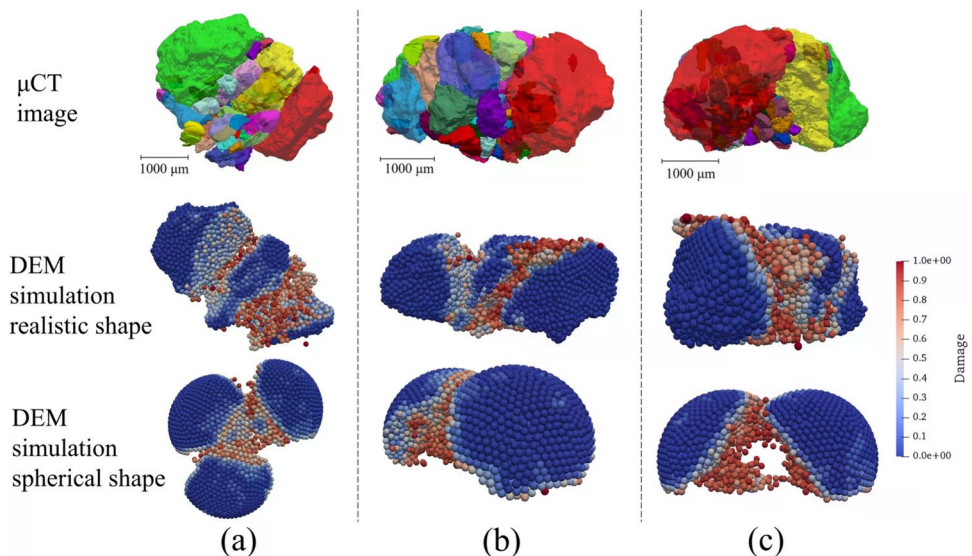
micrometers) and nano-CT (spot size down to 0.4 microns), based on spatial resolution (Wang and Miller 2020). As shown in Fig. 22, a typical micro-CT system usually consists of a high-intensity X-ray source, a detector, a sample stage, and a rotation device. The X-ray source passes through the rock, and the detector receives the X-rays that pass through the rock, converting them into electrical signals to generate 2D projection images. By rotating the sample, multiple 2D projection images from different angles can be obtained. These 2D images are reconstructed into 3D images using CT reconstruction algorithms, ultimately revealing the microstructure inside the rock (Yang et al. 2019c). The process of CT reconstructing rock images is essentially the digitalization of rock cores, also referred to as digital core reconstruction. The high-resolution 3D image reconstruction capability of micro-CT provides crucial support for digital rock physics research. Zhu et al. (2018) and Kong et al. (2019) utilized micro-CT to study the behavior of crack propagation and microstructural evolution of rocks under external forces, and further analyzed by printing 3D rock specimens with 3D imaging information. As shown in Fig. 23, Zhao et al. (2024) generated realistic-shaped particles with internal defects based on micro-CT images for investigating the effect of granite morphology on micro-damage behavior. Yang et al. (2023) utilized micro-CT and digital image processing techniques to establish three-dimensional non-uniform numerical models reflecting the fine-scale structure of rock masses for investigating the fracture mechanisms of pre-existing fractures in shale. These studies demonstrate that digital core reconstruction combined with 3D printing technology and numerical simulations, enables precise investigation of the evolution of crack propagation in rocks at both micro and macro scales. It has become an important method in the study of macro

and micro mechanics of rocks. Currently, micro-CT and in-situ micro-CT are mainly applied in uniaxial compression tests and small-scale triaxial compression tests, but their application in large-scale true triaxial experiments has not been reported. This is mainly because micro-CT equipment cannot accommodate large-scale true triaxial instruments. It is worth noting that the quality (resolution) of CT images determines the accuracy of digital core reconstruction work. The image resolution is influenced by various factors such as voxel size, field of view, and signal-to-noise ratio. Zhao et al. (2023) suggest that image resolution of micro-CT can be artificially enhanced using super-resolution algorithms to obtain higher resolution images.

In addition to the aforementioned characterization methods, electromagnetic radiation techniques (Wei et al. 2020), three-dimensional morphology of rock fracture surfaces (Li et al. 2016b), fractal theory (Ding et al. 2021), and digital image techniques (Aliabadian et al. 2019) have been widely used to characterize rock fractures. Unfortunately, these methods are less frequently used in true triaxial experiments.

SEM and AE can characterize rock fractures from two-dimensional images and interpret the process of cracks initiation and propagation of cracks in the rock surface. However, in reality, cracks are distributed non-uniformly within the rock in 3D space. 2D characterization methods can only describe the crack distribution on a specific 2D plane within the 3D space. Therefore, 2D characterization methods have technical limitations in comprehensively characterizing crack distribution under true triaxial conditions. In contrast, the 3D characterization capabilities of AE and CT can more accurately reveal the initiation and propagation processes of internal cracks throughout the rock, providing a basis for studying rock fracture mechanisms.

Fig. 23 Final failure patterns of particles in micro-CT tests and DEM simulations: **a** top view, **b** front view, **c** side view, after Zhao et al. (2024)



However, AE and CT also have drawbacks. CT is difficult to apply in large-scale true triaxial experiments, mainly because it cannot accommodate large-scale true triaxial apparatus within CT machines. During experiments, microscopic fractures within the rock are not visible, and AE results cannot directly correlate with microscopic fractures. Considering the distinctive features of different characterization methods, combining various methods can be achieved to accurately quantitatively analyze the fracture mechanisms of rocks under true triaxial conditions. For instance, integrating AE with CT and utilizing CT to establish the correlation between AE and microscopic fractures can facilitate linking AE with microscopic fractures, thereby enabling a quantitative characterization of micro–macro fractures in rocks. Additionally, novel experimental methods can be designed, such as fabricating transparent rock specimens according to similarity principle. Conducting experiments with transparent rocks can address the challenge of "difficulty in observing internal fracture," enabling comprehensive three-dimensional observations of the exterior and interior of rock specimens.

4 Theoretical Analysis

Theoretical analysis is the basic method to analyze the deformation and fracture of rock using the constitutive relation and strength criterion of rock, also called mechanical analysis. The constitutive model of rock reveals the relationship between stress and strain, including the elastic, nonlinear, plastic, damage, and strain softening models. The constitutive model can be used to study the behavior of rock under different loading conditions to provide an essential basis for engineering design, resource exploitation, and disaster prediction. The strength criterion is the critical condition to describe the failure of rock under different stress states. In deep underground mining, the bearing capacity of rock determines whether the surrounding rock breaks, which is the most critical factor in controlling the stability of surrounding rock. Selecting the appropriate strength criterion is the key to correctly calculating rock fracture, and incorrectly calculating the critical conditions for rock damage in a real stress environment can lead to serious engineering waste or even result in major casualties and property damage. Therefore, establishing rock strength criterion to accurately predict the rock bearing capacity is of great significance to ensure the rational design and safe construction of underground projects. Compared with the intrinsic relationship, the strength criteria focus more on studying the fracture mechanism of the rock. Therefore,

the traditional strength criteria and its modified criteria will be introduced in this Section.

4.1 Mohr–Coulomb (MC) Criterion and Its Modified Criteria

The MC criterion has been widely used due to its simplicity of form and clarity of physical significance, etc. The MC criterion considers that shear damage occurs when a rock reaches its extreme strength under the combined action of normal stress (σ_n) and shear (τ) stresses, and it can be determined by Eq. (11):

$$\tau = c + \sigma_n \tan \varphi, \quad (11)$$

where, c is cohesion and φ is angle of internal friction.

A linear expression for its principal stress can be obtained by Eq. (12):

$$\sigma_1 = \frac{2c \cos \varphi}{1 - \sin \varphi} + \frac{1 + \sin \varphi}{1 - \sin \varphi} \sigma_3. \quad (12)$$

In numerical calculations, to facilitate a uniform treatment of the expressions for different strength and elastic–plastic constitutive relationships, the MC criterion is often expressed in a tensor-invariant form, with the stress tensor versus strain invariant given by Eq. (13) (Cai et al. 2022b):

$$\begin{bmatrix} \sigma_1 \\ \sigma_2 \\ \sigma_3 \end{bmatrix} = \frac{2}{\sqrt{3}} \sqrt{J_2} \begin{bmatrix} \sin(\theta_\sigma + \frac{2}{3}\pi) \\ \sin(\theta_\sigma) \\ \sin(\theta_\sigma - \frac{2}{3}\pi) \end{bmatrix} + \begin{bmatrix} \frac{I_1}{3} \\ \frac{I_1}{3} \\ \frac{I_1}{3} \end{bmatrix}, \quad (13)$$

$$\theta_\sigma = \tan^{-1} \left[\frac{2\sigma_2 - (\sigma_1 + \sigma_3)}{\sqrt{3}(\sigma_1 - \sigma_3)} \right], \quad (14)$$

where θ_σ is the lode angle, I_1 , I_2 and I_3 are the first, second and third invariants of stress tensor, respectively, and J_2 is the second stress bias tensor invariant. As can be seen from Eq. 12 and Eq. 13, the MC criterion has two main limitations: (i) it expresses the rock strength as a linear function of the circumferential pressure or positive stress; (ii) it neglects the effect of the σ_2 (Singh et al. 2011). The MC criterion is often chosen by assuming the rock strength parameters as constants and converting them to a plane strain model. As a result, MC is able to accurately predict the strength of rocks in shallow burial conditions, while it is conservative for deeply buried rocks (Xie et al. 2022). The limitations of the MC criterion have been improved by some scholars. For example, Zhang et al. (2023) modified

the MC criterion using a vein angular shape function based on a spatial slip surface, which considers the intermediate principal stresses and satisfies the smoothness and convexity requirements in the π -plane. Shen et al. (2018) modified the cohesion and internal friction angle parameters based on the original expression, which changed the linear relationship between the original expression's shear stress and positive stress. In addition, this modified criterion also links the, cohesion, and angle of internal friction, which breaks the linear relationship and the invariant strength parameters of the original expression and obtains the nonlinear MC strength criterion. Where, the relationship between the three parameters of uniaxial compressive strength (σ_c), cohesion (c_0) and apparent angle of internal friction (ϕ_0) can be determined by Eq. (15):

$$\sigma_c = \frac{2c_0 \cos \phi_0}{1 - \sin \phi_0} c_0 = \frac{1 - \sin \phi_0}{2 \cos \phi_0} \sigma_c. \tag{15}$$

Singh et al. (2011) considered the concept of critical state proposed by Barton and modified the MC criterion under conventional triaxial conditions. The expression is as Eq. (16):

$$(\sigma_1 - \sigma_3) = \sigma_{ci} + \frac{2 \sin \phi_{i0}}{1 - \sin \phi_{i0}} \sigma_3 - \frac{1}{\sigma_{ci} (1 - \sin \phi_{i0})} \sigma_3^2, \text{ for } 0 \leq \sigma_3 \leq \sigma_{ci}, \tag{16}$$

where σ_{ci} is uniaxial compressive strength (UCS), $(\sigma_1 - \sigma_3)$ is the deviatoric stress of rock failure. Considering its application to a deeply buried true triaxial state of stress, Singh then introduced σ_2 to generalize Eq. (17). The expression is as Eq. (17):

$$(\sigma_1 - \sigma_3) = \sigma_{ci} + \frac{2 \sin \phi_{i0}}{1 - \sin \phi_{i0}} \left(\frac{\sigma_2 + \sigma_3}{2} \right) - \frac{1}{\sigma_{ci} (1 - \sin \phi_{i0})} \left(\frac{\sigma_2^2 + \sigma_3^2}{2} \right), \text{ for } 0 \leq \sigma_3 \leq \sigma_{ci}, \tag{17}$$

where σ_{ci} is UCS here. Although the formula has considered the effect of σ_2 , the criterion shows a large error when the σ_2 is more significant than the UCS. Therefore, Singh suggests that it should be used for $0 \leq \sigma_3 \leq \sigma_2 \leq \sigma_{ci}$.

4.2 Drucker–Prager (DP) Criterion and Its Modified Criteria

Considering the effect of intermediate principal stresses and bias stresses in rock damage, Drucker and Prager (1952) proposed the DP criterion based on the generalized Mises yield criterion, whose yield function can be expressed as Eq. (18):

$$\alpha I_1 + \sqrt{J_2} - K = 0, \tag{18}$$

where α and k are material yield parameters determined by cohesion (c) and angle of internal friction (φ). Depending on the fitting method, the parameters (α, k) are expressed inconsistently and, in general, have the following five forms (Deng et al. 2006):

(1) MC external contact external circle (compression cone):

$$\alpha = \frac{2 \sin \varphi}{\sqrt{3}(3 - \sin \varphi)} k = \frac{6c \cos \varphi}{\sqrt{3}(3 - \sin \varphi)}. \tag{19}$$

(2) MC internal contact external circle (elongation cone):

$$\alpha = \frac{2 \sin \varphi}{\sqrt{3}(3 + \sin \varphi)} k = \frac{6c \cos \varphi}{\sqrt{3}(3 + \sin \varphi)} \tag{20}$$

(3) MC tangent circle (internal tangent cone):

$$\alpha = \frac{\sin \varphi}{\sqrt{3}\sqrt{3 + \sin^2 \varphi}} k = \frac{3c \cos \varphi}{\sqrt{3}\sqrt{3 + \sin^2 \varphi}}. \tag{21}$$

(4) MC equal area circle (DP criterion yields area equal to MC in the π -plane):

$$\alpha = \frac{2\sqrt{3} \sin \varphi}{\sqrt{2\sqrt{3}\pi(9 - \sin^2 \varphi)}} k = \frac{6\sqrt{3} \cos \varphi}{\sqrt{2\sqrt{3}\pi(9 - \sin^2 \varphi)}}. \tag{22}$$

(5) MC Match DP Circle:

$$\alpha = \frac{\sin \varphi}{3} k = c \cos \varphi. \tag{23}$$

The parameters (α, k) of the DP criterion in geotechnical engineering are generally determined by fitting the parameters of the MC criterion. Therefore, the DP series of criterion can also be considered as a modification of the MC strength criterion. Although the DP criterion considers the σ_2 and hydrostatic pressure, the Lode angle effect of rock strength is not considered. Therefore, the DP criterion cannot match the state of triaxial compression and triaxial tension. In this regard, Guo et al. (2021) modified the DP criterion from the perspective of elastic strain energy to solve the problems of the large tensile-shear zone and Lode angle effect, and proposed a generalized DP strength criterion. The yield function expression is determined by Eq. (24):

$$\sqrt{J_2 - \frac{1 - 2\nu}{3} I_2} = k + \alpha I_1, \tag{24}$$

where ν is the Poisson's ratio.

Notably, different forms of the DP criterion predict rock strengths quite differently. For example, the DP criterion in the form of internal tangent cone underestimates the strength of the rock, and the DP criterion in the form of equal area

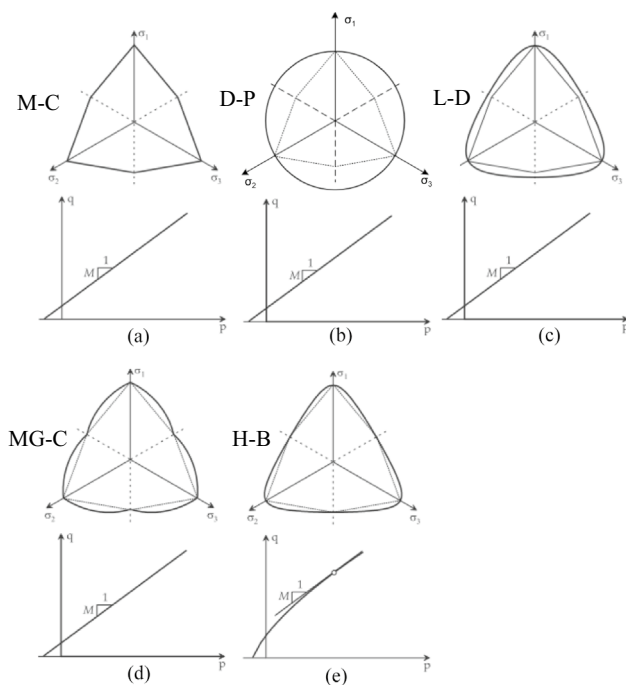


Fig. 24 Failure criterion in principal stress space and in the deviatoric plane, after Benz and Schwab (2008)

circle overestimates the strength of the rock. In addition, the DP criterion overestimates the strengthening effect of intermediate principal stresses on rock strength and must be used cautiously in geotechnical engineering (Zhang et al. 2023). Although DP overcomes the disadvantages of the MC criterion, it is more applicable to brittle rocks at low perimeter pressures (Bavdekar and Subhash 2018).

4.3 Lade–Duncan Criterion and Its Modified Criteria

Considering the shortcomings of the DP criterion and the MC criterion, Lade and Duncan (1975) proposed a strength criterion that includes three principal stresses. The criterion is simple in form, being a curved triangle in the π -plane, with the three outer corner points of the MC criterion connected to the outside (see Fig. 24c). The strength criterion expression is determined by Eq. (25):

$$\frac{I_1^3}{I_3} = \eta_{LD} \tag{25}$$

where η_{LD} is a strength parameter related to the angle of internal friction with the expression is determined by Eq. (26):

$$\eta_{LD} = \frac{(3 - \sin \varphi)^3}{(1 + \sin \varphi) \cdot (1 - \sin \varphi)^2}, \tag{26}$$

I_1, I_2 are calculated as Eq. (27):

$$I_1 = \sigma_1 + \sigma_2 + \sigma_3, I_3 = (\sigma_1)(\sigma_2)(\sigma_3). \tag{27}$$

According to Eq. (26), the LD criterion does not take into account the effect of cohesion. Therefore, the criterion is only applicable to weakly cemented sandy soil materials. Later, Lade (1977) modified the original criterion by considering the damaged form of cohesionless soils at the flexural yield surface, and the new strength criterion expression is determined by Eq. (28):

$$(I_1^3/I_3 - 27)(I_1/p_a)^m = \eta_1, \tag{28}$$

where η_1, m are material constants. Consistent with the original criterion, the modified DP criterion still does not consider the effect of cohesion, which limits the application of the DP criterion in rock mechanics. Later, Ewy (1999) introduced cohesion into the LD criterion, which led to a wide range of applications in rock mechanics. This is also known as the Modified Lade criterion (MLC), whose strength criterion is expressed as Eq. (29):

$$\frac{(I_1'')^3}{I_3''} = 27 + \eta, \tag{29}$$

where I_1'' and I_3'' are the effective first and third principal stress invariants, respectively, which can be determined from the translation distance along the hydrostatic pressure axis (S_a), the fluid pressure (P_p), and its expression is determined by Eq. (30):

$$I_1'' = (\sigma_1 + S_a + P_p) + (\sigma_2 + S_a + P_p) + (\sigma_3 + S_a + P_p), \\ I_3'' = (\sigma_1 + S_a + P_p)(\sigma_2 + S_a + P_p)(\sigma_3 + S_a + P_p). \tag{30}$$

S_a, P_p are determined by the angle of internal friction and cohesion, calculated as Eq. (31):

$$S_a = \frac{c}{\tan \varphi} \eta = 4(\tan \varphi)^2 \left(\frac{9 - 7 \sin \varphi}{1 - \sin \varphi} \right). \tag{31}$$

The MLC criterion is a curved triangle with a smooth envelope in the π -plane, which is more accurate than the MC criterion and the DP criterion for predicting the true triaxial strength of rocks. However, in the triaxial tensile stress state, the envelope is not connected to the MC criterion, which overestimates the rock strength (Xie et al. 2022; Zhang et al. 2023).

4.4 Mogi–Coulomb Criterion(MG-C) and Its Modified Criteria

The effect of the σ_2 on rock damage was clarified by Mogi in his study of rock triaxial experiments. Although its impact is smaller than the σ_3 , it is still not negligible. Subsequently, according to the triaxial experimental results and von Mises theory, Mogi suggested a criterion considering that the fracture plane of rocks strikes in the σ_2 direction, in which the octahedral shear stress τ_{oct} is a function of average normal stress σ_m in true triaxial state (Mogi 1971):

$$\tau_{oct} = f_1(\sigma_m), \quad (32)$$

where

$$\tau_{oct} = \frac{1}{3} \sqrt{(\sigma_1 - \sigma_2)^2 + (\sigma_2 - \sigma_3)^2 + (\sigma_1 - \sigma_3)^2} \quad (33)$$

$$\sigma_m = \frac{\sigma_1 + \sigma_3}{2},$$

where f_1 is a monotonically increasing function. On this basis, Chang and Haimson (2000) further developed the Mogi strength criterion by proposing an exponential form of the Mogi strength criterion, which can be expressed as Eq. (34):

$$\tau_{oct} = A \left(\frac{\sigma_1 + \sigma_3}{2} \right)^n, \quad (34)$$

where A and n are rock material parameters (The specific values need to fit by true triaxial experimental data, for amphibolite A is 1.77 and n is 0.86). Al-Ajmi and Zimmerman (2005) cast doubt on the validity of the power-law form of the Mogi strength criterion because it cannot be related to the parameters calibrated by Coulomb's destruction law, such as cohesion and angle of internal friction. Second, Al-Ajmi proposed a linear expression of the Mogi strength criterion, also known as the Mogi–Coulomb strength criterion, after a large amount of rock triaxial experimental data combined with cohesion and internal friction angle. The modified strength criterion expression is determined by Eq. (35):

$$\tau_{oct} = a + b\sigma_{m,2}, \quad (35)$$

where a and b are determined by Eq. (36):

$$a = \frac{2\sqrt{2}}{3} c \cos \varphi, \quad b = \frac{2\sqrt{2}}{3} \sin \varphi. \quad (36)$$

Although scholars have proposed different expressions of the Mogi–Coulomb criterion, we consider the assumption of $\tau_{oct} = f(\sigma_m)$ to be the key point of Mogi's contribution, and the specific algebraic form of the

function f being a somewhat secondary matter of convenience. The Mogi criterion in its original form can accurately describes the strength of rocks under true triaxial conditions, however, its shape in the π -plane (see Fig. 24d) does not conform to the assumption of continuity, limiting its further development into an intrinsic model. Mogi–Coulomb combines Mogi's theory of elasticity and Coulomb's theory of sliding friction, making its application in rock mechanics widespread. However, the fact that it is based on axisymmetric assumptions leads to deviations from the results of many true triaxial experiments, especially when the predicted intensity tends to be low at large lode angle (Xie et al. 2022).

4.5 Hoek–Brown Criterion (HB) and Its Modified Criteria

Hoek and Brown (1980) discarded assumptions about the damage mechanism of rocks and obtained the profoundly influential two-dimensional nonlinear Hoek–Brown strength criterion (HB) by fitting the data into a curve from several hundred sets of rock triaxial test data and a large number of field tests. The expression of the HB strength criterion is determined by Eq. (37):

$$\sigma_1 = \sigma_3 + \sigma_{ci} \left(m_i \frac{\sigma_3}{\sigma_c} + 1 \right)^{0.5}, \quad (37)$$

where m_i is a material constant for the intact rock reflecting the brittleness of the rock, σ_{ci} is the unconfined compressive strength (The parameters of m_i and σ_{ci} can be obtained by fitting Eq. (37) to results of laboratory tests on intact samples of rocks). Since the HB strength criterion is derived from fitting a large amount of experimental data, it can accurately predict the strength of conventional triaxial of rocks. In addition, the HB criterion can distinguish between triaxial compressive and triaxial tensile stress states, and the envelope has a nonlinear characteristic, which is more applicable under high-stress conditions (Zhang et al. 2023). To apply it widely to practical geotechnical engineering, Hoek et al. introduced the geological strength parameter (GSI) into the original criterion to modify it, which is called the Generalized HB Strength Criterion (GHB) (Hoek and Brown 2019). The strength criterion for the GHB is expressed by Eq. (38):

$$\sigma_1 = \sigma_3 + \sigma_{ci} \left(m_b \frac{\sigma_3}{\sigma_{ci}} + s \right)^a, \quad (38)$$

where m_b , s and a are the rock mass material constants, which are related to geological strength (For intact rock, $s = 1$ and $a = 0.5$). Their calculation formula is determined by Eq. (39):

$$m_b = m_i \exp\left(\frac{GSI - 100}{28 - 14D}\right)$$

$$s = \exp\left(\frac{GSI - 100}{9 - 3D}\right) \quad (39)$$

$$a = \frac{1}{2} + \frac{1}{6} \left[\exp(-GSI/15) - \exp(-20/3) \right],$$

where D is the excavation disturbance factor and GSI reflects the structural surface characteristics of the rock mass. In a recent study, Hoek and Brown further refined the values of these parameters, discussing the range of GSI values and the selection criteria for D (Hoek and Brown 2019).

However, neither HB nor GHB takes into account the effect of intermediate principal stresses and belongs to the two-dimensional strength criterion. Considering the high accuracy of its prediction under conventional triaxial, some scholars have tried to construct a three-dimensional HB strength criterion using the HB strength criterion as a framework. Pan and Hudson (1988) proposed a three-dimensional HB strength criterion called Pan-Hudson strength criterion (GPH). GPH can be expressed as Eq. (40):

$$F_{GPH} = \frac{1}{\sigma_c^{1/a-1}} \left(\frac{3}{\sqrt{2}} \tau_{oct} \right)^{1/a} + \frac{3}{2\sqrt{2}} m_b \tau_{oct} - m_b \frac{I_1}{3} - s \sigma_c = 0. \quad (40)$$

This criterion has a similar shape to the DP criterion in the π -plane. Both are circular. Therefore, GPH does not consider the vein angle effect and is more applicable to weak rock bodies (Su et al. 2022). Zhang and Zhu (2007) proposed another form of 3D HB strength criterion based on the MGC and HB strength criterion, which Zhang (2008) later generalized as generalized Zhang-Zhu strength (GZZ). The expression of the strength criterion is:

$$\frac{9}{2\sigma_c} \tau_{oct}^2 + \frac{3}{2\sqrt{2}} m_b \tau_{oct} - m_b \sigma_m = s \sigma_c. \quad (41)$$

The GZZ criterion can be degraded to the HB criterion in regular triaxial elongation and regular triaxial compression and to the Pan-Hudson criterion in pure shear radial surfaces (Zhang 2008). However, the GZZ criterion does not comply with the assumptions of outer convexity and continuity of the π -plane under triaxial conditions and is defective in numerical calculations. Considering this, Cai et al. (2021) modified it to overcome the defects of the original criterion in the π -plane. They successfully applied it in 3D finite element numerical simulation software, and the modified strength criterion is also called the Smooth GZZ strength criterion. The strength criterion is expressed by Eq. (42):

$$F_{GZZ} = \frac{1}{\sigma_c^{(1/a-1)}} (\sqrt{3} J_2)^{1/a} + \left(\frac{3 + \sin 3\theta_\sigma}{2\sqrt{3}} \right) m_b \sqrt{J_2} - m_b \frac{I_1}{3} - s \sigma_c, \quad (42)$$

where J_3 is the third stress bias tensor invariant. The calculation formula is:

$$\sin 3\theta_0 = -\frac{3\sqrt{3}}{2} \frac{J_3}{J_2^{3/2}}$$

$$J_2 = \frac{(\sigma_1 - \sigma_2)^2 + (\sigma_2 - \sigma_3)^2 + (\sigma_3 - \sigma_1)^2}{6} \quad (43)$$

$$J_3 = S_1 S_2 S_3 = \left(\sigma_1 - \frac{I_1}{3} \right) \left(\sigma_2 - \frac{I_1}{3} \right) \left(\sigma_3 - \frac{I_1}{3} \right).$$

Similarly, Wu (2018a) also noticed this problem and adopted a new bias plane and corrected it to overcome the defect that GZZ is not fully convex in the bias plane. Different from Smooth GZZ, this correction preserves the characteristics of the original criterion in the meridional plane. After continuous development and refinement by Hoek, Brown, and other scholars, the HB criterion has formed a more complete system, which can better respond to the effects of structural surfaces and anisotropy on rock strength. The series of strength criterion has now become the most influential strength criterion in geotechnical engineering. Because of their high accuracy of prediction, the GPH criterion and the GZZ criteria have become the recommended strength criterion of the International Society for Rock Mechanics and Engineering (Su et al. 2022).

4.6 Unified Strength Theory (UST) and Its Modified Criteria

Yu et al. (1992) proposed the Unified Strength Theory (UST) based on the mechanical model and mathematical modelling method of a double shear unit body. The principal stresses for metal-like materials are expressed as Eq. (44):

$$F = \sigma_2 - \frac{b\sigma_2 + \sigma_3}{1+b} \frac{1 + \sin \varphi}{1 - \sin \varphi} = \frac{2c \cos \varphi}{1 - \sin \varphi} \left(\sigma_2 \leq \frac{\sigma_1 + \sigma_3}{2} - \frac{\sigma_1 - \sigma_3}{2} \sin \varphi \right),$$

$$F' = \frac{\sigma_1 + b\sigma_2}{1+b} - \sigma_3 \frac{1 + \sin \varphi}{1 - \sin \varphi} = \frac{2c \cos \varphi}{1 - \sin \varphi} \left(\sigma_2 > \frac{\sigma_1 + \sigma_3}{2} - \frac{\sigma_1 - \sigma_3}{2} \sin \varphi \right), \quad (44)$$

where F represents the strength function of the material, b is the intermediate principal shear stress effect factor ($0 \leq b \leq 1$). After that, the rock mechanics double shear unified strength theory was established after considering the specificity of rock materials with hydrostatic pressure, and the strength criterion expression is as Eq. (45):

$$F = \sigma_1 - \frac{\alpha}{1+b} (b\sigma_2 + \sigma_3) = \sigma_i; \sigma_2 \leq \frac{\sigma_1 + \alpha\sigma_3}{1+\alpha}$$

$$F' = \frac{1}{1+b} (\sigma_1 + b\sigma_2) - \alpha\sigma_3 = \sigma_i; \sigma_2 \geq \frac{\sigma_1 + \alpha\sigma_3}{1+\alpha}, \quad (45)$$

where α is the ratio of uniaxial tensile strength to UCS of the rock.

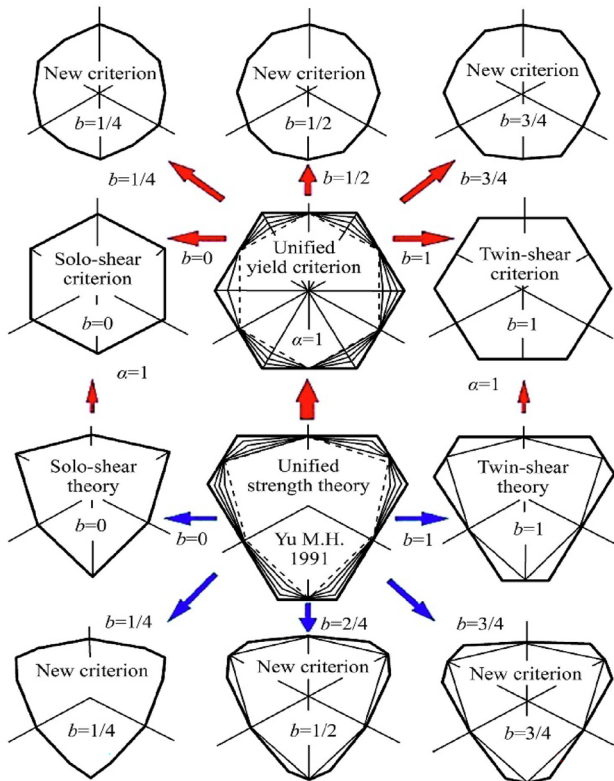


Fig. 25 UST yield trajectory, after Xie et al. (2022)

According to different values of b , a series of different yield trajectories can be determined from hexagons and 12 deformations. As shown in Fig. 25, when $b=0$, UST becomes the solo-shear strength criterion; when $b=1$, UST becomes the double-shear strength criterion and when b takes other values, new strength criteria are obtained (Yu and He 1992). After decades of development, the UST has been systematically improved and elaborated, and an original new strength criterion system has been formed (Xie et al. 2022). More importantly, the proposal of the UST provides new ideas to solve the two major problems of the strength criterion proposed by Voigt–Josenko (First, the shear stresses on all surfaces except the maximum shear stresses in the faces are not considered in the damage analysis; secondly, the strength criterion of rocks cannot be

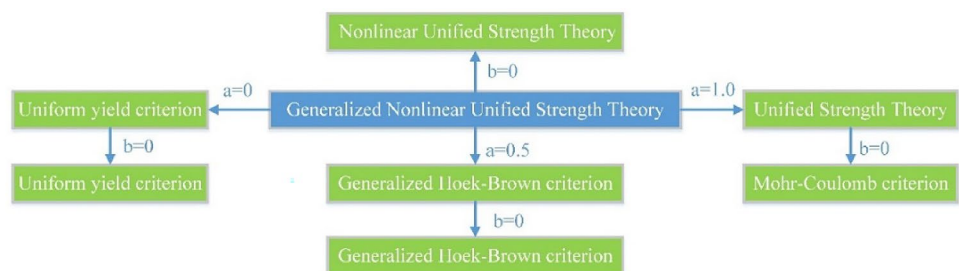
unified into a single damage criterion) (Zhang et al. 2023). However, Li et al. (2023a) believed that the UST predicts the same strength at $\sigma_2 = \sigma_3$ and $\sigma_2 = \sigma_1$, which contradicts with the test results of some rock types and limits its application. Therefore, in their study, they reinterpreted the contribution of σ_2 in the UST. By introducing a mobilization factor χ to characterize the weakening effect of σ_2 on rock strength at high σ_2 values and proposed the Generalized Unified Strength Theory (GUST). By examining true triaxial data from fourteen types of rocks, the GUST's high precision predictive capability was verified.

Considering the ability of the HB criterion to reflect the nonlinear characteristics of deep rock and its limitation of not accounting for the influence of the intermediate principal stress. Zan and Yu (2013) modified the HB criterion using the UCT and proposed the generalized nonlinear unified strength theory (GNUST). The expression is as Eq. (46):

$$\sigma_1 - \frac{1}{1+b}(b\sigma_2 + \sigma_3) = \sigma_c \left[\frac{m}{(1+b)\sigma_c}(b\sigma_2 + \sigma_3) + s \right]^a, \tag{46}$$

where m , s and a correspond to m_b , s and a in the GHB strength criterion, respectively. The GNUST can transform into different strength theories depending on the parameter values. When $a=0$, GNUST becomes the unified strength criterion; when $a=0.5$, it becomes the nonlinear unified strength theory; when $a=1.0$, it transforms into the unified strength theory represented by the Mohr–Coulomb (MC) criterion; when $0 < a < 1$, GNUST can produce numerous new strength criteria. The relationship between GNUST and other strength criterion is shown in Fig. 26. GNUST encompasses most existing nonlinear strength theories, elevating rock strength criteria to a new level. However, similar to the HB strength criterion, GNUST heavily relies on the experience of researchers for parameter selection. There are various strength criteria at present. The strength criteria have the same theoretical basis, but their mathematical forms and parameter meanings are not the same, and even the physical meanings of the parameters are not clear. The introduction of UST and GNUST addresses the problem. It is worth noting that other scholars have also improved on the single strength criterion based on the idea of "unification" and have attempted to encompass the current

Fig. 26 GNUST in relation to other intensity theories



strength criterion with a unified mathematical expression. Zienkiewicz (1971) proposed a general formula for strength criteria and integrated most strength criterion into the framework of existing procedures. Desai et al. (1986) proposed a unified strength criterion in polynomial form. Aubertin et al. (1999) proposed Mises–Schleicher and DP unified (MSDPu) criterion. Benz et al. (2008) combined the HB criterion with the Matsukawa–Nakagawa (MN) criterion, proposing a unified HB and MN (HBMN) criterion. These strength criteria have highly theoretical. However, Wang et al. (2023) argued that these unified strength criteria have some limitations, such as, it is difficult to characterize the hydrostatic pressure effect, and some of the strength criterion have complex expressions. To overcome these limitations, Wang et al. (2023) utilized the nonlinear properties of power functions to establish a new three-dimensional nonlinear unified strength criterion.

Overall, the two-dimensional strength criteria have achieved excellent results in assessing rock damage on shallow buried underground works and remains the preferred choice for most geotechnical projects. However, with the gradual increase of the mining depth, the true three-dimensional stress characteristics of the rock become increasingly obvious, and the two-dimensional strength criteria will make the calculation results too conservative. The three-dimensional strength criteria existing at present does not have a clear understanding of the failure surfaces in the three-dimensional stress space. Therefore, many true triaxial experiments on rocks need to be carried out in the future to clarify the effects of intermediate principal stress, hydrostatic pressure, and lode angle on the rock damage surface in the three-dimensional stress space. Constructing a three-dimensional strength criterion for rocks that conforms to the convexity and smoothness is necessary to detect the mechanism of rock fracture in deep mining more accurately.

5 Numerical Simulation

Rock fracture in deep underground space excavation is a complex problem requiring large-scale numerical calculations for fine results. Numerical calculations can be divided into analytical, semi-analytical and numerical solutions according to the ease of solution. Analytical and semi-analytical solutions are simpler and faster than numerical solutions (Su et al. 2022). The numerical solution is a tool for analysis and computation when dealing with multiple complex problems for which no analytical solution can be proposed, which is also called numerical simulation. Due to the complexity of the mechanical properties of deep rocks, it is challenging to study the fracture mechanism of rocks using the traditional analytical method. Numerical

simulation has become one of the main approaches to this problem, enabling complex calculations and visualization.

5.1 Numerical Simulation Methods

At present, several scholars have reviewed numerical simulation methods for rock mechanics. Initially, Jing and Hudson (2003; 2002) reviewed the numerical simulation techniques and their progress in rock mechanics and engineering. Nikolić et al. (2016) updated the 2002 version of the review with the latest numerical modelling techniques. Bobet et al. (2009a, b) reviewed the numerical simulation methods of discontinuous media and their progress. Sun et al. (2012) reviewed the contact relationship of numerical simulation in rock mechanics. Lisjak et al. (2014) analytically summarized the application of discrete elements in discontinuous rock fracture. Mohammadnejad et al. (2018) summarized the research progress of computational fracture mechanics of rocks. Recently, Tahmasebi (2023) reviewed the experimental and numerical simulation research status of granular materials, and clarified the future research direction.

This Section presents a brief summary and discussion of numerical modelling methods and several key points involved in studying rock fracture mechanisms, building on previous work. In general, there are three most common numerical simulation methods in rock mechanics: (1) the continuous medium method, which contains finite difference (FDM), finite element (FEM), boundary element (BEM), mesh free method, and extended finite element method (XFEM); (2) the discontinuous medium method, which includes the discrete element method (DEM), and discrete fissure mesh method (DFN); and (3) the hybrid finite-discrete element method. Although there are numerous simulation methods, not all numerical techniques can correctly model rock fracture (Nikolic et al. 2016). The continuous methods simulate processes such as deformation and stress redistribution before damage occurs to the system. If the simulated area is large enough, applying the continuity method can respond to the mechanical behavior of the rock, even if there are joints and fissures within the rock. Still, it has some limitations in dealing with discontinuous structural surfaces such as faults, joints, and fissures. It is difficult to simulate the movement process of the material with an actual large displacement. The discontinuity method simulates the damage processes, such as crack initiation, extension, intersection, penetration, and the subsequent occurrence of large displacements in the system. The discontinuity method makes up for the shortcomings of the continuity method, but the technique cannot simulate the deformation and damage before the destruction of the rock mass. Therefore, the selection of the continuity

and discontinuity methods is based on the focus of the research problem. If only a small amount of fracture exists and contact between blocks is not a significant influence, the continuity method is a good choice. If the fractured rock is to have large-scale displacement, rotation, detachment, etc., the discontinuous method is a better choice. Hybrid finite discrete elements can avoid the shortcomings of both methods. Therefore, if it is necessary to study the deformation and stress distribution of rock before fracture, as well as the process of crack initiation, propagation, and eventual formation of block separation and movement, the hybrid continuous–discontinuous method is a better choice. First, the continuous method is used to describe the deformation and stress distribution of the rock; when the cracks further develop and lead to block separation, the discontinuous method is then employed to simulate the interaction and movement of the blocks.

Although there are numerous numerical simulation methods, no universal method can solve all rock mechanics problems. It is necessary to select the most appropriate method to solve the problem according to the focus of the problem. For the study of rock fracture, no matter which method is chosen, the core is to be able to accurately describe the emergence, expansion, and morphology of cracks in the rock. This requires researchers to have a certain knowledge and experience to focus on the core concepts of rock mechanics and geotechnical engineering to ensure that the selected methods and simulations meet engineering design requirements.

5.2 Fracture Technology

To realistically simulate the rock fracture process, the numerical simulation method needs to be able to simulate crack generation and expansion in any direction (Mohammadnejad et al. 2018). In other words, the fracture technique of the numerical simulation determines the realism of the results. Several typical fracture techniques will be described below.

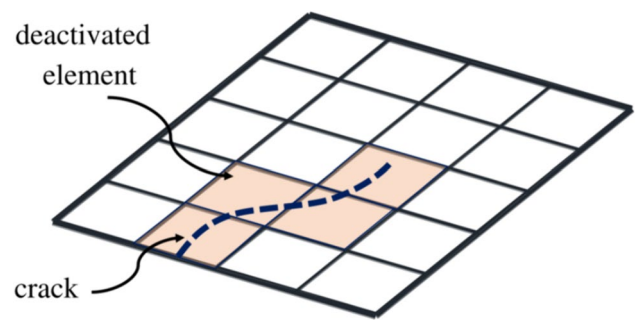
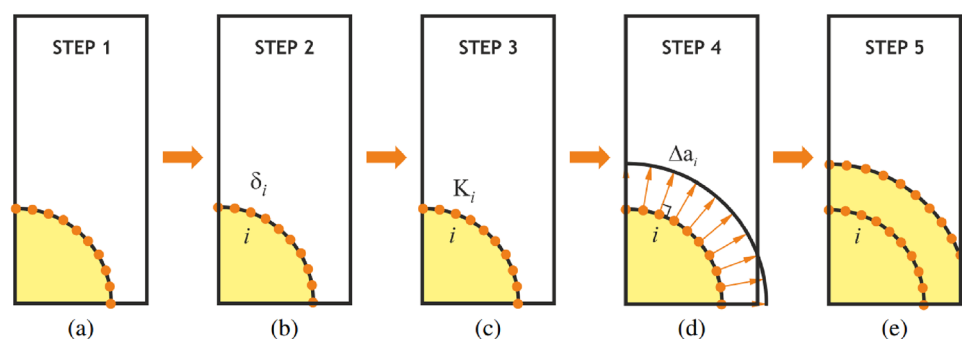


Fig. 28 Element erosion method to realize rock fracture, after Mohammadnejad et al. (2018)

5.2.1 Continuous Method

Among the standard continuous numerical simulation methods (excluding meshless techniques), FEM achieves rock fracture better than FDM and BEM. FEM implements crack expansion through adaptive mesh repartitioning. As shown in Fig. 27, the main steps are divided into four main stages (Branco et al. 2015): (1) establishing the finite element model, (2) calculating the strength factor at the tip, (3) determining the extension direction and extension distance using the crack extension criterion, and (4) re-meshing in conjunction with the morphology of the crack after extension. The above steps are repeated continuously, and the rock fracture simulation is finally realized. Although the adaptive meshing technique of the finite element method can deal with the complex three-dimensional crack extension problem, the crack extension is complicated in geotechnical engineering, and many extension sub-steps need to be set to obtain accurate results. This also leads to high computational costs and makes it difficult to meet the requirements for computational efficiency. In addition, various techniques have been used to achieve rock fracture within the framework of FEM, such as the internal unit cracking method, the embedded unit method, the elemental erosion method, and the XFEM. As shown in Fig. 28, the elemental erosion method simulates the generation of cracks in rocks by removing grid elements, and the element body

Fig. 27 Adaptive meshing technology: **a** Establish the model, **(b-c)** is the calculation of the intensity factor, **d** determines the extension distance and direction, **e** re-meshing, after Branco et al. (2015)



containing the cracks is deactivated by setting the stress to zero to indicate its deactivation (Rabczuk 2013). Although simple and easy to use, this method does not simulate crack extension. Belytschko and Black (1999) proposed a finite element method with minimal mesh rescaling, also known as the XFEM, to enrich the finite element method with cracks. The extended finite element method considers the effect of cracks and introduces a discontinuous enhancement function in the finite element approximation. The extended finite element method retains all the advantages of the traditional finite element method but also has unique benefits due to its characteristics: for example, the crack and the computational mesh are independent of each other, so there is no need for mesh re-drawing, which saves a lot of computational costs; the use of special enhancement functions can easily capture the discontinuity in the crack surface and the singularity near the tip of the crack, and very accurate results can be obtained with a small number of meshes.

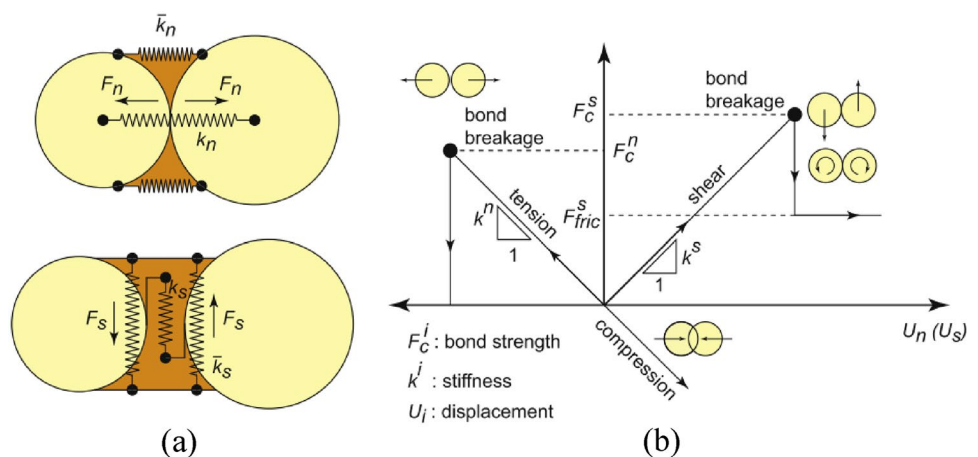
Unlike the FEM, which divides the elements in the continuous domain, the BEM divides the elements only on the boundaries of the domain of definition. It approximates the boundary conditions by functions of the control equations. Therefore, the number of BEM elements is less, and the pre-processing is simpler compared to FEM. In addition, the error of BEM only originates from the boundary nodes, and the computational accuracy is higher. The error BEM generates at the nodes is due to crack node overlap. For this reason, Subdomain Boundary Element Method (SBEM), Displacement Discontinuity Method (DDM), and Dual Boundary Element Method (DBEM) are generated to solve the problem.

Standard numerical simulations of continuity have achieved some success in implementing rock fracture, but the presence of discontinuities in the rock mass must be addressed. In standard continuous numerical simulation methods, homogenization techniques and continuous-interface combinations are usually used to implement

structural surfaces in the model. The first method is used for more discontinuous surfaces and responds to the deterioration effect of the rock mass by reducing its modulus of elasticity (Hoek and Diederichs 2006). This method does not accurately capture the slippage and separation of the rock mass due to size effects (Hammah et al. 2008). The second method accommodates large displacements and rotations with negligible contact variation between meshes. Therefore, both methods have certain limitations in modeling the structural planes of rock masses. Overall, homogenization techniques are suitable for studying the macroscopic failure of rocks containing structural planes, while the continuous-interface combination method can accurately simulate the microscopic failure of rocks with structural planes. Thus, in practical geotechnical engineering, these two methods should be used in combination. For instance, when simulating a large geotechnical engineering, homogenization techniques can be employed for most areas, while the continuous-interface combination method can be used to investigate the fracture process in critical fracture zones. This combined approach can ensure computational efficiency while enhancing the accuracy and reliability of the simulation results. Therefore, the continuous medium method can only simulate rock fracture to a certain extent.

A large part of the reason for the shortcomings of the continuous numerical modelling approach described above in modelling rock fracture is due to the mesh. In this reason, meshless methods have created a wave of research. Meshless method uses a set of scattered nodes to discretize the solution area. It constructs the approximation function with the help of the discrete points without establishing the connection relationship of the elements, thus avoiding the disadvantage of mesh redrawing. The characteristics of the meshless method make it widely used in rock fracture studies. For example, Das and Cleary (2010) used the SPH method to study the effect of rock shape on rock fracture. Deb and Pramanik (2013) used the SPH method to study the

Fig. 29 The parallel bond model implemented in PFC: **a** Normal and shear stiffnesses between particles, **b** Constitutive behavior in shear and tension, after Lisjak and Grasselli (2014)



fracture process of brittle rocks. Although meshless methods overcome the drawbacks of mesh-based numerical methods, the complex function construction methods for dealing with discontinuous surfaces make them computationally expensive, and the difficulty of developing suitable constitutive models makes them less popular than FEM.

5.2.2 Discontinuous Medium Method

The discontinuous medium method is narrowly defined as the DEM. The core idea of the DEM was proposed by Cundall (1971) and is widely used in numerical analysis software. The discrete element method divides the whole into single units and calculates the forces on each unit subjected to external forces. Numerical analysis software developed from discrete element methods have been widely used in geotechnical engineering, such as Particle Flow Code (PFC), Universal Distinct Element Code (UDEC), Engineering Discrete Element Method (EDEM), etc. (Cao et al. 2023; Cong et al. 2015). Most traditional discrete element software is based on particle flow, while the UDEC series is implemented as a mesh.

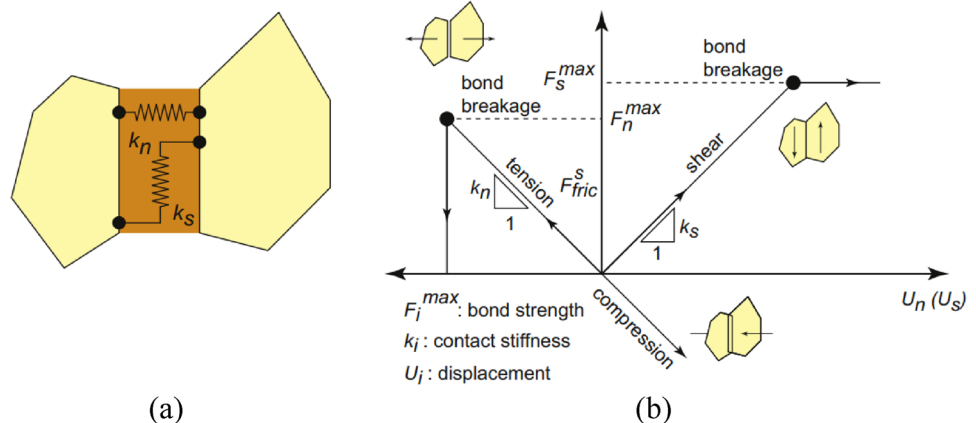
The discrete element method of particle flow is also known as the BPM method, represented by the PFC family of software. BPM divides the domain into circular and spherical rigid elements, which are non-uniformly distributed (Mohammadnejad et al. 2018). As shown in Fig. 29a and the PFC software, there are two contacts: contact bonding model (CBM) and parallel bonding model (PBM). CBM can be considered as two elastic springs with constant shear and normal stiffnesses at a given point. However, the parallel bond model approximates particle pair bonding as cement material, assuming elastic interactions between particles parallel to the sliding or contact bond constitutive model (Ao et al. 2022). Cracks initiation when the tensile, shear and compressive stresses in the element exceed the maximum tensile strength, maximum shear strength, and maximum compressive strength of the contact bonds, and

cracks extend along rigid element boundaries (Lisjak and Grasselli 2014). For CBM, the particles can move and rotate freely in the normal and tangential directions. As shown in Fig. 29b, the shear strength decreases to a constant, and the tensile strength decreases to 0 when the contact bond breaks, but the contact stiffness still exists. CBM does not enable rotation between particles, and the difference between the two contact models is that parallel bond breaking in the latter immediately reduces the model's stiffness.

In UDEC, the rock model is divided into numerous blocks interconnected by discontinuous surface. Each block and discontinuous surface exhibits distinct mechanical behavior, and the deformation and failure of the model are determined jointly by the blocks and discontinuous surface. UDEC considers the interaction between discontinuous blocks and discontinuous surfaces and divides rigid blocks into units that can slide, slip, interact, and separate. Therefore, this method enables accurate simulation of the mechanical behavior of underground rocks (Bobet et al. 2009b). As shown in Fig. 30a, the blocks in UDEC are connected by normal and tangential springs. As shown in Fig. 30b, the fracture mechanisms of UDEC software are normal tension damage and tangential shear damage. The blocks separate when the tensile stress between them exceeds their tensile strength. Shear failure is determined using the MC criterion, checking in each computational iteration whether the shear stress exceeds the maximum shear strength. Sliding between the blocks occurs when the shear stress exceeds their maximum shear strength. Otherwise, there is a linear relationship between displacement and stress between the blocks.

The discontinuous medium method has specific advantages over continuous software, particularly in accurately simulating block motion, crack initiation, and extension. For instance, it can better capture the discrete movements and interactions of individual blocks, predict the initiation of cracks more accurately, and model the propagation of these cracks under various stress conditions.

Fig. 30 UDEC modeling of fracture propagation in rock: **a** Normal and shear stiffnesses between blocks, **b** Constitutive behavior in shear and tension, after Lisjak and Grasselli (2014)



Studies such as Karampinos et al. (2015) and Gao et al. (2019) have demonstrated these benefits in underground geotechnical engineering applications. However, its drawbacks are also apparent, such as parameter calibration, difficulty in complex modeling, and difficulty in simulating the behavior of rocks before the damage.

5.2.3 Hybrid Continuous–Discontinuous Method

Munjiza et al. (1995) proposed the Combined Finite-Discrete Element Method to overcome the drawbacks of the continuous and discontinuous methods. The method

unites the principles of continuous and discontinuous media, allowing the creation of new discrete bodies when the material satisfies the fracture criterion. Hybrid continuous–discontinuous methods have been successfully used to simulate rock fracture and fragmentation to achieve the transition from continuous to discontinuous (An et al. 2017; Han et al. 2020a; Ma et al. 2022). At present, most of the hybrid continuous–discontinuous methods are extended based on the original version of Combined Finite-Discrete Element Method, and the methods to achieve rock fracture are similar. Among these methods, the parallel computation of HFDEM based on a graphical processing unit (GPGPU)

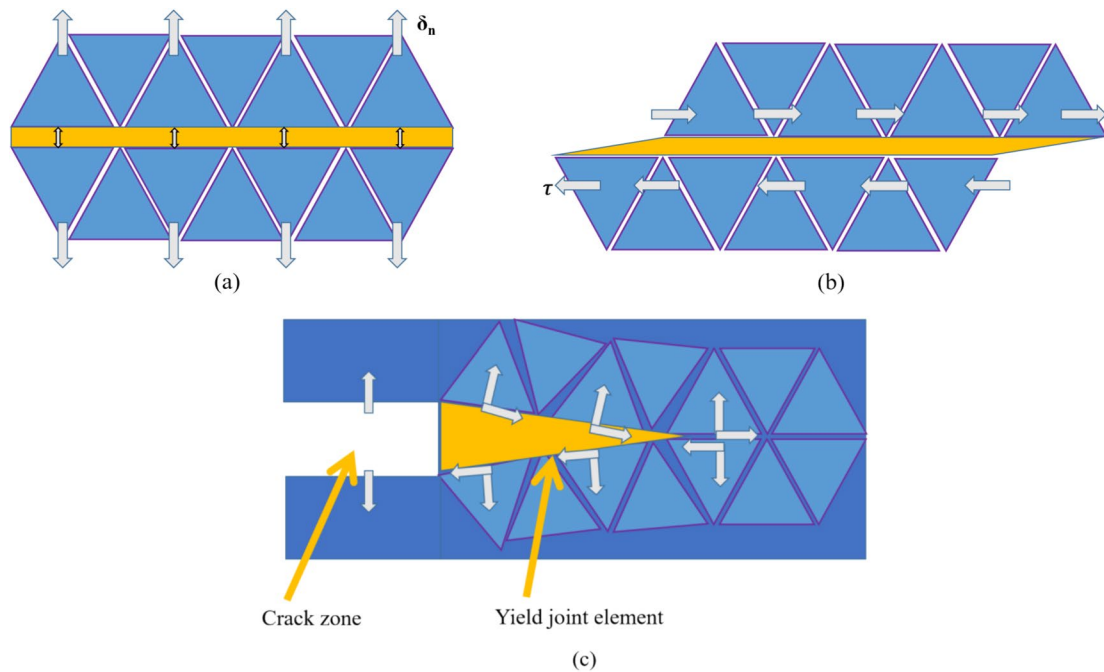


Fig. 31 Fracture types of rocks in HFDEM: **a** tensile failure, **b** shear failure, **c** mixed tensile-shear failure

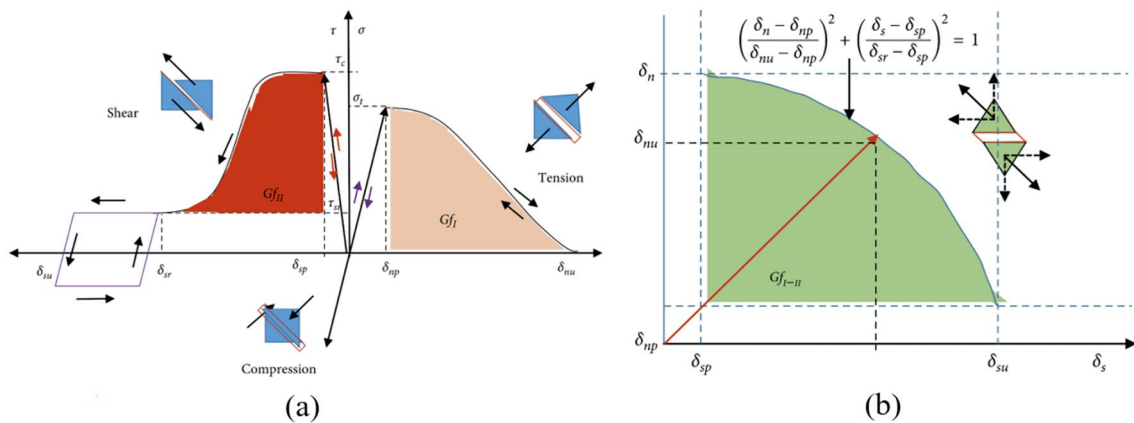


Fig. 32 **a** Relationship between bond stress and opening displacement under tensile and shear conditions, **b** failure criterion of mixed fracture mode, after An et al. (2021)

proposed by Liu et al (2013a) has dramatically improved the computational efficiency. It has been widely used, and this Section will briefly introduce the method of HFDEM to achieve the fracture. It is worth noting that the coupling of continuous and discontinuous methods at physical boundaries can also serve as a hybrid numerical simulation approach, such as BEM/DEM (Barros et al. 2023), FEM/DEM (Wu et al. 2018c), and FDM/DEM (Zhang et al. 2018). However, unlike the Combined Finite-Discrete Element Method, the coupling of continuous–discontinuous methods cannot freely simulate the continuous and discontinuous behaviors of rocks and their transitions.

HFDEM classifies rock fracture into three modes according to the rock being under different stress conditions. For example, Fig. 31a shows pure-mode-I fracture when subjected to pure tensile stress; Fig. 31b shows pure-mode-II fracture when subjected to pure shear stress; and Fig. 31c shows mixed-mode I-II fracture when subjected to mixed tensile-shear stress. In HFDEM, the whole can be discretized into several finite elements, and adhesive forces bond together the finite elements. The relationship between the bond force and the opening distance of the elements when they are subjected to tensile and shear stresses is shown in Fig. 32a. For tensile fracture, the tensile stress determines the opening (o) between the elements. The opening distance between the elements continues to increase as the normal bond stress σ^{coh} reaches the extreme tensile strength value (T_s). It is worth noting that the opening between the units cannot be reversed when the tensile strength between the units exceeds T_s . Subsequently, the σ^{coh} decreases gradually and tensile cracking starts to occur in the rock when its strength decreases to zero. Finally, when the element opening distance reaches the ultimate opening size (o_t), the finite element separates, and the rock undergoes tensile fracture. The shear fracture mechanism is much the same as tensile fracture. It is worth noting that the tangential bond stress τ^{coh} does not decrease to zero when the element is subjected to a shear-slip type of damage. At this point, τ^{coh} becomes pure frictional resistance, which also corresponds to some extent to the presence of residual strength after rock fracture. Whether a mixed type I-II fracture occurs is determined by the expression in Fig. 32b, which represents the maximum distance between the elements at which separation can occur. Mixed fracture arises in the green area, and the units separate in the other areas.

The hybrid continuous–discontinuous method integrates the advantages of both continuous method and discontinuous method, can simulate the behavior of rocks before and after damage, and can accurately simulate the initiation and propagation of rock cracks and the transition from continuous to discontinuous (An et al. 2017; Han et al. 2020b; Mohammadnejad et al. 2020). All three classes of methods enable the simulation of rock fracture, but there

are some differences in the methods used to achieve fracture. In addition, various methods have different advantages. Therefore, the selection of the method should be based on the focus of the study. For example, if it is dedicated to the study of rock fracture, the discontinuous method is a superior choice. However, it is also necessary to study the mechanical behavior of the rock prior to its destruction, the hybrid method is superior.

5.3 Ground Stress Equilibrium Method

Ground stress is an essential influence on the mechanics of deeply buried rocks. Therefore, the implementation of ground stress in numerical simulations must be fully considered. In numerical simulations, the initial stress balance is generally achieved by applying the ground stresses to different surfaces. This approach can have two major drawbacks: (1) three-way unequal pressure will cause the stress applied at the boundary of the model to be realized by interpolation, which is inconsistent with the actual stress applied, and (2) when multiple contact surfaces are involved, especially in the presence of nodal fissures, applying ground stresses by the conventional method can result in dissipation of the stresses during equilibrium (Tal et al. 2014). For this reason, Lisjak et al. (2014) proposed a new ground stress equilibrium technique in which the magnitude of predetermined ground stress is calculated at each node, and the calculated force is applied backward to the nodes during ground stress equilibrium to achieve initial ground stress equilibrium. Then, the node stresses are released by fixing the model boundary to achieve the final ground stress equilibrium.

5.4 Computational Efficiency

Currently, most numerical simulation methods require meshing, but meshing is not the focus of the study. Therefore, when simulating the generation and expansion of rock cracks, it is necessary to finely divide the mesh so that the fracture mode is independent of the mesh to give full play to the crack expansion technology of numerical simulation software to capture the fracture mechanism of the rock accurately (Vazaios et al. 2019). As the depth increases, the complexity of the model increases again. Complex models with mesh refinement can affect the computational efficiency of the software. Especially for quasi-static problems, the loading and unloading rates are small, and the dynamic energy dissipates over a considerable period. The combination of the above two factors can lead to an increase in the number of elements and time steps, making it possible for a simulation to take several weeks. This is unacceptable for numerical simulation, which is known for its efficiency and

convenience. At the same time, particle-based methods (BPM, SPH) also have problems with computational efficiency. The refinement of the model leads to an increase in the computation time for contact detection between particles, velocity and position reset of particles. Therefore, computational efficiency is a problem common to all numerical simulation software. For this reason, some scholars have successfully applied to hybrid finite discrete element and particle flow software (FDEM, CDEM, PFC, SPH) using parallel acceleration of graphical processing unit (GPGPU), which has improved the computational efficiency by dozens or even hundreds of times (Chen et al. 2020; Das and Cleary 2010; Gujjala et al. 2023; Tang et al. 2022). The computation of GPU parallel architecture takes the numerical simulation of rock mechanics to a new level, making it infinitely possible to simulate deep and complex scenarios such as large-scale and multi-coupling. Of course, it is also possible to simplify the model to improve computational efficiency, but this is not a wise choice for the study of rock fracturing in deep mining.

5.5 Mechanical Parameter

When studying the numerical simulation of rock fracture, the mechanical behavior of the model depends mainly on the microscopic parameters of the contact between the rock bodies (Han et al. 2020a). However, conventional rock mechanics experiments can only obtain conventional mechanical parameters (e.g., modulus of elasticity, Poisson's ratio, etc.). Microscopic mechanical parameters (bond modulus, bond stiffness, etc.) require back analysis for acquisition. Back analysis is the process of determining a set of input conditions that lead to outputs consistent with observed phenomena. In numerical simulation of geotechnical engineering, back analysis is always used to determine the input parameters. In numerical simulations of geotechnical engineering, back analysis is often used to determine input parameters inaccessible to direct measurement, a process commonly recognized as model calibration. However, at present, limited and non-unique data make it challenging to develop a universally usable framework for numerical back analysis of rock mechanics, resulting in the manual trial-and-error method remaining the dominant approach (Walton and Sinha 2022). Considering the limitations of back analysis on rock mechanical parameters, Cai et al. (2022a) proposed a real-time and fast forward analysis method for deep excavation. The rock strength parameters were obtained using digital in-situ inspection of the palm face information. The method requires a rigorous investigation of the geological and environmental formations. In addition, there are deterministic and uncertain relationships between parameters of deep rock mechanics. Uncertainty relationship refers to the change in parameters

caused by the disturbance of the rock, which in turn leads to changes in the associated parameters. However, most numerical simulations are analyzed and calculated deterministically, ignoring parameter changes (Tiwari et al. 2018). Although the correlations between rock parameters are widely recognized, research on this topic remains limited. Cao et al. (2017) argue that the use of probabilistic methods can adequately take into account the correlation between rock parameters. To this end, Zheng et al. (2021) proposed a multivariate distribution combined with a relevance vector machine (RVM) method, which considers the variability of all input parameters and can identify uncertainties and correlations between rock parameters. Therefore, the relationship between mechanical parameters should be fully considered in numerical simulations in the future, and a multivariate distribution model should be established to describe the multi-dependent characteristics of different parameters.

6 Field Measurement

Field measurements provide critical data for understanding geological conditions and predicting potential risks. In the context of researching rock fracture in deep mining, determining ground stress and field monitoring play significant roles. Field monitoring can obtain information on rock fracturing at different scales, providing data and validation for numerical simulations and laboratory experiments. The accuracy of ground stress values is the first step in correctly analyzing rock fracture process. Therefore, this Section will review field monitoring method and determination of ground stress.

6.1 Field Monitoring

At present, most field monitoring can only qualitatively study rock fracture mechanisms. The techniques currently used for monitoring rock fracture in the field encompass both the macroscopic and microscopic scales. Macro-monitoring is aimed at deformation and stresses in the rock and is generally achieved by means of stress gauges and strain gauges (Sun et al. 2018a). More importantly, this type of method only addresses the local deformation of the rock and does not allow for comprehensive monitoring of the rock and rock mass. With the development of digital image technology, non-contact deformation monitoring methods (DIC) are also used to study the deformation and fracture of rocks. The basic principle of DIC is to match the digital scattering images of different states of the object surface with geometric points and track the movement of the points to obtain the deformation information of the object surface

(Hou et al. 2021). The DIC technique is highly accurate and is widely used to study rock deformation and fracture. For example, Zhao et al. (2015) quantified the initiation law of rock specimens using DIC technique from the global strain field. Su et al. (2018) investigated the fracture law of marble using DIC. During field monitoring, the successful installation and consistent operation of monitoring instruments is not always guaranteed, due to the complex geological conditions in deep underground (Wu et al. 2018b). Especially when extremely severe deformation of the rock mass extrusion is encountered, which often leads to severe damage to the instrument. Therefore, DIC technique have high requirements for the on-site environment in field monitoring. Fiber-optic sensing technology, which is not site-specific, has been applied to underground excavation deformation monitoring and is an efficient and convenient method for monitoring rock deformation at the macro-scale (Ren et al. 2023, 2021; Song et al. 2021).

For microscopic monitoring there are microseismic monitoring techniques (MS), acoustic emission (AE), scanning electron microscopy (SEM) etc. (Li et al. 2017a; Wu et al. 2017; Xiao et al. 2019). In comparison, MS is suitable for field monitoring and the remaining techniques are more suitable for laboratory tests. MS technique is a micro-scale 3D monitoring method, which fills the gap in obtaining microscopic fracture information of rocks that cannot be acquired through field monitoring (Li et al. 2020a). It is worth noting that AE and MS theories are similar both are based on seismology. MS techniques can be considered as AE techniques in a broad sense. The AE technique is suitable for source-reception distances of a few meters or less, and specimens can be as small as millimeters (Liu et al. 2020). Although the principles of AE and MS are similar, their application scenarios differ. MS is primarily used to

monitor the stress state and fractures of underground rocks, while AE is commonly used to monitor the propagation of microcracks within laboratory-scale materials. And, due to the complexity of field test conditions, it is difficult to synchronize the information on the fracture process and AE signals (Zhu et al. 2020).

Under the influence of external disturbances, the rock mass generates microfractures internally and releases strain energy in the form of elastic waves, known as microseismic in MS. MS first collects the microseismic fluctuation signals emitted during the fracture of the rock mass. Then, using waveform analysis to obtain information on the time and location of the source event (microseismic event) of the rock mass fracture, as well as the intensity of the source of the earthquake. By accurately locating microseismic events, it is possible to determine the site of development of a rock fracture surface or the geometry of the fracture surface (Cai et al. 2001). As shown in Fig. 33, the microseismic signal is transmitted through the microseismic sensor. In underground cavern excavation, sensors generally form a spatial array along the axis of the cavern and the excavation elevation, which can effectively capture the fracture signals of the rock during the excavation process. The localization of seismic sources is a complex task, and the accuracy of the localization will directly affect the accuracy of the analysis. Field monitoring is mainly based on the theory of arrival-time difference (arrival time) to achieve seismic source localization.

The theory of arrival time source localization refers to establishing a function between the arrival time difference and wave velocity of the waves generated during rock fracture and the spatial coordinates of the sensors, which is then solved to obtain the location of the seismic source and the moment of seismicity. Methods based on the arrival time

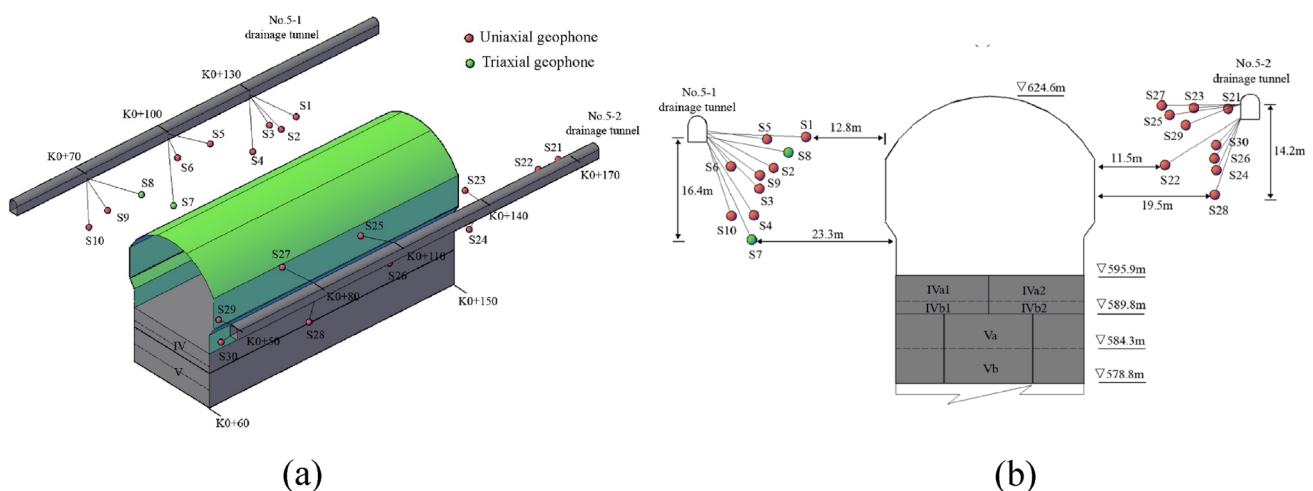


Fig. 33 MS sensor layout diagram of an underground cavern: **a** three-dimensional layout diagram, **b** front view diagram, after Zhao et al. (2022b)

theory include the Inglada method, Geiger iteration method, double residual localization method, simplex algorithm, and so on. These methods are susceptible to extraction accuracy and wave velocity modelling, and have poor positioning accuracy (Cheng et al. 2018). After entering the twenty-first century, some scholars have improved it, such as Lin et al. (2010) who used the linear positioning method combined with the Geiger iteration method to locate the seismic source. Dong et al. (2011) proposed a method of seismic source localization that does not need to measure the velocity in advance, which better solves the impact of the traditional method on the localization accuracy due to the velocity error. Bisrat et al. (2012) based on the particle swarm model to determine the wave velocity and the moment of seismicity, and solved the seismic source location using the seismic source hierarchical localization method. Li et al. (2014) used the statistics of paradoxical numbers to locate the source based on simplex algorithms, which improves the accuracy. In addition, the accuracy of the data can be improved by coordinating between automatic pickup, wave velocity modelling and positioning methods, and by installing microseismic sensors at specific locations (Cheng et al. 2018).

6.2 Determination of Ground Stress

Ground stress is the internal stress within a rock mass. Due to the presence of ground stress, the interior of the rock mass is in a constant state of deformation and movement. Accurately determining ground stress is the key point in using numerical simulations and laboratory tests to analyzing rock's fracture and stability in geotechnical engineering (Cai and Peng 2011; Zhao et al. 2012). The main methods of determining ground stress are field direct measurements and inverse reconstruction. Field direct measurement of ground stress is the most straightforward approach to obtaining an accurate stress field in a specific area (Liu et al. 2013b). At present, the main field direct measurement methods are as follows: strain relief, acoustic emission, borehole cores, and hydraulic fracturing tests (Qian et al. 2021). However, the measurement has limitations, including high costs, discreteness of results, and lack of representativeness (Kang et al. 2010). The results obtained from the measurement point can only reflect the

local stress distribution at that point. Therefore, researchers have engaged in extensive practical exploration and found various methods for obtaining ground stress. At present, methods for ground stress include: (1) Heim's hypothesis, (2) lateral pressure method, (3) regression analysis method, (4) boundary load adjustment method, and (5) artificial intelligence combining the above methods, such as genetic algorithms, neural networks and machine Learning (Yao et al. 2021).

Haimson proposed the "hydrostatic pressure" hypothesis in 1987. According to Haimson's hypothesis, ground stress stored in rock masses approximates a state of hydrostatic pressure. This means that ground stress in any direction within the rock mass equals the overburden stress i.e. $\sigma = \gamma H$ (σ is the stress in any direction, γ is gravity of the rock, H is buried depth). However, in reality, the lateral stress does not adhere to Haimson's hypothesis. Lateral pressure method is used to obtain the magnitude of ground stress by calculating the depth of burial, gravity, and lateral pressure coefficient, and the formula is as Eq. (47):

$$\begin{aligned}\sigma_v &= \gamma H, \\ \sigma_H &= K\gamma H,\end{aligned}\quad (47)$$

where σ_v is the vertical stress, σ_H is the maximum horizontal principal stress, K is the lateral pressure coefficient. The obtained principal stresses calculated using this formula do not consider the real stress environment (Jia et al. 2020). In order to be able to accurately calculate the ground stress, some scholars have given calculation formulas based on local ground stress measured data. For vertical stress, Brown and Hoek (1978) summarized the worldwide patterns of vertical stress variation with depth. Studies suggest that vertical stress is essentially equal to the weight of overlying rock layers. Although there may be some error under tectonic movement, this conclusion has been widely accepted by scholars and extensively applied in geotechnical engineering. For horizontal stresses, a linear regression can be fitted to the measured data (Haimson 1978; Jing et al. 2008; Stephansson et al. 1986). Therefore, the ground stress formula can be represented by a linear equation related to depth:

Table 4 The values of A, B, C and D are given in some regions
Note: In USA, H is measured in km

Number	Country or rock types	A	B	C	D	Reference
1	Fennoscandia	6.700	0.800	0.0444	0.0329	(Stephansson et al. 1986)
2	USA	70.000	20.000	0.1600	0.2400	(Haimson 1978)
3	China					
	Igneous rock	5.8950	0.2325	0.0318	0.0198	(Jing et al. 2008)
	sedimentary rock	4.9125	1.5673	0.0240	0.0183	
	metamorphic rock	4.0567	1.6589	0.0264	0.0194	

$$\begin{aligned}\sigma_v &= \gamma H, \\ \sigma_H^{\max} &= A + BH, \\ \sigma_H^{\min} &= C + DH,\end{aligned}\quad (48)$$

where σ_H^{\max} is the maximum horizontal principal stress, σ_H^{\min} is the minimum horizontal principal stress, A and C are the magnitude of horizontal stress at the surface, B and D are the gradient of horizontal principal stress change. As shown in Table 4, the values of A , B , C and D are given in some countries. It is noteworthy that this method is primarily suitable for regions characterized by weak geological structures and relatively flat geological formations (Long et al. 2020). According to the fitting formula, the ground stress field in deeper underground spaces can be approximated. However, the approximate ground stress field may not meet researcher' requirements for accurately determining stress values. Zhang et al. (2005) proposed an improved algorithm for calculating ground stress regression. Based on the determination of Eq. (48), this method employs distance interpolation for each Gauss point in the stress field to obtain its stress component. Consequently, an auxiliary stress field is formulated, which participates in multivariate linear regression, ultimately yielding the ground stress field for the entire computational domain. In addition, based on ground stress measured data, regression analysis can be combined with numerical simulation methods to accurately invert ground stress. This method first assumes the type and form of boundary loads, then establishes a multivariate regression equation between stress at measurement points and boundary loadings (Pu et al. 2021). Then, the obtained boundary loads are embedded into the finite element model to calculate the coefficients of the regression equation. The obtained boundary loadings would be embedded in the numerical simulation to calculate the coefficients of the regression equation. The actual ground stress field is a linear combination of these regression coefficients multiplied by the corresponding stress field. It is worth noting that ground stress multivariate linear regression analysis in engineering is mainly divided into stress regression analysis and displacement inversion analysis. However, displacements of surrounding rocks occur after engineering activities, hence stress regression analysis is preferred. The multivariate linear regression inversion method is convenient and efficient. However, as depth increases, ground stress often exhibits nonlinear variations. This method cannot address the problem of nonlinear relationships between ground stress and burial depth. To overcome this limitation, many researchers have attempted to utilize artificial neural networks and genetic algorithms for ground stress inversion. Li et al. (2020b) employed neural networks to establish the relationship between measured ground stress data and numerical calculations in the Luodu region of China. By comparing with measured data, the

combined approach of numerical analysis and neural network inversion was reliable. Yao et al. (2021) proposed a local stress field correction (LSFC) method to address the problem of discrete and nonlinear in measured stresses. The method of LSFC combines genetic algorithms and BP neural networks. By comparing with the inversion results of multivariate regression analysis, the effectiveness of LSFC was validated. Zhang et al. (2016) proposed a secondary inversion method capable of reflecting complex geological conditions, known as the stepwise regression-differential evolution-support vector Machine (SR-DE-SVM) secondary nonlinear inversion algorithm. This model can analyze the primary causes of initial ground stress formation and more accurately calculate the distribution patterns of the three-dimensional ground stress field. Nonlinear inversion methods such as neural networks and genetic algorithms offer advantages over traditional ground stress calculation methods, particularly under complex geological conditions. These methods have greater development prospects, especially for studying the distribution characteristics of initial ground stress fields in deep mining.

It is worth noting that the rationality of boundary condition settings is crucial to ensure the reliability of results during inversion (Li et al. 2009). In many studies, lateral boundary stresses are often simplified as constant values or represented through lateral pressure coefficients (Meng and He 2020). However, the relationship between lateral boundary stresses and depth is more complex. Therefore, setting reasonable boundary conditions is paramount.

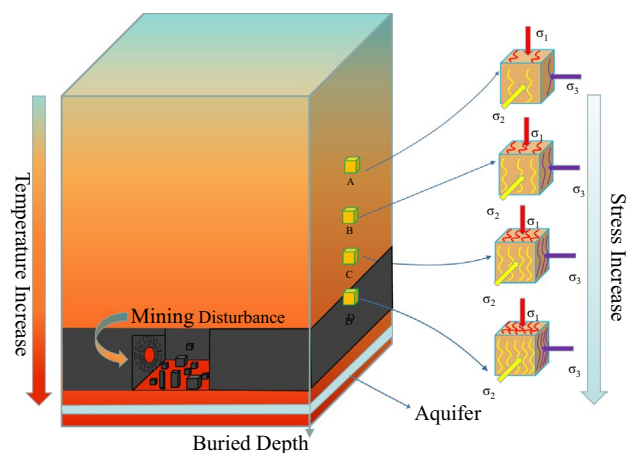


Fig. 34 Schematic diagram of deep rock environment under "three highs and one disturbance"

7 Prospect

High ground stress is the first problem that needs to be addressed in deep mining. Therefore, we provide a review of research methods for deep rock fracture under high ground stress disturbances in this paper. Researchers have conducted in-depth studies through laboratory experiments, theoretical analysis, numerical simulations, and field measurements, achieving significant results. However, the factors affecting rock fracture in deep mining extend beyond high stress. As shown in Fig. 34, deep rock is subjected to a "three highs and one disturbance" environment (high stress, high temperature, high osmotic pressure and dynamic disturbance) (He et al. 2005). In this environment, deep rock masses will exhibit more intense mechanical reactions and complex fracture mechanisms, leading to frequent occurrences of deep engineering disasters, and the mechanisms involved remain unclear, making prediction and effective control difficult.

Therefore, researchers have attempted to analyze multi-field coupling law from the perspective of multi-field coupling models, which is beneficial for understanding the mechanical responses and fracturing mechanisms of rocks, thereby reducing accidents and improving mining efficiency. Cao et al. (2020) suggested that crack instability under deep mining unloading results from gas desorption driving crack formation and expansion, and constructed models for gas pressure rise, crack formation and expansion, and instability criterion. Liu et al. (2023b) investigated crack instability in deep coal seams induced by the coupling of mining unloading and gas driving, as well as the transformation of failure modes. They established control equations for the evolution of tensile stress and gas pressure within coal-rock cracks during the unloading process and revealed the dynamic evolution patterns of tensile stress and gas pressure, along with their primary controlling factors. Fianu et al. (2020) developed an electromagnetic-thermal coupling model to describe the enhancement of shale gas production through microwave heating. The study suggests that thermal stimulation improves the rate of gas adsorption in the matrix and increases the diffusion rate of reservoir matrix, potentially boosting production by 25% within a year. Liu et al. (2023a) established an electromagnetic-thermal fluid-solid coupling model to conduct numerical simulations of the microwave heating process for shale gas. Their study suggests that the microwave power increased from 20 to 100 W, and the gas production-increasing efficiency increased from 24.6% to 156.0%. These studies have laid a solid foundation for the multi-field coupling theory in deep mining. However, the fracture mechanism and damage evolution law of rocks under the coupling of stress field, seepage field, temperature field and dynamic perturbation in

deep mining still need further research and breakthroughs. Future research should consider the influence of these factors to comprehensively understand the fracture mechanisms in deep mining, thereby enhancing the safety and efficiency of deep mining operations. The research methods reviewed in this paper can also provide some references for the selection of research methods in future deep mining studies.

8 Summary

In the past few decades, a large number of scholars from the experimental, theoretical, and computational perspectives to study the fracture mechanism of the deep rock mass have achieved fruitful results, laying a solid foundation for deep rock mechanics has dramatically promoted the human exploration of the underground space. In this paper, the key issues involving deep rock mechanics are summarized and discussed based on an extensive collection of literature. In addition, the research methods of rock fracture mechanisms for deep underground space development are reviewed. At present, there are four methods used to study the problem: laboratory tests, theoretical analysis, numerical simulation and field measurements. Some of the summaries are as follows.

(1) The lack of consensus on the boundaries of deep mining in different countries has hindered the development and communication of deep rock mechanics, but it has become an indisputable fact that deep means high ground stress. The unification of the concept of "deep" is an urgent task in the study of deep rock mechanics. Deep mining cannot be simplified and treated as a plane strain model, which would lead to conservative analyses. In addition, the deep rock body is affected by "three highs and one disturbance"; its physical and mechanical properties are very different from the shallow part, and the traditional rock mechanics theory and method no longer apply to deep mining. It is urgent to build a theory of deep rock mechanics.

(2) The rapid development of dynamic and static true triaxial apparatus has provided key technology to solve the problem of measuring various physical and mechanical properties exhibited by rocks under deep burial conditions and has promoted the development of deep rock mechanics. The testing machine and rock shape should be improved to overcome eccentric loading and end effects when performing true triaxial tests. In addition, flaws, initial damage, and stress paths in the rock should be considered in mechanical and similar experiments on rocks. In view of the fact that the mechanical properties of the rock mass are like a "black box" and the fracture mechanism cannot be derived directly from experiments, the identification of crack initiation stress and a series of characterization methods have been established.

Experimental materials can be improved in the future, e.g. by focusing on the production of "transparent rock bodies".

(3) MC, DP, LD, MGC, HB, UST and their associated modified strength criteria are analyzed in comparison. Most strength criteria make several assumptions that make their accuracy vary considerably under different conditions and in different rock types. Among the many strength criteria, the HB series of strength criteria are more suitable for deep underground works because it considers the geological structure, intermediate principal stress, lode angle, and excavation disturbance. The three-dimensional strength criteria existing at present does not have a clear understanding of the failure surfaces in the three-dimensional stress space. In the future, many true triaxial experiments on rocks need to be carried out to clarify the effects of intermediate principal stress, hydrostatic pressure, and lode angle on the rock damage surface in the three-dimensional stress space. Constructing a three-dimensional strength criterion for rocks that conforms to the convexity and smoothness is necessary to detect the mechanism of rock fracture in deep mining more accurately.

(4) There are many numerical simulation methods, and not all are good at simulating rock fractures. The methods need to be selected according to the focus of the study. More importantly, the real mechanical properties of the rock body should be represented as much as possible based on the existing data. Numerical simulations are performed with a refined mesh to maximize the fracture technique of the numerical simulation method to capture the fracture mechanism of the rock. In addition, the ground stress equilibrium method is directly related to the accuracy of the calculation results, and the traditional equilibrium method should be eliminated. Finally, for the numerical simulation to significantly contribute to the study of deep rock fracture mechanisms, more in-depth research should be carried out in dealing with rock anisotropy and nonlinearity, improving the computational efficiency and optimizing the acquisition of parameters.

(5) There are numerous monitoring techniques, but most are limited in their application due to site constraints. Through comparative analysis, fiber-optic technology and microseismic monitoring are superior methods to study rock fracture from both macro and fine-scale perspectives. The microseismic monitoring technique still has the disadvantages of low data transmission and prediction accuracy for fractured rocks, which can be improved to time theory or new positioning methods.

Among the four methods mentioned above, none of them has an absolute advantage over the others, and none of them can completely elaborate the fracture mechanism of the deep rock mass. Researchers should give full play to the characteristics and advantages of each method, link them closely, and establish a link between microscopic damage

and macroscopic fracture to jointly elaborate the essence of the damage mechanism of the deep rock mass.

Acknowledgements The authors would like to express their sincere gratitude for the support provided by the Yunnan Province "Caiyun" Postdoctoral Innovative Project Plan (No. CG24056E004A). This invaluable assistance has been fundamental in facilitating the research presented in this paper. We are deeply appreciative of the opportunity to advance our work through the resources and guidance offered by this esteemed program.

Funding No funding was received for conducting this study.

Data availability The data used to support the findings of this study are available from the corresponding author upon request.

Declarations

Conflict of interest The authors have no relevant financial or non-financial interests to disclose.

References

- Al-Ajmi AM, Zimmerman RW (2005) Relation between the Mogi and the Coulomb failure criteria. *Int J Rock Mech Mining Sci* 42(3):431–439. <https://doi.org/10.1016/j.ijrmms.2004.11.004>
- Aliabadian Z, Zhao G-F, Russell AR (2019) Crack development in transversely isotropic sandstone discs- subjected to Brazilian tests observed using digital image correlation. *Int Journal Rock Mech Mining Sci* 119:211–221. <https://doi.org/10.1016/j.ijrmms.2019.04.004>
- An HM, Liu HY, Han H et al (2017) Hybrid finite-discrete element modelling of dynamic fracture and resultant fragment casting and muck-piling by rock blast. *Comput Geotech* 81:322–345. <https://doi.org/10.1016/j.compgeo.2016.09.007>
- An H, Song Y, Liu H (2021) FDEM modelling of rock fracture process during three-point bending test under quasistatic and dynamic loading conditions. *Shock Vib* 2021:5566992. <https://doi.org/10.1155/2021/5566992>
- Ao Y, Sun C, Jia B et al (2022) Meso fracture characteristics of granite and instability evolution law of surrounding rock in deep cavern. *Sci Rep* 12(1):2994. <https://doi.org/10.1038/s41598-022-06833-0>
- Aubertin M, Li L, Simon R et al (1999) Formulation and application of a short-term strength criterion for isotropic rocks. *Can Geotech J* 36(5):947–960. <https://doi.org/10.1139/t99-056>
- Barros G, Sapucaia V, Hartmann P et al (2023) A novel BEM-DEM coupling in the time domain for simulating dynamic problems in continuous and discontinuous media. *Comput Methods Appl Mech Eng* 410:116040. <https://doi.org/10.1016/j.cma.2023.116040>
- Bavdekar S, Subhash G (2018) Comparison of pressure-sensitive strength delts for ceramics under ultrahigh confinement. *Int J Impact Eng* 118:60–66. <https://doi.org/10.1016/j.ijimpeng.2018.04.007>
- Belytschko T, Black T (1999) Elastic crack growth in finite elements with minimal remeshing. 45:601–620
- Benz T, Schwab R (2008) A quantitative comparison of six rock failure criteria. *Int J Rock Mech Mining Sci* 45(7):1176–1186. <https://doi.org/10.1016/j.ijrmms.2008.01.007>
- Benz T, Schwab R, Kauter RA et al (2008) A Hoek-Brown criterion with intrinsic material strength factorization. *Int J Rock Mech Mining Sci* 45(2):210–222. <https://doi.org/10.1016/j.ijrmms.2007.05.003>

- Bi J, Zhao Y, Wu Z et al (2024) Research on crack classification method and failure precursor index based on RA-AF value of brittle rock. *Theoretical and Applied Fracture Mechanics* 129:104179. <https://doi.org/10.1016/j.tafmec.2023.104179>
- Bisrat S, Deshon HR, Rowe C (2012) Microseismic swarm activity in the new madrid seismic zone. *Bull Seismol Soc Am* 102(3):1167–1178. <https://doi.org/10.1785/0120100315>
- Bobet A, Fakhimi A, Johnson S et al (2009a) Numerical models in discontinuous media: review of advances for rock mechanics applications. *J Geotech Geoenviron Eng*. [https://doi.org/10.1061/\(ASCE\)GT.1943-5606.0000133](https://doi.org/10.1061/(ASCE)GT.1943-5606.0000133)
- Bobet A, Fakhimi A, Johnson S et al (2009b) Numerical models in discontinuous media: review of advances for rock mechanics applications. *J Geotech Geoenviron Eng* 135(11):1547–1561. [https://doi.org/10.1061/\(ASCE\)GT.1943-5606.0000133](https://doi.org/10.1061/(ASCE)GT.1943-5606.0000133)
- Brace WF, Paulding Jr BW, Scholz C (1966) Dilatancy in the fracture of crystalline rocks. *Journal of Geophysical Research*. 3939–3953. <https://doi.org/10.1029/JZ071i016p03939>
- Branco R, Antunes FV, Costa JD (2015) A review on 3D-FE adaptive remeshing techniques for crack growth modelling. *Eng Fracture Mech* 141:170–195. <https://doi.org/10.1016/j.engfracmech.2015.05.023>
- Brown ET, Hoek E (1978) Trends in relationships between measured in-situ stresses and depth. *Int J Rock Mech Mining Sci Geomech Abstracts* 15(4):211–215. [https://doi.org/10.1016/0148-9062\(78\)91227-5](https://doi.org/10.1016/0148-9062(78)91227-5)
- Cai M (2010) Practical estimates of tensile strength and hoek-brown strength parameter m_i of brittle rocks. *Rock Mech Rock Eng* 43(2):167–184. <https://doi.org/10.1007/s00603-009-0053-1>
- Cai M, Kaiser PK, Martin CD (2001) Quantification of rock mass damage in underground excavations from microseismic event monitoring. *Int J Rock Mech Mining Sci* 38(8):1135–1145. [https://doi.org/10.1016/S1365-1609\(01\)00068-5](https://doi.org/10.1016/S1365-1609(01)00068-5)
- Cai M, Peng H (2011) Advance of in-situ stress measurement in China. *J Rock Mech Geotech Eng* 3(4):373–384. <https://doi.org/10.3724/SP.J.1235.2011.00373>
- Cai W, Zhu H, Liang W et al (2021) A New Version of the Generalized Zhang-Zhu Strength Criterion and a Discussion on Its Smoothness and Convexity. *Rock Mech Rock Eng* 54(8):4265–4281. <https://doi.org/10.1007/s00603-021-02505-z>
- Cai W, Zhu H, Liang W (2022a) Three-dimensional stress rotation and control mechanism of deep tunneling incorporating generalized Zhang-Zhu strength-based forward analysis. *Engineering Geology*. 308:106806. <https://doi.org/10.1016/j.enggeo.2022.106806>
- Cai W, Zhu H, Liang W et al (2022b) Three-dimensional forward analysis and real-time design of deep tunneling based on digital in-situ testing. *International Journal of Mechanical Sciences*. 226:107385. <https://doi.org/10.1016/j.ijmecsci.2022.107385>
- Cai W, Zhu H, Liang W et al (2023) A post-peak dilatancy model for soft rock and its application in deep tunnel excavation. *Journal of Rock Mechanics and Geotechnical Engineering*. 15(3):683–701. <https://doi.org/10.1016/j.jrmge.2022.05.014>
- Cao W, Shi J-Q, Durucan S et al (2020) Gas-driven rapid fracture propagation under unloading conditions in coal and gas outbursts. *Int J Rock Mech Mining Sci* 130:104325. <https://doi.org/10.1016/j.ijrmms.2020.104325>
- Cao Z, Wang Y, Li D (2017) Practical reliability analysis of slope stability by advanced monte carlo simulations in a spreadsheet. *Can Geotech J* 48(1):162–172. https://doi.org/10.1007/978-3-662-52914-0_7
- Cao J, Dou L, He J et al (2023) Mechanism of the coal bursts in the working face during mining of steeply inclined and extra thick coal seam. *Geomatics, Natural Hazards and Risk*. <https://doi.org/10.1080/19475705.2023.2206511>
- Chang C, Haimson B (2000) True triaxial strength and deformability of the German Continental Deep Drilling Program (KTB) deep hole amphibolite. *Journal of Geophysical Research: Solid Earth* 105(B8):18999–19013. <https://doi.org/10.1029/2000JB900184>
- Chen Z-Q, He C, Hu X-Y et al (2021) Effect of stress paths on failure mechanism and progressive damage of hard-brittle rock. *J Mt Sci* 18(9):2486–2502. <https://doi.org/10.1007/s11629-020-6554-9>
- Chen J-Y, Lien F-S, Peng C et al (2020) GPU-accelerated smoothed particle hydrodynamics modeling of granular flow. *Powder Technol* 359:94–106. <https://doi.org/10.1016/j.powtec.2019.10.017>
- Chen B, Zuo Y, Zheng L et al (2022) Deformation failure mechanism and concrete-filled steel tubular support control technology of deep high-stress fractured roadway. *Tunnell Underground Space Technol* 129:104684. <https://doi.org/10.1016/j.tust.2022.104684>
- Cheng J, Song G, Sun X et al (2018) Research developments and prospects on microseismic source location in mines. *Engineering* 4(5):653–660. <https://doi.org/10.1016/j.eng.2018.08.004>
- Cheon D-S, Jeon S, Ryu C (2006) An experimental study on the brittle failure under true triaxial conditions. *Tunnell Underground Space Technol* 21:448–449. <https://doi.org/10.1016/j.tust.2005.12.087>
- Cong Y, Wang ZQ, Zheng YR et al (2015) Experimental study on microscopic parameters of brittle materials based on particle flow theory. *Yantu Gongcheng Xuebao/Chinese Journal of Geotechnical Engineering*. 37:1031–1040. <https://doi.org/10.11779/CJGE201506009>
- Cui L, Zheng J-J, Dong Y-K et al (2017) Prediction of critical strains and critical support pressures for circular tunnel excavated in strain-softening rock mass. *Eng Geol* 224:43–61. <https://doi.org/10.1016/j.enggeo.2017.04.022>
- Cundall PA (1971) A computer model for simulating progressive large-scale movements in blocky rock systems. *Proc.int.symp.on Rock Fracture, 1(ii-b)*, 11–8
- Das R, Cleary PW (2010) Effect of rock shapes on brittle fracture using Smoothed Particle Hydrodynamics. *Theoretical Appl Fracture Mech* 53(1):47–60. <https://doi.org/10.1016/j.tafmec.2009.12.004>
- Deb D, Pramanik R (2013) Failure process of brittle rock using smoothed particle hydrodynamics. *J Eng Mech* 139:1551–1565. [https://doi.org/10.1061/\(ASCE\)JEM.1943-7889.0000592](https://doi.org/10.1061/(ASCE)JEM.1943-7889.0000592)
- Deng CJ, He GJ (2006) Zheng YR (2006) Studies on Drucker-Prager yield criteria based on M-C yield criterion and application in geotechnical engineering. *Chinese Journal of Geotechnical Engineering* 28(6):735–739
- Desai CS, Somasundaram S, Frantzikonis G (1986) A hierarchical approach for constitutive modelling of geologic materials. *Int J Num Analyt Methods Geomech* 10(3):225–257. <https://doi.org/10.1002/nag.1610100302>
- Diederichs MS (2007) The 2003 Canadian Geotechnical Colloquium: Mechanistic interpretation and practical application of damage and spalling prediction criteria for deep tunnelling. 44(9): 1082–1116. <https://doi.org/10.1139/t07-033>
- Diering DH (1997) Ultra-deep level mining - future requirements 496KB). *Journal of the Southern African Institute of Mining and Metallurgy*. 97(6): 249–255. https://doi.org/10.10520/AJA0038223X_2438
- Ding C, Yang R, Yang L (2021) Experimental results of blast-induced cracking fractal characteristics and propagation behavior in deep rock mass. *Int J Rock Mech Mining Sci* 142:104772. <https://doi.org/10.1016/j.ijrmms.2021.104772>
- Dong L, Li X, Tang L et al (2011) Mathematical functions and parameters for microseismic source location without pre-measuring speed. *Chin J Rock Mech Eng* 30:2057–2067
- Dong L, Zhang Y, Ma J (2020) Micro-crack mechanism in the fracture evolution of saturated granite and enlightenment to the precursors of instability. *Sensors*. <https://doi.org/10.3390/s20164595>

- Drucker DC (1952) Prager WJQoAm. Soil Mechanics and Plastic Analysis or Limit Design 10:157–165
- Du K, Li X-B, Li D-Y et al (2015) Failure properties of rocks in true triaxial unloading compressive test. Transactions of Nonferrous Metals Society of China. 25(2):571–581. [https://doi.org/10.1016/S1003-6326\(15\)63639-1](https://doi.org/10.1016/S1003-6326(15)63639-1)
- Du K, Luo X, Liu M et al (2024) Understanding the evolution mechanism and classification criteria of tensile-shear cracks in rock failure process from acoustic emission (AE) characteristics. Engineering Fracture Mechanics. 296:109864. <https://doi.org/10.1016/j.engfracmech.2024.109864>
- Duan Y, Feng X-T, Li X et al (2022) Mesoscopic damage mechanism and a constitutive model of shale using in-situ X-ray CT device. Eng Fract Mech 269:108576. <https://doi.org/10.1016/j.engfracmech.2022.108576>
- Duan D, Zhao Y, Zhang R et al (2020) Acoustic emission characterization of uniaxial compression failure characteristics of mudstone based on Micro-CT. Zhendong yu Chongji/Journal of Vibration and Shock. 39:163–170 and 195. <https://doi.org/10.13465/j.cnki.jvs.2020.16.023>
- Eberhardt E, Stead D, Stimpson B et al (1998) Identifying crack initiation and propagation thresholds in brittle rock. Can Geotech J 35:222–233. <https://doi.org/10.1139/cgj-35-2-222>
- Ewy RT (1999) Wellbore-stability predictions by use of a modified lade criterion. SPE Drill Complet 14(02):85–91. <https://doi.org/10.2118/56862-PA>
- Feng F, Chen S, Li D et al (2019) Analysis of fractures of a hard rock specimen via unloading of central hole with different sectional shapes. Energy Sci Eng 7(6):2265–2286. <https://doi.org/10.1002/ese3.432>
- Feng X-T, Chen S, Zhou H (2004) Real-time computerized tomography (CT) experiments on sandstone damage evolution during triaxial compression with chemical corrosion. Int J Rock Mech Mining Sci 41(2):181–192. [https://doi.org/10.1016/S1365-1609\(03\)00059-5](https://doi.org/10.1016/S1365-1609(03)00059-5)
- Feng X-T, Kong R, Yang C et al (2020) A three-dimensional failure criterion for hard rocks under true triaxial compression. Rock Mech Rock Eng 53(1):103–111. <https://doi.org/10.1007/s00603-019-01903-8>
- Feng X-T, Tian M, Yang C et al (2023) A testing system to understand rock fracturing processes induced by different dynamic disturbances under true triaxial compression. J Rock Mech Geotech Eng 15(1):102–118. <https://doi.org/10.1016/j.jrmge.2022.02.002>
- Feng X-T, Yang C-X, Kong R et al (2022) Excavation-induced deep hard rock fracturing: Methodology and applications. J Rock Mech Geotech Eng 14(1):1–34. <https://doi.org/10.1016/j.jrmge.2021.12.003>
- Feng X-T, Zhang X, Kong R et al (2016) A novel mogi type true triaxial testing apparatus and its use to obtain complete stress-strain curves of hard rocks. Rock Mech Rock Eng 49(5):1649–1662. <https://doi.org/10.1007/s00603-015-0875-y>
- Feng X-T, Zhang J, Yang C et al (2021) A novel true triaxial test system for microwave-induced fracturing of hard rocks. J Rock Mech Geotech Eng 13(5):961–971. <https://doi.org/10.1016/j.jrmge.2021.03.008>
- Feng X-T, Zhao J, Zhang X et al (2018) A novel true triaxial apparatus for studying the time-dependent behaviour of hard rocks under high stress. Rock Mech Rock Eng 51(9):2653–2667. <https://doi.org/10.1007/s00603-018-1516-z>
- Feng X-T, Pei S-F, Jiang Q et al (2017a) Deep Fracturing of the Hard Rock Surrounding a Large Underground Cavern Subjected to High Geostress: In Situ Observation and Mechanism Analysis. Rock Mechanics and Rock Engineering. 50(8): 2155–2175. <https://doi.org/10.1007/s00603-017-1220-4>
- Feng X-T, Zhang X, Yang C et al (2017b) Evaluation and reduction of the end friction effect in true triaxial tests on hard rocks. International Journal of Rock Mechanics and Mining Sciences 97:144–148. <https://doi.org/10.1016/j.ijrmms.2017.04.002>
- Fianu J, Gholinezhad J, Hassan M (2020) Thermal simulation of shale gas recovery involving the use of microwave heating. Journal of Petroleum Science and Engineering. 186:106768. <https://doi.org/10.1016/j.petrol.2019.106768>
- Frenelus W, Peng H, Zhang J (2021) Long-term degradation, damage and fracture in deep rock tunnels: A review on the effect of excavation methods. Frattura Ed Integrità Strutturale 15:128–150. <https://doi.org/10.3221/IGF-ESIS.58.10>
- Furuzumi M, Sugimoto F (1986) Effect of intermediate principal stress on failure of rocks and failure condition of rocks under multiaxial stresses. J Jpn Soc Eng Geol 27(1):13–20. <https://doi.org/10.5110/jjseg.27.13>
- Gao M-B, Li T-B, Meng L-B et al (2018) Identifying crack initiation stress threshold in brittle rocks using axial strain stiffness characteristics. J Mt Sci 15(6):1371–1382. <https://doi.org/10.1007/s11629-018-4847-z>
- Gao Y, Gao F, Yeung MR (2019) Modeling large displacement of rock block and a work face excavation of a coal mine based on discontinuous deformation analysis and finite deformation theory. Tunnelling and Underground Space Technology. 92:103048. <https://doi.org/10.1016/j.tust.2019.103048>
- Gao Q, Ma L, Liu W et al (2023) Research on the denoising method of infrared thermogram during rock fracture. Infrared Physics & Technology. 131:104651. <https://doi.org/10.1016/j.infrared.2023.104651>
- Gong W, Wang J, Gong Y et al (2013) Thermography analysis of a roadway excavation experiment in 60° inclined stratified rocks. Int J Rock Mech Min Sci 60:134–147. <https://doi.org/10.1016/j.ijrmms.2012.12.047>
- Gong F-Q, Luo Y, Li X-B et al (2018) Experimental simulation investigation on rockburst induced by spalling failure in deep circular tunnels. Tunnelling and Underground Space Technology. 81:413–427. <https://doi.org/10.1016/j.tust.2018.07.035>
- Gong F, Wuxing W, Tianbin L et al (2019) Experimental simulation and investigation of spalling failure of rectangular tunnel under different three-dimensional stress states. International Journal of Rock Mechanics and Mining Sciences 122:104081. <https://doi.org/10.1016/j.ijrmms.2019.104081>
- Gu L, Feng X-T, Kong R et al (2023) Excavation stress path induced fracturing mechanism of hard rock in deep tunnel. Rock Mech Rock Eng 56(3):1779–1806. <https://doi.org/10.1007/s00603-022-03151-9>
- Guan K, Zhu W, Wei J et al (2018) A finite strain numerical procedure for a circular tunnel in strain-softening rock mass with large deformation. International Journal of Rock Mechanics and Mining Sciences. 112:266–280. <https://doi.org/10.1016/j.ijrmms.2018.10.016>
- Gujjala YK, Kim H-M, Ryu D-W (2023) GPGPU-based parallel computation using discrete elements in geotechnics: a state-of-art review. Arch Comput Methods Eng 30(3):1601–1622. <https://doi.org/10.1007/s11831-022-09851-3>
- Guo JQ, Jiang JG, Liu XR et al (2021). Modification of Drucker-Prager strength criterion based on the elastic strain energy. China Civil Engineering Journal. 54(6): 110–116. <https://doi.org/10.15951/j.tmgxcb.06.010>
- Haimson B, Chang C (2000) A new true triaxial cell for testing mechanical properties of rock, and its use to determine rock strength and deformability of Westerly granite. International Journal of Rock Mechanics and Mining Sciences. 37(1):285–296. [https://doi.org/10.1016/S1365-1609\(99\)00106-9](https://doi.org/10.1016/S1365-1609(99)00106-9)
- Haimson BC (1978) The hydrofracturing stress measuring method and recent field results. International Journal of Rock Mechanics and

- Mining Sciences & Geomechanics Abstracts. 15(4):167–178. [https://doi.org/10.1016/0148-9062\(78\)91223-8](https://doi.org/10.1016/0148-9062(78)91223-8)
- Hammah RE, Yacoub T, Corkum B et al. (2008). The Practical Modelling of Discontinuous Rock Masses with Finite Element Analysis. The 42nd U.S. Rock Mechanics Symposium (USRMS),
- Han H, Fukuda D, Liu H et al (2020) Combined finite-discrete element modelling of rock fracture and fragmentation induced by contour blasting during tunnelling with high horizontal in-situ stress. *Int J Rock Mech Mining S* 127:104214. <https://doi.org/10.1016/j.ijrmms.2020.104214>
- Han H, Fukuda D, Liu H et al (2020a) FDEM simulation of rock damage evolution induced by contour blasting in the bench of tunnel at deep depth. *Tunnelling and Underground Space Technology*. 103:103495. <https://doi.org/10.1016/j.tust.2020.103495>
- He M, Li J, Liu D et al (2021) A Novel True Triaxial Apparatus for Simulating Strain Bursts Under High Stress. *Rock Mech Rock Eng* 54(2):759–775. <https://doi.org/10.1007/s00603-020-02285-y>
- He M, Wang Q (2022) Excavation compensation method and key technology for surrounding rock control. *Engineering Geology* 307:106784. <https://doi.org/10.1016/j.enggeo.2022.106784>
- He M, Xie H, Peng S et al (2005) Study on rock mechanics in deep mining engineering. *Chinese Journal of Rock Mechanics and Engineering* 24:2803–2813. <https://doi.org/10.3321/j.issn:1000-6915.2005.16.001>
- He M, Miao J, Dejian L et al (2007) Experimental study on rockburst processes of granite specimen at great depth. *Chinese Journal of Rock Mechanics and Engineering* 26:865–876. <https://doi.org/10.3321/j.issn:1000-6915.2007.05.001>
- He M-C, Gong W-L, Li D-J et al (2009) Physical modeling of failure process of the excavation in horizontal strata based on IR thermography. *Mining Science and Technology (China)* 19(6):689–698. [https://doi.org/10.1016/S1674-5264\(09\)60128-9](https://doi.org/10.1016/S1674-5264(09)60128-9)
- He M, Jia X, Gong W et al (2010a) Physical modeling of an underground roadway excavation in vertically stratified rock using infrared thermography. *International Journal of Rock Mechanics and Mining Sciences* 47(7):1212–1221. <https://doi.org/10.1016/j.ijrmms.2010.06.020>
- He MC, Gong WL, Zhai HM et al (2010b) Physical modeling of deep ground excavation in geologically horizontal strata based on infrared thermography. *Tunnelling and Underground Space Technology* 25(4):366–376. <https://doi.org/10.1016/j.tust.2010.01.012>
- He M, Xia H, Jia X et al (2012) Studies on classification, criteria and control of rockbursts. *Journal of Rock Mechanics and Geotechnical Engineering* 4(2):97–114. <https://doi.org/10.3724/SP.J.1235.2012.00097>
- Heping XIE (2019) Research review of the state key research development program of China: Deep rock mechanics and mining theory. *Journal of China Coal Society*(5). <https://doi.org/10.13225/j.cnki.jccs.2019.6038>
- Hoek E, Brown Edwin T (1980) Empirical Strength Criterion for Rock Masses. *J Geotech Eng Div* 106(9):1013–1035. <https://doi.org/10.1061/AJGEB6.0001029>
- Hoek E, Brown ET (1997) Practical estimates of rock mass strength. *International Journal of Rock Mechanics and Mining Sciences* 34(8):1165–1186. [https://doi.org/10.1016/S1365-1609\(97\)80069-X](https://doi.org/10.1016/S1365-1609(97)80069-X)
- Hoek E, Brown ET (2019) The Hoek–Brown failure criterion and GSI – 2018 edition. *Journal of Rock Mechanics and Geotechnical Engineering* 11(3):445–463. <https://doi.org/10.1016/j.jrmge.2018.08.001>
- Hoek E, Diederichs MS (2006) Empirical estimation of rock mass modulus. *International Journal of Rock Mechanics and Mining Sciences* 43(2):203–215. <https://doi.org/10.1016/j.ijrmms.2005.06.005>
- Hou D, Fu X, Lu C (2021) Research on Failure Process and Precursor Information of Surrounding Rock of Deep Layered Roadway Based on Digital Image Correlation Method. *Geotech Geol Eng* 39(7):4817–4831. <https://doi.org/10.1007/s10706-021-01795-y>
- Hounsfield GN (1973) Computerized transverse axial scanning (tomography): Part 1. Description of system. *British Journal of Radiology* 46(552):1016–1022. <https://doi.org/10.1259/0007-1285-46-552-1016>
- Huang R, Wang X, Chan L (2001) Triaxial unloading test of rocks and its implication for rock burst. *Bull Eng Geol Env* 60:37–41. <https://doi.org/10.1007/s100640000082>
- Jia Z, Xie H, Zhang R et al (2020) Acoustic Emission Characteristics and Damage Evolution of Coal at Different Depths Under Triaxial Compression. *Rock Mech Rock Eng* 53(5):2063–2076. <https://doi.org/10.1007/s00603-019-02042-w>
- Jiang Q, Zhang M, Yan F et al (2021) Effect of initial minimum principal stress and unloading rate on the spalling and rockburst of marble: a true triaxial experiment investigation. *Bull Eng Geol Env* 80(2):1617–1634. <https://doi.org/10.1007/s10064-020-01995-5>
- Jiang Y, Zhou H, Lu J et al (2023) Strength, deformation, and failure characteristics of hollow cylinder sandstone under axial–torsional tests. *Bull Eng Geol Env* 82(8):296. <https://doi.org/10.1007/s10064-023-03295-0>
- Jiang Y, Zou W (2023) Sensitivity Analysis of Factors Affecting the Stability of Deep Buried Tunnel. 15(1):381. <https://www.mdpi.com/2071-1050/15/1/381>
- Jing L (2003) A review of techniques, advances and outstanding issues in numerical modelling for rock mechanics and rock engineering. *Int J Rock Mech Mining Sci* 40(3):283–353. [https://doi.org/10.1016/S1365-1609\(03\)00013-3](https://doi.org/10.1016/S1365-1609(03)00013-3)
- Jing L, Hudson JA (2002) Numerical methods in rock mechanics. *Int J Rock Mech Mining Sci* 39(4):409–427. [https://doi.org/10.1016/S1365-1609\(02\)00065-5](https://doi.org/10.1016/S1365-1609(02)00065-5)
- Jing F, Sheng Q, Zhang Y-H et al (2008) Statistical analysis of geostress distribution laws for different rocks. *Rock Soil Mech* 29:1877–1883. <https://doi.org/10.3969/j.issn.1000-7598.2008.07.028>
- Kaiser PK, Kim B-H (2015) Characterization of strength of intact brittle rock considering confinement-dependent failure processes. *Rock Mech Rock Eng* 48(1):107–119. <https://doi.org/10.1007/s00603-014-0545-5>
- Kang H, Zhang X, Si L et al (2010) In-situ stress measurements and stress distribution characteristics in underground coal mines in China. *Eng Geol* 116(3):333–345. <https://doi.org/10.1016/j.enggeo.2010.09.015>
- Karampinos E, Hadjigeorgiou J, Hazzard J et al (2015) Discrete element modelling of the buckling phenomenon in deep hard rock mines. *Int J Rock Mech Mining Sci* 80:346–356. <https://doi.org/10.1016/j.ijrmms.2015.10.007>
- Kong R, Feng X-T, Zhang X et al (2018) Study on crack initiation and damage stress in sandstone under true triaxial compression. *Int J Rock Mech Mining Sci* 106:117–123. <https://doi.org/10.1016/j.ijrmms.2018.04.019>
- Kong L, Ostadhassan M, Hou X et al (2019) Microstructure characteristics and fractal analysis of 3D-printed sandstone using micro-CT and SEM-EDS. *J Petroleum Sci Eng* 175:1039–1048. <https://doi.org/10.1016/j.petrol.2019.01.050>
- Kong R, Tuncay E, Ulusay R et al (2021) An experimental investigation on stress-induced cracking mechanisms of a volcanic rock. *Eng Geol* 280:105934. <https://doi.org/10.1016/j.enggeo.2020.105934>
- Kong B, Wang E, Li Z et al (2016) Nonlinear characteristics of acoustic emissions during the deformation and fracture of sandstone subjected to thermal treatment. *Int J Rock Mech Mining Sci* 90:43–52. <https://doi.org/10.1016/j.ijrmms.2016.10.004>
- Košek F, Dudák J, Týmlová V et al (2024) Evaluation of pore-fracture microstructure of gypsum rock fragments using micro-CT.

- Micron. 181:103633. <https://doi.org/10.1016/j.micron.2024.103633>
- Lade PV (1977) Elasto-plastic stress–strain theory for cohesionless soil with curved yield surfaces. *Int J Solids Struct* 13(11):1019–1035. [https://doi.org/10.1016/0020-7683\(77\)90073-7](https://doi.org/10.1016/0020-7683(77)90073-7)
- Lade P, Duncan J (1975) Elastoplastic stress–strain theory for Cohesionless soil. *ASCE J Geotech Eng Div* 101:1037–1053. <https://doi.org/10.1061/AJGEB6.0000204>
- Lajtai EZ (1974) Brittle fracture in compression. *Int J Fract* 10(4):525–536. <https://doi.org/10.1007/BF00155255>
- Lee D-H, Juang CH, Chen J-W et al (1999) Stress paths and mechanical behavior of a sandstone in hollow cylinder tests. *Int J Rock Mech Mining Sci* 36(7):857–870. [https://doi.org/10.1016/S0148-9062\(99\)00063-7](https://doi.org/10.1016/S0148-9062(99)00063-7)
- Lee Y-Z, Schubert W (2008) Determination of the round length for tunnel excavation in weak rock. *Tunnell Underground Space Technol* 23(3):221–231. <https://doi.org/10.1016/j.tust.2007.04.001>
- Li B, Ding Q-F, Xu N-W et al (2020a) Mechanical response and stability analysis of rock mass in high geostress underground powerhouse caverns subjected to excavation. *J Central South University* 27(10):2971–2984. <https://doi.org/10.1007/s11771-020-4522-8>
- Li X, Du K, Li D (2015b) True triaxial strength and failure modes of cubic rock specimens with unloading the minor principal stress. *Rock Mech Rock Eng* 48(6):2185–2196. <https://doi.org/10.1007/s00603-014-0701-y>
- Li G, Hu Y, Li QB et al (2020b) Inversion method of in-situ stress and rock damage characteristics in dam site using neural network and numerical simulation—a case study. *IEEE Access* 8:46701–46712. <https://doi.org/10.1109/ACCESS.2020.2979024>
- Li X, Li D, Guo L et al (2007) Study on mechanical response of highly-stressed pillars in deep mining under dynamic disturbance. *Chinese J Rock Mech Eng*. <https://doi.org/10.3321/j.issn:1000-6915.2007.05.008>
- Li H-B, Liu M-C, Xing W-B et al (2017a) Failure mechanisms and evolution assessment of the excavation damaged zones in a large-scale and deeply buried underground powerhouse. *Rock Mech Rock Eng* 50(7):1883–1900. <https://doi.org/10.1007/s00603-017-1208-0>
- Li G, Ma F, Liu G et al (2019) A strain-softening constitutive model of heterogeneous rock mass considering statistical damage and its application in numerical modeling of deep roadways. *Sustainability*. <https://doi.org/10.3390/su11082399>
- Li G, Mizuta Y, Ishida T et al (2009) Stress field determination from local stress measurements by numerical modelling. *Int J Rock Mech Mining Sci* 46(1):138–147. <https://doi.org/10.1016/j.ijrmms.2008.07.009>
- Li Y, Oh J, Mitra R et al (2016) A constitutive model for a laboratory rock joint with multi-scale asperity degradation. *Comput Geotech* 72:143–151. <https://doi.org/10.1016/j.compgeo.2015.10.008>
- Li L, Shang C, Chu K et al (2021) Large-scale geo-mechanical model tests for stability assessment of super-large cross-section tunnel. *Tunnell Underground Space Technol* 109:103756. <https://doi.org/10.1016/j.tust.2020.103756>
- Li SC, Wang Q, Wang HT et al (2015) Model test study on surrounding rock deformation and failure mechanisms of deep roadways with thick top coal. *Tunnell Underground Space Technol* 47:52–63. <https://doi.org/10.1016/j.tust.2014.12.013>
- Li S, Wang Z, Wang J et al (2023c) Analysis on mechanical behavior and progressive failure of deep-buried marble based on complete stress–strain curves. *Bull Eng Geol Environ* 82(4):133. <https://doi.org/10.1007/s10064-023-03123-5>
- Li S, Wang Z, Wang JG et al (2023) Analysis on mechanical behavior and progressive failure of deep-buried marble based on complete stress–strain curves. *Bull Eng Geol Environ*. <https://doi.org/10.1007/s10064-023-03123-5>
- Li H, Xu J-T, Zhang Z-L et al (2023a) A generalized unified strength theory for rocks. *Rock Mech Rock Eng* 56:1–18. <https://doi.org/10.1007/s00603-023-03471-4>
- Li M, Yin G, Xu J et al (2016a) A novel true triaxial apparatus to study the geomechanical and fluid flow aspects of energy exploitations in geological formations. *Rock Mech Rock Eng* 49(12):4647–4659. <https://doi.org/10.1007/s00603-016-1060-7>
- Li B, Zhang W, Xue Y et al (2022) An image segmentation-based method for quantifying the rock failure mechanism under true triaxial compression. *Int J Rock Mech Mining Sci* 158:105195. <https://doi.org/10.1016/j.ijrmms.2022.105195>
- Li H, Zhong R, Pel L et al (2023b) A new volumetric strain-based method for determining the crack initiation threshold of rocks under compression. *Rock Mech Rock Eng*. <https://doi.org/10.1007/s00603-023-03619-2>
- Li N, Wang E, Ge M et al (2014) A method for identifying outlier signals for microseismic event based on arrival time difference. *Yanshilixue Yu Gongcheng Xuebao/Chinese Journal of Rock Mechanics and Engineering*. 33: 1654–1661. <https://doi.org/10.13722/j.cnki.jrme.2014.08.016>
- Li X, Zhou J, Wang S et al (2017b) Review and practice of deep mining for solid mineral resources. *Chinese Journal of Nonferrous Metals*. 27:1236–1262. <https://doi.org/10.19476/j.ysxb.1004.0609.2017.06.021>
- Lin P, Liu H, Zhou W (2015) Experimental study on failure behaviour of deep tunnels under high in-situ stresses. *Tunnell Underground Space Technol* 46:28–45. <https://doi.org/10.1016/j.tust.2014.10.009>
- Lin F, Li S, Xue Y et al (2010) Microseismic sources location methods based on different initial values. *Chinese Journal of Rock Mechanics and Engineering* 29:996–1002. <http://dspace.xmu.edu.cn:8080/dspace/handle/2288/17803>
- Lisjak A, Figi D, Grasselli G (2014) Fracture development around deep underground excavations: Insights from FDEM modeling. *J Rock Mech Geotech Eng*. <https://doi.org/10.1016/j.jrmge.2014.09.003>
- Lisjak A, Grasselli G (2014) A review of discrete modeling techniques for fracturing processes in discontinuous rock masses. *J Rock Mech Geotech Eng* 6(4):301–314. <https://doi.org/10.1016/j.jrmge.2013.12.007>
- Liu H, Kang Y, Lin P (2013a) Hybrid finite–discrete element modeling of geomaterials fracture and fragment muck-piling. *Int J Geotech Eng* 9(1939787913Y):1939787000. <https://doi.org/10.1179/1939787913Y.0000000035>
- Liu Y, Li H, Luo C et al (2013) In situ stress measurements by hydraulic fracturing in the Western Route of South to North Water Transfer Project in China. *Eng Geol*. <https://doi.org/10.1016/j.enggeo.2013.11.008>
- Liu T, Li M, Zou Q et al (2023) Crack instability in deep coal seam induced by the coupling of mining unloading and gas driving and transformation of failure mode. *Int J Rock Mech Mining Sci* 170:105526. <https://doi.org/10.1016/j.ijrmms.2023.105526>
- Liu W, Ma L, Gao Q et al (2023c) Fracture precursor recognition and damage quantitative characterization of stressed rock using infrared radiation. *Rock Mech Rock Eng* 56(8):5567–5584. <https://doi.org/10.1007/s00603-023-03344-w>
- Liu Z, Ma C, Wei X-A (2022) Electron scanning characteristics of rock materials under different loading methods: a review. *Geomech Geophys Geo-Energy Geo-Resources* 8(2):80. <https://doi.org/10.1007/s40948-022-00392-4>
- Liu J-P, Wang R, Lei G et al (2020) Studies of stress and displacement distribution and the evolution law during rock failure process based on acoustic emission and microseismic monitoring. *Int J Rock Mech Mining Sci* 132:104384. <https://doi.org/10.1016/j.ijrmms.2020.104384>

- Liu J, Xue Y, Fu Y et al (2023) Numerical investigation on microwave-thermal recovery of shale gas based on a fully coupled electromagnetic, heat transfer, and multiphase flow model. *Energy* 263:126090. <https://doi.org/10.1016/j.energy.2022.126090>
- Long Y, Liu J-P, Lei G et al (2020) Progressive fracture processes around tunnel triggered by blast disturbances under biaxial compression with different lateral pressure coefficients. *Transactions of Nonferrous Metals Society of China*. 30(9):2518–2535. [https://doi.org/10.1016/S1003-6326\(20\)65398-5](https://doi.org/10.1016/S1003-6326(20)65398-5)
- Lou Q, He X (2018) Experimental study on infrared radiation temperature field of concrete under uniaxial compression. *Infrared Physics & Technology* 90:20–30. <https://doi.org/10.1016/j.infrared.2018.01.033>
- Lu J, Jiang C, Jin Z et al (2021) Three-dimensional physical model experiment of mining-induced deformation and failure characteristics of roof and floor in deep underground coal seams. *Process Safety Environ Protect* 150:400–415. <https://doi.org/10.1016/j.psep.2021.04.029>
- Lu J, Yin G, Gao H et al (2020) True Triaxial Experimental Study of Disturbed Compound Dynamic Disaster in Deep Underground Coal Mine. *Rock Mech Rock Eng* 53(5):2347–2364. <https://doi.org/10.1007/s00603-019-02041-x>
- Lu J, Yin G, Zhang D et al (2021) Mechanical properties and failure mode of sandstone specimen with a prefabricated borehole under true triaxial stress condition. *Geomech Energy Environ* 25:100207. <https://doi.org/10.1016/j.gete.2020.100207>
- Ma H, Wang W, Liu Q et al (2022) Extremely large deformation of tunnel induced by rock mass fracture using GPGPU parallel FDEM. *Int J Numerical Analyt Methods Geomech* 46(9):1782–1807. <https://doi.org/10.1002/nag.3368>
- Malan F, Basson DJJOTSaIOM, Metallurgy (1998) Ultra-deep mining: The increased potential for squeezing conditions. *Journal of The South African Institute of Mining and Metallurgy*. <https://doi.org/10.1007/s11837-998-0290-x>
- Maolin T, Han L, Yang X et al (2022) Asymmetric deformation failure mechanism and support technology of roadways under non-uniform pressure from a mining disturbance. *Bull Eng Geol Env* 81:211. <https://doi.org/10.1007/s10064-022-02710-2>
- Martin CD, Chandler NA (1994) The progressive fracture of Lac du Bonnet granite. *Int J Rock Mech Mining Sci Geomech Abstracts* 31(6):643–659. [https://doi.org/10.1016/0148-9062\(94\)90005-1](https://doi.org/10.1016/0148-9062(94)90005-1)
- Mccullough EC (1975) Photon attenuation in computed tomography. *Med Phys* 2(6):307–320. <https://doi.org/10.1118/1.594199>
- Meng Q-B, Liu J-F, Xie L-X et al (2021) Experimental mechanical strength and deformation characteristics of deep damaged-fractured rock. *Bull Eng Geol Env* 81(1):32. <https://doi.org/10.1007/s10064-021-02529-3>
- Meng W, He C. (2020). Back Analysis of the Initial Geo-Stress Field of Rock Masses in High Geo-Temperature and High Geo-Stress. *Energies*. <https://doi.org/10.3390/en13020363>
- Michelis P (1985) Polyaxial Yielding of Granular Rock. *J Eng Mech* 111(8):1049–1066. [https://doi.org/10.1061/\(ASCE\)0733-9399\(1985\)111:8\(1049\)](https://doi.org/10.1061/(ASCE)0733-9399(1985)111:8(1049))
- Mogi K (1967) Effect of the intermediate principal stress on rock failure. *J Geophys Res* 72(20):5117–5131. <https://doi.org/10.1029/JZ072i020p05117>
- Mogi K (1971) Fracture and flow of rocks under high triaxial compression. *J Geophys Res* 76(5):1255–1269. <https://doi.org/10.1029/JB076i005p01255>
- Mogi K. (1962). Study of Elastic Shocks Caused by the Fracture of Heterogeneous Materials and its Relations to Earthquake Phenomena.
- Mohammadnejad M, Dehkhoda S, Fukuda D et al (2020) GPGPU-parallelised hybrid finite-discrete element modelling of rock chipping and fragmentation process in mechanical cutting. *J Rock Mech Geotech Eng* 12(2):310–325. <https://doi.org/10.1016/j.jrmge.2019.12.004>
- Mohammadnejad M, Liu H, Chan A et al (2018) An overview on advances in computational fracture mechanics of rock. *Geosyst Eng* 24:1–24. <https://doi.org/10.1080/12269328.2018.1448006>
- Munjiza A, Owen DRJ, Bicanic N (1995) A combined finite-discrete element method in transient dynamics of fracturing solids. *Eng Comput* 12(2):145–174. <https://doi.org/10.1108/02644409510799532>
- Nasseri MHB, Goodfellow SD, Lombos L et al (2014) 3-D transport and acoustic properties of Fontainebleau sandstone during true-triaxial deformation experiments. *Int J Rock Mech Mining Sci* 69:1–18. <https://doi.org/10.1016/j.ijrmmms.2014.02.014>
- Nicksiar M, Martin CD (2012) Evaluation of methods for determining crack initiation in compression tests on low-porosity rocks. *Rock Mech Rock Eng* 45(4):607–617. <https://doi.org/10.1007/s00603-012-0221-6>
- Nikolic M, Roje-Bonacci T, Ibrahimbegovic A (2016) Overview of the numerical methods for the modelling of rock mechanics problems. *Technical Gazette, Scientific-professional Journal of Technical Faculties of University in Osijek*. 23:627–637. <https://doi.org/10.17559/TV-20140521084228>
- Ohno K, Ohtsu M (2010) Crack classification in concrete based on acoustic emission. *Construct Building Mater* 24(12):2339–2346. <https://doi.org/10.1016/j.conbuildmat.2010.05.004>
- Pan XD, Hudson JA. (1988). A Simplified Three Dimensional Hoek-Brown Yield Criterion. *ISRM International Symposium*.
- Pu Y, Apel DB, Prusek S et al (2021) Back-analysis for initial ground stress field at a diamond mine using machine learning approaches. *Nat Hazards* 105(1):191–203. <https://doi.org/10.1007/s11069-020-04304-1>
- Qian Q, Li S (2008) Review of research on zonal disintegration phenomenon in deep rock mass engineering. *Chinese J Rock Mech Eng* 27:1278–1284. <https://doi.org/10.3321/j.issn:1000-6915.2008.06.024>
- Qian L, Yao T, Mo Z et al (2021) GAN inversion method of an initial in situ stress field based on the lateral stress coefficient. *Sci Rep* 11:21825. <https://doi.org/10.1038/s41598-021-01307-1>
- Qian Q, Zhou X (2018) Failure behaviors and rock deformation during excavation of underground cavern group for jinping i hydropower station. *Rock Mech Rock Eng* 51(8):2639–2651. <https://doi.org/10.1007/s00603-018-1518-x>
- Rabczuk T (2013) Computational Methods for Fracture in Brittle and Quasi-Brittle Solids: State-of-the-Art Review and Future Perspectives. *ISRN Applied Mathematics* 2013. <https://doi.org/10.1155/2013/849231>
- Ren B, Shen Y, Zhao T et al (2023) Deformation monitoring and remote analysis of ultra-deep underground space excavation. *Underground Space* 8:30–44. <https://doi.org/10.1016/j.undsp.2022.04.005>
- Ren B, Zhu H, Shen Y et al. (2021). Deformation monitoring of ultra-deep foundation excavation using distributed fiber optic sensors. *IOP Conference Series: Earth and Environmental Science*. <https://doi.org/10.1088/1755-1315/861/7/072057>
- Shen B, Shi J, Barton N (2018) An approximate nonlinear modified Mohr-Coulomb shear strength criterion with critical state for intact rocks. *Journal of Rock Mechanics and Geotechnical Engineering*. 10(4):645–652
- Shi D, Wang J, Xiong L (2022a) Study on Noise Correction Algorithm of Infrared Emissivity of Rock under Uniaxial Compression. *Sustainability* 14(19):12769. <https://www.mdpi.com/2071-1050/14/19/12769>

- Shi H, Song L, Zhang H et al (2022b) Experimental and numerical studies on progressive debonding of grouted rock bolts. *International Journal of Mining Science and Technology*. 32(1):63–74. <https://doi.org/10.1016/j.ijmst.2021.10.002>
- Sibai M, Henry JP, Gros JC (1997) Hydraulic fracturing stress measurement using a true triaxial apparatus. *Int J Rock Mech Mining Sci* 34(3):289.e281–289.e210. [https://doi.org/10.1016/S1365-1609\(97\)00058-0](https://doi.org/10.1016/S1365-1609(97)00058-0)
- Singh M, Raj A, Singh B (2011) Modified Mohr–Coulomb criterion for non-linear triaxial and polyaxial strength of intact rocks. *International Journal of Rock Mechanics and Mining Sciences*. 48(4):546–555
- Skoczylas F, Henry JP (1995) A study of the intrinsic permeability of granite to gas. *International Journal of Rock Mechanics and Mining Sciences & Geomechanics Abstracts*. 32(2):171–179. [https://doi.org/10.1016/0148-9062\(94\)00022-U](https://doi.org/10.1016/0148-9062(94)00022-U)
- Smart BGD (1995) A true triaxial cell for testing cylindrical rock specimens. *Int J Rock Mech Mining Sci Geomech Abstracts* 32(3):269–275. [https://doi.org/10.1016/0148-9062\(94\)00042-2](https://doi.org/10.1016/0148-9062(94)00042-2)
- Song L, Li H-Z, Chan CL et al (2016) Reliability analysis of underground excavation in elastic-strain-softening rock mass. *Tunnell Underground Space Technol* 60:66–79. <https://doi.org/10.1016/j.tust.2016.06.015>
- Song H, Pei H, Zhu HJM (2021) Monitoring of tunnel excavation based on the fiber Bragg grating sensing technology. *Measurement*. <https://doi.org/10.1016/j.measurement.2020.108334>
- Spetzler HA, Sobolev GA, Sondergeld CH et al (1981) Surface deformation, crack formation, and acoustic velocity changes in pyrophyllite under polyaxial loading. *Journal of Geophysical Research: Solid Earth*. 86(B2):1070–1080. <https://doi.org/10.1029/JB086iB02p01070>
- Stephansson O, Särkkä P, Myrvang A. (1986). State of Stress In Fennoscandia. ISRM International Symposium.
- Su G, Chen Z, Ju JW et al (2017) Influence of temperature on the strainburst characteristics of granite under true triaxial loading conditions. *Eng Geol* 222:38–52. <https://doi.org/10.1016/j.enggeo.2017.03.021>
- Su G, Zhai S, Jiang J et al (2017b) Influence of Radial Stress Gradient on Strainbursts: An Experimental Study. *Rock Mech Rock Eng* 50(10):2659–2676. <https://doi.org/10.1007/s00603-017-1266-3>
- Su F, Pan P, Gao Y et al (2018) Experimental study on failure process and mechanism of marble containing natural hard structural plane. *Yanshilixue Yu Gongcheng Xuebao/Chinese Journal of Rock Mechanics and Engineering*. 37:611–620. <https://doi.org/10.13722/j.cnki.jrme.2017.1279>
- Su C, Cai W, Zhu H (2022) Elastoplastic semi-analytical investigation on a deep circular tunnel incorporating generalized Zhang–Zhu rock mass strength. *Computers and Geotechnics*. 150:104926. <https://doi.org/10.1016/j.compgeo.2022.104926>
- Sun C, Jin C, Wang L et al (2022a) Creep damage characteristics and local fracture time effects of deep granite. *Bull Eng Geol Env* 81(2):79. <https://doi.org/10.1007/s10064-022-02578-2>
- Sun H, Ma L, Konietzky H et al (2022b) Characteristics and generation mechanisms of key infrared radiation signals during damage evolution in sandstone. *Acta Geotech* 17(5):1753–1763. <https://doi.org/10.1007/s11440-021-01331-5>
- Sun X, Song P, Zhao C et al (2018b) Physical modeling experimental study on failure mechanism of surrounding rock of deep-buried soft tunnel based on digital image correlation technology. *Arab J Geosci* 11(20):624. <https://doi.org/10.1007/s12517-018-3979-3>
- Sun X, Xu H, He M et al (2017) Experimental investigation of the occurrence of rockburst in a rock specimen through infrared thermography and acoustic emission. *Int J Rock Mech Mining Sci* 93:250–259. <https://doi.org/10.1016/j.ijrmms.2017.02.005>
- Sun X, Zhao C, Tao Z et al (2021b) Failure mechanism and control technology of large deformation for Muzhailing Tunnel in stratified rock masses. *Bull Eng Geol Env* 80(6):4731–4750. <https://doi.org/10.1007/s10064-021-02222-5>
- Sun L, Zhao J, Zhao G (2012) Contact description in numerical simulation for Rock mechanics. *Harmonising Rock Engineering and the Environment - Proceedings of the 12th ISRM International Congress on Rock Mechanics*:541–544. <https://doi.org/10.1201/b11646-94>
- Sun H, Ma L, Adeleke N et al (2017a) Background thermal noise correction methodology for average infrared radiation temperature of coal under uniaxial loading. *Infrared Physics & Technology* 81:157–165. <https://doi.org/10.1016/j.infrared.2017.01.001>
- Sun X, Chen F, Miao C et al (2018a) Physical modeling of deformation failure mechanism of surrounding rocks for the deep-buried tunnel in soft rock strata during the excavation. *Tunnelling and Underground Space Technology* 74:247–261. <https://doi.org/10.1016/j.tust.2018.01.022>
- Sun Q, Ma F, Guo J et al (2021a) Excavation-induced deformation and damage evolution of deep tunnels based on a realistic stress path. *Computers and Geotechnics* 129:103843. <https://doi.org/10.1016/j.compgeo.2020.103843>
- Tahmasebi P (2023) A state-of-the-art review of experimental and computational studies of granular materials: properties, advances, challenges, and future directions. *Progress Mater Sci* 138:101157. <https://doi.org/10.1016/j.pmatsci.2023.101157>
- Tal Y, Hatzor YH, Feng X-T (2014) An improved numerical manifold method for simulation of sequential excavation in fractured rocks. *Int J Rock Mech Mining Sci* 65:116–128. <https://doi.org/10.1016/j.ijrmms.2013.10.005>
- Tang H, Ji X, Zhang H et al (2022) Numerical simulation of large compression deformation disaster and supporting behavior of deep buried soft rock tunnel with high in situ stress based on CDEM. *Adv Civil Eng* 2022:5985165. <https://doi.org/10.1155/2022/5985165>
- Tang CA, Wang J, Zhang J (2010) Preliminary engineering application of microseismic monitoring technique to rockburst prediction in tunneling of Jinping II project. *J Rock Mech Geotech Eng* 2(3):193–208. <https://doi.org/10.3724/SP.J.1235.2010.00193>
- Tao M, Huatao Z, Momeni A et al (2020) Fracture failure analysis of elliptical hole bored granodiorite rocks under impact loads. *Theoret Appl Fract Mech* 107:102516. <https://doi.org/10.1016/j.tafmec.2020.102516>
- Ting A, Ru Z, Jianfeng L et al (2012) Space–time evolution rules of acoustic emission location of unloaded coal sample at different loading rates. *Int J Mining Sci Technol* 22(6):847–854. <https://doi.org/10.1016/j.ijmst.2012.12.001>
- Tiwari G, Pandit B, Latha Gali M et al (2018) Analysis of tunnel support requirements using deterministic and probabilistic approaches in average quality rock mass. *Int J Geomech* 18(4):04018017. [https://doi.org/10.1061/\(ASCE\)/GM.1943-5622.0001113](https://doi.org/10.1061/(ASCE)/GM.1943-5622.0001113)
- Vazaios I, Vlachopoulos N, Diederichs MS (2019) Assessing fracturing mechanisms and evolution of excavation damaged zone of tunnels in interlocked rock masses at high stresses using a finite-discrete element approach. *J Rock Mech Geotech Eng* 11(4):701–722. <https://doi.org/10.1016/j.jrmge.2019.02.004>
- Verman M, Singh B, Viladkar MN et al (1997) Effect of tunnel depth on modulus of deformation of rock mass. *Rock Mech Rock Eng* 30(3):121–127. <https://doi.org/10.1007/BF01047388>
- Vogel M, Rast HP (2000) AlpTransit—safety in construction as a challenge: health and safety aspects in very deep tunnel construction. *Tunnell Underground Space Technol* 15(4):481–484. [https://doi.org/10.1016/S0886-7798\(01\)00018-9](https://doi.org/10.1016/S0886-7798(01)00018-9)
- Walton G, Sinha S (2022) Challenges associated with numerical back analysis in rock mechanics. *J Rock Mech Geotech Eng* 14(6):2058–2071. <https://doi.org/10.1016/j.jrmge.2022.01.010>

- Wang Y, Huang J, Wang G (2022) Numerical analysis for mining-induced stress and plastic evolution involving influencing factors: high stress, excavation rate and multilayered heterogeneity. *Eng Comput* 39(8):2928–2957. <https://doi.org/10.1108/EC-10-2021-0614>
- Wang M, Li J, Ma L et al (2016b) Study on the characteristic energy factor of the deep rock mass under weak disturbance. *Rock Mech Rock Eng* 49(8):3165–3173. <https://doi.org/10.1007/s00603-016-0968-2>
- Wang Y, Li X, Wu Y et al (2014) Research on relationship between crack initiation stress level and brittleness indices for brittle rocks. *Chinese J Rock Mech Eng* 33:264–275. <https://doi.org/10.13722/j.cnki.jrme.2014.02.003>
- Wang C, Lu Z, Liu L et al (2016) Predicting points of the infrared precursor for limestone failure under uniaxial compression. *Int J Rock Mech Mining Sci* 88:34–43. <https://doi.org/10.1016/j.ijrmms.2016.07.004>
- Wang Y, Miller JD (2020) Current developments and applications of micro-CT for the 3D analysis of multiphase mineral systems in geomaterials. *Earth-Sci Rev* 211:103406. <https://doi.org/10.1016/j.earscirev.2020.103406>
- Wang J, Wu S, Chang X et al (2023) A novel three-dimensional nonlinear unified failure criterion for rock materials. *Acta Geotech*. <https://doi.org/10.1007/s11440-023-02114-w>
- Wang J, Chen W, Su R et al (2006) Geological disposal of high-level radioactive waste and its key scientific issues. *Chinese Journal of Rock Mechanics and Engineering*. 25: 801–812
- Wawersik WR, Carlson LW, Holcomb DJ et al (1997) New method for true-triaxial rock testing. *Int J Rock Mech Mining Sci* 34(3):331–314. [https://doi.org/10.1016/S1365-1609\(97\)00049-X](https://doi.org/10.1016/S1365-1609(97)00049-X)
- Wei M, Song D, He X et al (2020) Effect of rock properties on electromagnetic radiation characteristics generated by rock fracture during uniaxial compression. *Rock Mech Rock Eng* 53(11):5223–5238. <https://doi.org/10.1007/s00603-020-02216-x>
- Wen T, Tang H, Ma J et al (2018) Evaluation of methods for determining crack initiation stress under compression. *Eng Geol* 235:81–97. <https://doi.org/10.1016/j.enggeo.2018.01.018>
- Wu S, Chen L, Cheng Z (2019) Macro and meso research on the zonal disintegration phenomenon and the mechanism of deep brittle rock mass. *Eng Fract Mech* 211:254–268. <https://doi.org/10.1016/j.engfracmech.2019.02.023>
- Wu G, Chen W, Dai Y et al (2017) Application of a type of strain block FBG sensor for strain measurements of squeezing rock in a deep-buried tunnel. *Meas Sci Technol* 28(11):115001. <https://doi.org/10.1088/1361-6501/aa8336>
- Wu P, Fang Z, Wang X et al (2023) Reliability evaluation and prediction of deep buried tunnel based on similarity theory and model test. *KSCE J Civ Eng* 27(6):2654–2665. <https://doi.org/10.1007/s12205-023-0386-4>
- Wu Z, Jiang Y, Liu Q et al (2018) Investigation of the excavation damaged zone around deep TBM tunnel using a Voronoi-element based explicit numerical manifold method. *Int J Rock Mech Mining Sci* 112:158–170. <https://doi.org/10.1016/j.ijrmms.2018.10.022>
- Wu L, Liu S, Wu Y et al (2006) Precursors for rock fracturing and failure—Part II: IRR T-Curve abnormalities. *Int J Rock Mech Mining Sci* 43(3):483–493. <https://doi.org/10.1016/j.ijrmms.2005.09.001>
- Wu Z, Ma L, Fan L (2018) Investigation of the characteristics of rock fracture process zone using coupled FEM/DEM method. *Eng Fract Mech* 200:355–374. <https://doi.org/10.1016/j.engfracmech.2018.08.015>
- Wu L, Wang J (1998) Infrared radiation features of coal and rocks under loading. *Int J Rock Mech Mining Sci* 35:969–976. [https://doi.org/10.1016/S0148-9062\(98\)00007-2](https://doi.org/10.1016/S0148-9062(98)00007-2)
- Wu S, Zhang S, Zhang G (2018a) Three-dimensional strength estimation of intact rocks using a modified Hoek-Brown criterion based on a new deviatoric function. *Int J Rock Mech Min Sci*. 107:181–190
- Xiao P, Li T, Xu N et al (2019) Microseismic monitoring and deformation early warning of the underground caverns of Lianghekou hydropower station. *Southwest China Arabian J Geosci* 12(16):496. <https://doi.org/10.1007/s12517-019-4683-7>
- Xie H, Lu J, Li C et al (2022) Experimental study on the mechanical and failure behaviors of deep rock subjected to true triaxial stress: a review. *Int J Mining Sci Technol* 32(5):915–950. <https://doi.org/10.1016/j.ijmst.2022.05.006>
- Xie H, Ju Y, Li LY (2005) Criteria for strength and structural failure of rocks based on energy dissipation and energy release principles. *Chinese Journal of Rock Mechanics and Engineering*. 24: 3003–3010.
- Xu J, Li S, Tang X et al (2008) Influential factors of acoustic emission location experiment of rock under uniaxial compression. *Chinese J Rock Mech Eng* 27:765–772. <https://doi.org/10.3321/j.issn:1000-6915.2008.04.016>
- Yan P, Lu W-B, Chen M et al (2015) Contributions of in-situ stress transient redistribution to blasting excavation damage zone of deep tunnels. *Rock Mech Rock Eng* 48(2):715–726. <https://doi.org/10.1007/s00603-014-0571-3>
- Yang S-Q, Ni H-M, Wen S (2014) Spatial acoustic emission evolution of red sandstone during multi-stage triaxial deformation. *J Central South Univ* 21(8):3316–3326. <https://doi.org/10.1007/s11771-014-2305-9>
- Yang S-Q, Tao Y, Xu P et al (2019) Large-scale model experiment and numerical simulation on convergence deformation of tunnel excavating in composite strata. *Tunnell Underground Space Technol* 94:103133. <https://doi.org/10.1016/j.tust.2019.103133>
- Yang S-Q, Tian W-L, Jing H-W et al (2019b) Deformation and damage failure behavior of mudstone specimens under single-stage and multi-stage triaxial compression. *Rock Mech Rock Eng* 52(3):673–689. <https://doi.org/10.1007/s00603-018-1622-y>
- Yang Y, Wu Z, Zuo Y et al (2023) Three-dimensional numerical simulation study of pre-cracked shale based on CT technology. *Front Earth Sci*. <https://doi.org/10.3389/feart.2022.1120630>
- Yang S-Q, Yin P-F, Huang Y-H et al (2019c) Strength, deformability and X-ray micro-CT observations of transversely isotropic composite rock under different confining pressures. *Eng Fract Mech* 214:1–20. <https://doi.org/10.1016/j.engfracmech.2019.04.030>
- Yao T, Mo Z, Qian L et al (2021) Local stress field correction method based on a genetic algorithm and a BP neural network for in situ stress field inversion. *Adv Civil Eng* 2021:4396168. <https://doi.org/10.1155/2021/4396168>
- Yong W, Ai Xiang W, Jun Y et al (2023) Progress and prospective of the mining key technology for deep metal mines. *Chinese J Eng*. <https://doi.org/10.13374/j.issn2095-9389.2022.11.12.004>
- Yu MH, He LN. (1992). TS2e4-A New Model and Theory on Yield and Failure of Materials Under The Complex Stress State. *Mechanical Behaviour of Materials VI* <https://doi.org/10.1016/B978-0-08-037890-9.50389-6>
- Yu MH, H LN, L CY (1992) Generalized twin shear stress yield criterion and its generalization
- Yu YZ, Zhang XT, Wang Y. et al. 2020 State-Of-The-Art: Experimental Study On Mechanical Properties Of Rockfill Materials Under True Triaxial Conditions. *Engineering Mechanics*. 37(4): 1–21,29. <https://doi.org/10.6052/j.issn.1000-4750.2019.07.ST04>
- Yuan C, Guo Y, Wang W et al (2020) Study on "Triaxial Loading-Unloading-Uniaxial Loading" and Microscopic Damage Test of Sandstone. <https://doi.org/10.3389/feart.2020.00078>

- Zhan Y, Yu M (2013) Generalized nonlinear unified strength theory of rock. *J Southwest Jiaotong Univ* 48:616–624. <https://doi.org/10.3969/j.issn.0258-2724.2013.04.005>
- Zhang L (2008) A generalized three-dimensional Hoek-Brown strength criterion. *Rock Mech Rock Eng* 41(6):893–915. <https://doi.org/10.1007/s00603-008-0169-8>
- Zhang Y, Feng X-T, Yang C et al (2021b) Evaluation method of rock brittleness under true triaxial stress states based on pre-peak deformation characteristic and post-peak energy evolution. *Rock Mech Rock Eng* 54(3):1277–1291. <https://doi.org/10.1007/s00603-020-02330-w>
- Zhang S-R, Hu A-K, Wang C (2016) Three-dimensional inversion analysis of an in situ stress field based on a two-stage optimization algorithm. *J Zhejiang Univ, Sci, A* 2016:782–802. <https://doi.org/10.1631/jzus.A1600014>
- Zhang C, Jiang B, Li N et al (2017) Elastoplastic coupling solution of circular openings in strain-softening rock mass considering pressure-dependent effect. *Int J Geomech*. [https://doi.org/10.1061/\(ASCE\)GM.1943-5622.0001043](https://doi.org/10.1061/(ASCE)GM.1943-5622.0001043)
- Zhang Q, Li F, Duan K et al (2021) Experimental investigation on splitting failure of high sidewall cavern under three-dimensional high in-situ stress. *Tunnell Underground Space Technol* 108:103725. <https://doi.org/10.1016/j.tust.2020.103725>
- Zhang M, Li D, Liu J et al (2023) The modification of Mohr-Coulomb criteria based on shape function and determination method of undetermined parameters. *Mech Mater* 185:104772. <https://doi.org/10.1016/j.mechmat.2023.104772>
- Zhang P, Mishra B, Heasley KA (2015) Experimental investigation on the influence of high pressure and high temperature on the mechanical properties of deep reservoir rocks. *Rock Mech Rock Eng* 48(6):2197–2211. <https://doi.org/10.1007/s00603-015-0718-x>
- Zhang Z, Xie H, Zhang R et al (2019b) Deformation damage and energy evolution characteristics of coal at different depths. *Rock Mech Rock Eng* 52(5):1491–1503. <https://doi.org/10.1007/s00603-018-1555-5>
- Zhang K, Yang T, Bai H et al (2018) Longwall mining-induced damage and fractures: field measurements and simulation using FDM and DEM coupled method. *Int J Geomech* 18(1):04017127. [https://doi.org/10.1061/\(ASCE\)GM.1943-5622.0001040](https://doi.org/10.1061/(ASCE)GM.1943-5622.0001040)
- Zhang G, Zhang W, Wang H et al (2019a) Microscopic failure mechanism analysis of sandstone under triaxial compression. *Geotech Geol Eng* 37(2):683–690. <https://doi.org/10.1007/s10706-018-0638-0>
- Zhang L, Zhu H (2007) Three-dimensional hoek-brown strength criterion for rocks. *J Geotech Geoenviron Eng*. [https://doi.org/10.1061/\(ASCE\)1090-0241\(2007\)133:9\(1128\)](https://doi.org/10.1061/(ASCE)1090-0241(2007)133:9(1128))
- Zhang YX, Cai MF, Wang KZ. (2005) Algorithm of in situ stress field and its application. *Chinese Journal of Engineering*. 27(5): 520–523. <https://doi.org/10.13374/j.issn1001-053x.2005.05.033>
- Zhang X, Feng X, Kong R et al (2017b) Key technology in development of true triaxial apparatus to determine stress–strain curves for hard rocks. *Yanshilixue Yu Gongcheng Xuebao/Chinese Journal of Rock Mechanics and Engineering*. 36: 2629–2640. <https://doi.org/10.13722/j.cnki.jrme.2017.1215>
- Zhao XG, Cai M, Wang J et al (2013) Damage stress and acoustic emission characteristics of the Beishan granite. *Int J Rock Mech Mining Sci* 64:258–269. <https://doi.org/10.1016/j.ijrmmms.2013.09.003>
- Zhao J, Feng X-T, Zhang X-W et al (2018) Brittle-ductile transition and failure mechanism of Jinping marble under true triaxial compression. *Eng Geol* 232:160–170. <https://doi.org/10.1016/j.enggeo.2017.11.008>
- Zhao H, Gun H, Jiang C et al (2022a) Mechanical properties and fracture mode transformation of rocks subjected to asymmetric radial stresses. *Bull Eng Geol Env* 81(10):434. <https://doi.org/10.1007/s10064-022-02891-w>
- Zhao Y-M, Han Y, Kou Y-Y et al (2021) Three-dimensional, real-time, and intelligent data acquisition of large deformation in deep tunnels. *Adv Civil Eng* 2021:6671118. <https://doi.org/10.1155/2021/6671118>
- Zhao J-S, Jiang Q, Lu J-F et al (2022) Rock fracturing observation based on microseismic monitoring and borehole imaging: In situ investigation in a large underground cavern under high geostress. *Tunnell Underground Space Technol* 126:104549. <https://doi.org/10.1016/j.tust.2022.104549>
- Zhao H, Ma F, Xu J et al (2012) In situ stress field inversion and its application in mining-induced rock mass movement. *Int J Rock Mech Mining Sci* 53:120–128. <https://doi.org/10.1016/j.ijrmmms.2012.05.005>
- Zhao B, Saxena N, Hofmann R et al (2023) Enhancing resolution of micro-CT images of reservoir rocks using super resolution. *Comput Geosci* 170:105265. <https://doi.org/10.1016/j.cageo.2022.105265>
- Zhao X, Tang C, Li Y et al (2006) Study on Ae activity characteristics under uniaxial compression loading. *Chinese J Rock Mech Eng* 25:3673–3678. <https://doi.org/10.3321/j.issn:1000-6915.2006.z2.053>
- Zhao C, Tian J, Matsuda H et al (2015) Crack propagation and damage of rock under uniaxial compression based on global strain field analysis. *Yanshilixue Yu Gongcheng Xuebao/Chinese J Rock Mech Eng* 34:763–769. <https://doi.org/10.13722/j.cnki.jrme.2015.04.013>
- Zhao X, Wu Y, Jia Y et al (2024) Impact of particle shape on crushing behaviour of rock particles using X-ray micro-CT testing and DEM modelling. *Rock Mech Rock Eng*. <https://doi.org/10.1007/s00603-024-03916-4>
- Zhao Y, Zhang Z-G (2015) Mechanical response features and failure process of soft surrounding rock around deeply buried three-centered arch tunnel. *J Central South University* 22(10):4064–4073. <https://doi.org/10.1007/s11771-015-2951-6>
- Zheng Z, Feng X-T, Yang C-X et al (2020) Post-peak deformation and failure behaviour of Jinping marble under true triaxial stresses. *Eng Geol* 265:105444. <https://doi.org/10.1016/j.enggeo.2019.105444>
- Zheng M, Li S, Zhao H et al (2021) Probabilistic analysis of tunnel displacements based on correlative recognition of rock mass parameters. *Geosci Front* 12(4):101136. <https://doi.org/10.1016/j.gsf.2020.12.015>
- Zhou HW, Wang ZH, Wang CS et al (2019) On acoustic emission and post-peak energy evolution in beishan granite under cyclic loading. *Rock Mech Rock Eng* 52(1):283–288. <https://doi.org/10.1007/s00603-018-1614-y>
- Zhou HW, Xie HP, Zuo JP et al (2010) Experimental study of the effect of depth on mechanical parameters of rock. *Chinese Sci Bull* 55:3276–3284. <https://doi.org/10.1360/972010-786>
- Zhu G-Q, Feng X-T, Zhou Y et al (2019) Experimental study to design an analog material for Jinping marble with high strength, high brittleness and high unit weight and ductility. *Rock Mech Rock Eng*. <https://doi.org/10.1007/s00603-018-1710-z>
- Zhu G-Q, Feng X-T, Zhou Y-Y et al (2020) Physical model experimental study on spalling failure around a tunnel in synthetic marble. *Rock Mech Rock Eng* 53(2):909–926. <https://doi.org/10.1007/s00603-019-01952-z>
- Zhu JB, Zhou T, Liao ZY et al (2018) Replication of internal defects and investigation of mechanical and fracture behaviour of rock using 3D printing and 3D numerical methods in combination with X-ray computerized tomography. *Int J Rock Mech Mining Sci* 106:198–212. <https://doi.org/10.1016/j.ijrmmms.2018.04.022>
- Zienkiewicz OC. (1971). *The Finite Element Method In Engineering Science*.

Publisher's Note Springer Nature remains neutral with regard to jurisdictional claims in published maps and institutional affiliations.

Springer Nature or its licensor (e.g. a society or other partner) holds exclusive rights to this article under a publishing agreement with the

author(s) or other rightsholder(s); author self-archiving of the accepted manuscript version of this article is solely governed by the terms of such publishing agreement and applicable law.